NORTHEAST COOL-SEASON CYCLONES ASSOCIATED WITH SIGNIFICANT UPPER-LEVEL EASTERLY WIND ANOMALIES

by

Adrian N. Mitchell

A Thesis

Submitted to the University at Albany, State University of New York

in Partial Fulfillment of

the Requirements for the Degree of

Master of Science

College of Arts & Sciences

Department of Atmospheric and Environmental Sciences

2014

ABSTRACT

A subset of Northeast U.S. cool-season cyclones is associated with upper-level easterly flow and, occasionally, well-defined easterly jet streaks. These events occur approximately once per year and may be associated with retrograding surface cyclones and precipitation caused by northerly warm-air advection, leading to forecast challenges. The deepest extratropical cyclone that affected the Northeast U.S. during the 2009–2010 cool-season was associated with an upper-level easterly jet streak, and produced a record snowfall total of 85 cm in Burlington, Vermont. Orographic precipitation enhancement in this case resulted from an interaction of the low-level flow with the complex topography of northern Vermont. This thesis explores the multi-scale aspects of similar anomalous cyclone events (ACEs) in the Northeast U.S. through climatological, composite and case study analyses.

The NCEP–NCAR dataset was used to develop an ACE climatology consisting of 78 events from 1948–2010. ACEs are defined as cyclones associated with a 300-hPa standardized zonal wind anomaly ≤ -3 SD and a sea level pressure < 1000 hPa for at least a 12-h period. ACEs are separated into three categories based on the most commonly observed upper-level structures: open wave, cutoff low and easterly jet streak (EJS). Results from a composite analysis reveal that all ACEs develop during periods of anomalous high-latitude blocking; however, distinct differences in the strength and location of blocking exist within each category and govern the configuration of key synoptic-scale forcing features.

Case study analyses of two EJS events (2–3 January 2010; 25–27 February 2010) that were associated with historic snowfall totals and significant forecast challenges are

presented. Both events displayed considerable alteration of the low-level flow by the orography of the northeastern U.S. and, as a result, were studied using high-resolution model simulations. Results indicate that upslope precipitation enhancement occurred in conjunction with northerly warm-air advection beneath the equatorward exit region of an easterly jet streak in both cases. Based upon the results of the composite and case study analyses, conceptual models are presented depicting important synoptic-scale features including blocking anticyclones, upper-level jet streaks, trowal locations, and surface fronts.

ACKNOWLEDGEMENTS

First, I would like to thank my family and my girlfriend, Melina, for the unwavering love, support and encouragement they have given me over the years. It has motivated me to accomplish many of my goals including the completion of this M.S. thesis. Next, I would like to thank my co-advisors Dr. Lance Bosart and Dr. Kristen Corbosiero for their guidance and support throughout my undergraduate and graduate career. Their vast knowledge and continuous enthusiasm has been a great inspiration and has advanced my own abilities as a scientist, and for that I am forever grateful.

I would also like to thank the entire faculty and staff of the UAlbany Department of Atmospheric and Environmental Sciences for providing a friendly and supportive learning environment for the last six years. Special thanks go to Ross Lazear and Kevin Tyle for their technical assistance, as well as Justin Minder, whose guidance and suggestions helped to further the extent of this research. I also thank Barbara Zampella, Sandra George, Denise Church, Maria Moon and Chaina Porter for their assistance in administrative matters.

Special thanks go out to my fellow graduate students for delivering a relaxed and fun experience, amidst the challenges of graduate studies. In particular I would like to thank Nick Schiraldi and Adam Turchioe, whose programming assistance and valuable input were instrumental in the development of this thesis. Lastly I would like to thank Neil Stuart of the Albany, NY, NWS forecast office for providing valuable advice while serving as my NWS focal point for this research. This research was supported by the National Oceanic and Atmospheric Administration (NOAA) grant NA01NWS4680002,

awarded to the University at Albany, SUNY, as part of the Collaborative Science, Technology, and Applied Research (CSTAR) program.

TABLE OF CONTENTS

LIST OF TABLES

LIST OF FIGURES

1. Introduction

1.1 Motivation and Objectives

East Coast cool-season cyclones have been studied and well documented since the introductory papers of the 1940's (Austin 1941; Miller 1946). The synoptic-scale structure and dynamic processes associated with northeastern U.S. snowstorms have been investigated thoroughly by a variety of authors, but most notably by Kocin and Uccellini (1990, 2004). The cool-season of 2009–2010 brought several historic snowstorms to parts of the Mid-Atlantic and Northeast, and as a result, has been the focus of multiple attribution studies (e.g., Seager et al. 2010; Wang et al. 2010; Chang et al. 2011). The two deepest extratropical cyclones that impacted the northeastern U.S. during the 2009–2010 cool-season occurred on 1–3 January and 25–27 February 2010, and were both associated with upper-level easterly jet streaks and low-level wrap around warm air advection. An anomalous feature common to each of these two events was the surface cyclone track, which began northeastward off the Virginia coast only to turn westward while approaching the New England coast. The 1–3 January 2010 cyclone produced a record snowfall of 33.1 in (84 cm) in Burlington, VT and the 25–27 February 2010 cyclone produced a record snowfall upwards of 48 in (122 cm) in the Catskill Mountains of New York. In both cases, significant snowfall enhancement resulted from mesoscale forcing for ascent associated with the topography of New York and New England. Numerical models poorly forecast the track and precipitation distribution of the

aforementioned cyclones at lead times greater than 24 h, partially as a result of the complex large-scale flow regime that was in place.

Northeast cool-season cyclones associated with significant upper-level easterly wind anomalies (henceforth referred to as anomalous cyclone events; ACEs) have been scrutinized in various case studies, but due to their rarity have not been comprehensively studied through climatological and composite analyses. The goals of this study are to: (1) define criteria to objectively compile a list of ACEs spanning the years 1948–2010; (2) explore linkages between the occurrence of ACEs and various teleconnection indices; and (3) investigate synoptic-scale and mesoscale processes associated with ACEs. The antecedent environments conducive to the development of ACEs, and the mechanisms that govern their evolution will be of particular interest. The degree to which mesoscale forcing can modify dynamically forced synoptic-scale circulations will also be considered. A literature review of scientific findings relevant to the topic of northeastern U.S. cool-season cyclogenesis is contained in chapter 1, and an overview of the data and methodology used in this study is covered in chapter 2. Climatological and composite results are presented in chapter 3, and case study results are presented in chapter 4. Chapter 5 contains a research summary and key conclusions.

1.2 Literature Review

1.2.1 Characteristics of Northeast Cool-Season Cyclones

Cool-season cyclogenesis is favored along the East Coast of the U.S. due to the complex moisture, kinematic and thermal boundaries that can result from the physiography of the region (e.g., Colucci 1976; Sanders and Gyakum 1980; Roebber 1984; Maglaras et al. 1995). As a result, cyclones that affect the East Coast of the U.S. can come in a variety of "flavors" depending on the synoptic-scale pattern. Miller (1946) classified East Coast cyclones as either type A or B based on the orientation of observed surface features. Type A cyclones develop as a wave along a cold front and track northeastward along the Atlantic seaboard, interacting with the inherent land-ocean thermal boundary. Type B cyclones involve coastal secondary cyclogenesis along the shared warm front of an occluded primary low approaching the Great Lakes region, and a developing coastal low. Figure 1.1 displays two cyclones that typify each cyclone type defined by Miller (1946). Both Miller type A and type B cyclones are typically associated with pronounced upper-level jet streaks somewhere in the vicinity of the eastern U.S. Uccellini and Kocin (1987) investigated the role of vertical transverse jet streak circulations in East Coast snow events, and the link between the configuration of surface and upper-level features. Figure 1.2 shows a schematic of relevant surface and upper-level features associated with a "typical" heavy snow event. Using observational analysis, Uccellini and Kocin (1987) were able to demonstrate how ageostrophic circulations associated with coupled jet streaks can determine the orientation of surface cyclones, temperature advection and heavy precipitation in East Coast snowstorms. Kocin and Uccellini (2004) later described in exquisite detail the evolution of surface and upper-level features associated with thirty northeastern U.S. snowstorms. Figure 1.3 shows a schematic of jet streak circulation patterns common during Northeast snowstorms. The

overlap between the thermally direct transverse circulation in the entrance region of the northern jet streak and thermally indirect transverse circulation in the exit region of the southern jet streak nicely illustrate how enhanced forcing for surface cyclogenesis can occur.

Kocin and Uccellini (2004) analyze the track and configuration of surface cyclones, anticyclones, 500-hPa vorticity maxima and 500-hPa closed lows associated with northeastern U.S. snowstorms. They categorize cases as either "self development" (Sutcliffe 1947; Sutcliffe and Forsdyke 1950; Petterssen 1956; Palmén and Newton 1969), open-wave (Petterssen 1956), or cutoff lows (Petterssen 1956), based on the evolution of the 500-hPa trough. Kocin and Uccellini (2004) note that the most intense cyclones tend to be associated with the evolution of a 500-hPa trough into a closed vortex, termed "self development", while the longest duration cyclones consist of a closed, or cutoff, 500-hPa circulation prior to cyclogenesis. They note the importance of a downstream ridge or "Greenland block" during Northeast cyclogenesis events, consistent with Bell and Bosart's (1989) finding of positive thickness anomalies in the vicinity of Greenland prior to East Coast cyclogenesis in an 11-case composite.

In cases of intense cyclogenesis, Kocin and Uccellini (2004) stress the importance of trough mergers (e.g., Gaza and Bosart 1990; Lefevre and Nielsen-Gammon 1995; Dean and Bosart 1996), defined as the amalgamation of two separate 500-hPa vorticity centers, or shortwaves, into one coherent system. Gaza and Bosart (1990) note that trough mergers can lead to the development of a negatively tilted upper-level trough, enhanced thermal and differential vorticity advection, and ultimately intense surface cyclogenesis. The phasing of northern and southern stream shortwaves was observed in seventeen of

thirty cases by Kocin and Uccellini (2004) and in numerous historic cases such as the Cleveland "Superbomb" (Salmon and Smith 1980; Hakim et al. 1995, 1996). A southern stream shortwave and embedded vorticity maximum that phases with a northern stream shortwave will produce more favorable dynamics for rapid surface cyclogenesis than a southern stream shortwave that damps the northern stream shortwave or ejects around its periphery.

Shapiro and Keyser (1990) refined the Norwegian frontal-cyclone model (Bjerknes 1919) by using data from various observational and numerical modeling studies. During the Experiment on Rapidly Intensifying Cyclones over the Atlantic (ERICA) field study, observational data was gathered that led to new insights into maritime cyclone evolution; thus, it is applicable to most all Northeast cool-season cyclones. The Shapiro-Keyser model can be seen in Figure 1.4 and illustrates the evolution toward a frontal fracture near the cyclone center, a frontal T-bone and bent-back warm front, and ultimately a warm-core seclusion. The lifecycle of many Northeast cool-season cyclones takes place over the western North Atlantic Ocean, and thus evolve in a similar manner as that proposed by Shapiro and Keyser (1990). Rapidly intensifying Northeast cyclones, like those that occur in conjunction with shortwave mergers, tend to typify the stages of development proposed by Shapiro and Keyser (1990).

1.2.2 Northeast Cool-Season Cyclones and Anomalous Easterly Flow

Mid-latitude cyclones are understood to intensify by extracting energy from the surrounding baroclinic environment. The most intense cyclones can significantly weaken or even reverse the meridional temperature gradient during their lifecycle, through strong low-level temperature advection. The thermal wind equation illustrates how the vertical shear of the zonal wind is related to the meridional gradient of temperature:

$$\frac{\partial u_{\mathrm{g}}}{\partial p} = \frac{R_{\mathrm{d}}}{fp}\frac{\partial T}{\partial y} \tag{1.1}$$

where $\frac{\partial u_{\mathrm{g}}}{\partial p}$ is the change in zonal geostrophic wind with pressure, R_{d} is the gas constant for dry air, f is the Coriolis parameter, p is pressure and $\frac{\partial T}{\partial y}$ is the meridional temperature gradient. When the low-level temperature gradient is directed poleward, the zonal wind will become increasingly negative with height leading to an easterly wind aloft. Palmén and Newton (1969) discuss a cyclone in the advanced stages of development and note how the upper level height contours are strongly distorted, indicative of a negatively tilted trough. They remark how a substantial part of the moist-adiabatic ascent can occur in a region of easterly flow aloft, north of the surface cyclone center. As a result of the mean meridional temperature gradient over North America, and the aforementioned thermal wind relationship, well-defined easterly jet streaks are somewhat rare. Rochette and Market (2011) performed a case study of a northeastern U.S. cyclone associated with an upper-level easterly jet streak in February 2010. They remark how the jet streak is strikingly similar to the idealized "four-quadrant" model (e.g., Uccellini and Johnson 1979); however, the features are reversed (Figure 1.5). The authors carry out a quasigeostrophic (QG) diagnosis of the easterly jet streak and conclude that the forcing for upward motion in the right entrance and left exit regions of

the jet streak significantly influenced the sensible weather. Payer (2010) analyzed a cutoff cyclone associated with an upper-level easterly jet streak in January 2010. Forcing for upward vertical motion was found to be significant in the equatorward exit region of the jet streak and in regions of northeasterly warm air advection. Payer (2010) also found that a pattern of high latitude blocking over the North Atlantic Ocean was coincident with the development of a cutoff cyclone over the eastern U.S.

Cutoff cyclones have very slow forward speeds as a result of their separation from background westerly flow (e.g., Bell and Bosart 1989) and thus tend to be long duration events. Previous studies have found common precursors for cutoff cyclone development, including a large trough in place, and a high amplitude ridge upstream (Palmén 1949; Palmén and Nagler 1949; Keyser and Shapiro 1986; Bell and Bosart 1993, 1994; Bell and Keyser 1993). Using numerical simulations, Thorncroft et al. (1993) described two different scenarios in which cutoff cyclones can develop. The LC1 scenario is associated with a positively tilted trough that thins and is pinched off as anticyclonic wave breaking occurs. This leads to a cutoff cyclone equatorward of the primary jet stream. The LC2 scenario involves a negatively tilted trough that eventually wraps up cyclonically, allowing for a cutoff cyclone poleward of the mean jet stream. The LC2 scenario has been associated with rapidly deepening extratropical cyclones (e.g., Sanders and Gyakum 1980; Konrad and Colucci 1998). It has been observed that cutoff cyclones can support the maintenance of atmospheric blocking regimes (Rex 1950). Colucci (1985, 1987) documented multiple cutoff cyclones that led to the formation of Rex (1950) blocking patterns at 500 hPa. Similarly, Pelly and Hoskins (2003) found that intensifying cyclones

help to initiate blocking regimes in the North Atlantic, as warm air advection downstream of the surface cyclone enhances upper-level ridging.

Stuart and Grumm (2006) proved the usefulness of analyzing 300-hPa zonal wind standardized anomalies associated with East Coast winter storms. The authors refer to a feature as anomalous if the standardized anomaly departs from the 30-yr mean by more than 2.5 SD (standard deviations), indicating a situation that occurs less than 16% of the time. They note that a 300-hPa zonal wind anomaly threshold of −2.5 SD can be used to identify slow-moving, long duration cyclones that tend to be cutoff from the background westerly flow.

1.2.3 Teleconnections and Planetary-Scale Influences

Sanders and Gyakum (1980) found that rapidly intensifying extratropical cyclones (bombs) tend to occur in the western Atlantic, just off the East Coast of the United States. They note that this region is characterized by strong sea surface temperature gradients as a result of the warm Gulf Stream waters and cold continental air. The authors also found that extratropical bombs tend to develop just ahead of a planetary-scale trough, within or just poleward of the main belt of westerlies. Similarly, Hoskins and Valdes (1990) proposed that the North Atlantic storm track is somewhat self-maintaining, due to the mean baroclinicity and diabatic heating in the region. Sanders (1988) found that mobile upper-level troughs over North America tend to form in the vicinity of the Rocky Mountains, within a quasi-stationary planetary scale wave. These mobile troughs

effectively act as predecessor disturbances that, in the presence of a low-level baroclinic zone, can help initiate cyclogenesis farther eastward along the Atlantic coast. Lackmann et al. (1996) discuss how low-frequency planetary scale flow patterns can govern the behavior of various synoptic scale features, including cyclones and cyclogenetic precursors. Using composite analysis, the authors found several persistent features prior to explosive cyclogenesis in the western North Atlantic. These included a North Pacific trough, an enhanced Pacific jet and a ridge over western North America. Their composite analysis also depicted an enhanced cyclogenetic trough over the eastern U.S. Figure 1.6 illustrates the progression of explosive cyclone composite 500-hPa geopotential height anomalies beginning 72 h prior to the event, in 24-h intervals.

The anomalous features that were observed by Lackmann et al. (1996) prior to, and during, western North Atlantic cyclogenesis can also be associated with certain phases of teleconnection indices such as the North Atlantic Oscillation (NAO; Walker and Bliss 1932; Wallace and Gutzler 1981; Barnston and Livezey 1987; Feldstein 2003), the Pacific-North American (PNA) pattern (Wallace and Gutzler 1981; Barnston and Livezey 1987; Feldstein 2002), the Arctic Oscillation (AO; Thompson and Wallace 1998, 2000), and the El Niño-Southern Oscillation (ENSO; Bjerknes 1969; Halpert and Bell 1997; Bell and Halpert 1998). The NAO is a measure of sea level pressure or geopotential height difference between the Azores and Iceland, and can manifest as an anomalously weak (strong) North Atlantic jet stream during negative (positive) NAO events. Barnes and Hartmann (2010) found that jet stream anomalies associated with a negative NAO regime tend to persist longer than anomalies associated with a positive NAO regime as a result of eddy feedback. More than half of the heavy snow events

studied by Kocin and Ucellini (2004) developed during periods in which the NAO was distinctly negative.

The PNA is a stationary Rossby wave train-like pattern originating in the tropical Pacific and extending to the southeastern U.S. The positive (negative) phase of the PNA is associated with positive (negative) geopotential height anomalies near Hawaii and the western U.S. and negative (positive) height anomalies near the Aleutian Islands and southeastern U.S. (Archambault et al. 2008). During the positive phase of the PNA, an enhanced jet stream is typically found over the eastern Pacific with upper-level ridging over western North America. The PNA pattern can be significantly affected by the phase of ENSO (Straus and Shukla 2002), occasionally allowing for enhanced predictability. The AO is an index of the dominant pattern of sea level pressure and geopotential height variations north of 20°N latitude, and is characterized by pressure and geopotential height anomalies of one sign in the Arctic, with the opposite anomaly centered near 37-45°N. The negative (positive) phase of the AO is associated with positive (negative) geopotential height anomalies in high latitude polar regions and a weak (strong) mid-latitude jet stream.

Archambault et al. (2008) examined the influence of large-scale flow regimes on cool-season precipitation in the northeastern U.S. using statistical and composite analyses. The authors found that a negative NAO and positive PNA regime leads to a meridional flow pattern conducive for cyclone tracks along the East Coast. During negative NAO and positive PNA precipitation events, the precipitable water (PW) axis and low-level jet were bent toward the northeastern U.S. from the western North Atlantic, implying substantial moisture transport. In this regime, an amplified ridge was found over

the western U.S. with a downstream trough over the eastern U.S. Archambault et al. (2010) extended their research to the effects of transitioning NAO and PNA regimes on northeastern U.S. cool-season precipitation events, using similar methods. They found that NAO^+ to NAO^- and PNA^- to PNA^+ transitions favor wet conditions in the Northeast, with precipitation events occurring nearly twice as frequently during NAO^+ to NAO^- transitions. Figure 1.7 shows composite analyses of the five-day period surrounding the onset of a cool-season Northeast precipitation event associated with a NAO^+ to NAO^- transition. Archambault et al.'s (2010) composite results indicate that the development of a surface cyclone over the eastern U.S. helps to enhance a North Atlantic ridge, and develop a North Atlantic blocking pattern. The occurrence of cyclonic wave breaking enhances this process as strong warm air advection brings low potential vorticity (PV) air poleward. The conclusions of Archambault et al. (2010) are in agreement with Kocin and Uccellini (2004), who note that there appears to be a significant relationship between Northeast winter storms and a sign change in the short-term fluctuation of the NAO.

ENSO has long been known to affect global weather patterns, and typically has an observed time scale of 3-7 years. The Southern Oscillation is defined as sea level pressure difference between the Indian Ocean-western tropical Pacific and the east-central tropical Pacific (e.g., Bjerknes 1969; Halpert and Bell 1997; Bell and Halpert 1998). The sea level pressure anomalies are associated with the heating (El Niño) and cooling (La Niña) of the equatorial Pacific waters. During El Niño episodes, an enhanced Pacific jet stream brings warmer air into the western and northern portions of North America with enhanced storm frequency over the southern U.S. In La Niña episodes, a weaker Pacific jet stream inhibits storminess as cold air develops over northwest North

America and affects the western and central U.S. Hirsh et al. (2001) analyzed the relationship between the ENSO and the frequency of East Coast winter storms (ECWS). They found that ECWS frequency increases significantly during El Niño regimes, possibly as a result of an increased subtropical jet stream. This agrees with the results of Noel and Changon (1998) who concluded that during the warm phase of ENSO there is increased cyclone activity in New England. Both studies found little linkage between cyclone occurrence and the cool phase of ENSO. Smith and O'Brien (2001) performed a composite study relating ENSO with regional snowfall distributions. They found that the warm phase of ENSO was associated with enhanced snowfall in the Northeast urban corridor as a result of a favorable storm track and enhanced subtropical jet stream over the Southeast U.S. Figure 1.8 illustrates the dominant jet streams and temperature anomalies associated with the cool and warm phases of ENSO.

The tropics are linked to the extratropics through Rossby wave trains (e.g., Kim et al. 2006), a response to synoptic scale divergence aloft associated with deep, moist convection in the tropics. The Madden-Julian oscillation (MJO) represents a large-scale coupling between the atmospheric circulation and deep tropical convection. The MJO is characterized by an eastward moving pattern of deep tropical convection and a time scale of 30–60 days (Madden and Julian 1972, 1994). A study by Matthews et al. (2004) found that when MJO convection is centered over the western Pacific Ocean, a large-scale ridge tends to be in place over western North America. Alternatively, Zhou et al. (2012) concluded that during winter months, negative 500-hPa height anomalies are favored over the eastern U.S. when MJO convection is over the eastern Pacific Ocean. These results suggests that a favorable scenario for East Coast cyclogenesis may develop when

the MJO is either over the western or eastern Pacific Ocean, and a trough is in place over the eastern U.S. The combined effect of various teleconnection patterns and modes of low-frequency variability can lead to a pattern conducive for northeastern U.S. cool season cyclogenesis. It is thus important to document the phase and trend of these teleconnection patterns, prior to and during cyclogenesis events, in an effort to improve predictability.

1.3 Research Goals

This research will aim to: (1) objectively compile a list of ACEs, using a classification scheme to categorize individual events; (2) develop a climatology of ACEs from 1948–2010, and determine whether or not the phase of the AO, NAO, PNA and ENSO affects event occurrence; (3) perform composite analyses of ACEs to reveal important synoptic-scale forcing features; and (4) conduct case study analyses of high impact ACEs using the Weather Research and Forecasting (WRF) Model as a primary tool. The central objective of this research is to gain insight into multiscale aspects of this subset of northeastern U.S. cyclones, while presenting the anticipated findings in a way that is valuable to an operational forecaster in northeastern U.S. The development of conceptual models and event checklists will serve to increase situational awareness of forecasters at the National Weather Service prior to and during these cyclone events.

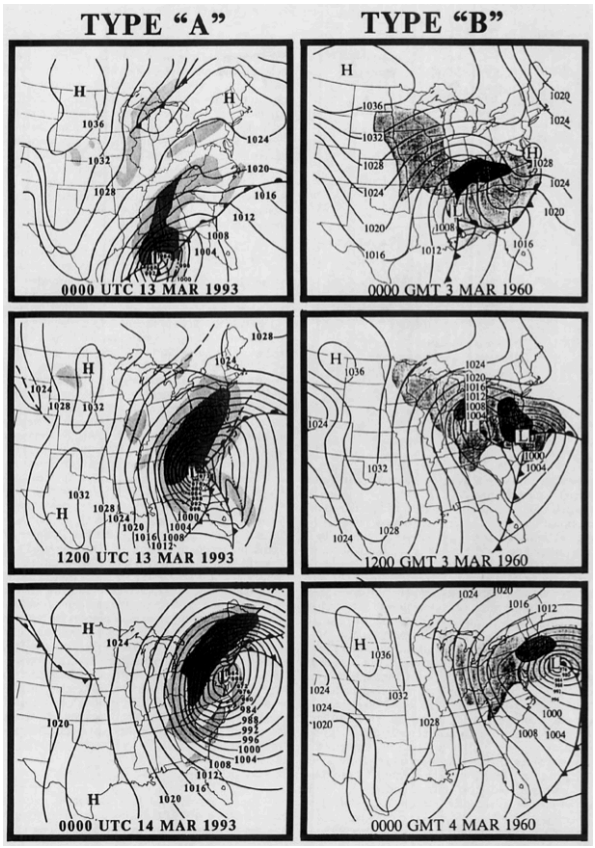

Fig. 1.1. Examples of Miller type A (left) and Miller type B (right) cyclones [adapted in part from Kocin and Uccellini (1990)].

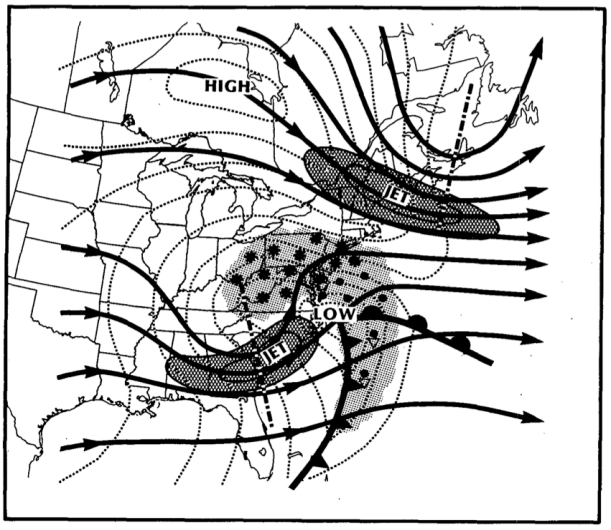

Fig. 1.2. Schematic of surface cold and warm fronts, high and low pressure centers, sea level isobars (dotted), precipitation (shading: asterisks represent snowfall; dots represent rain), upper-level flow (arrows), upper-level trough axes (dot-dashed), and jet streaks (cross-hatched shading) associated with a "typical" heavy snow event along the East Coast [Fig. 1 and adapted caption from Uccellini and Kocin (1987)].

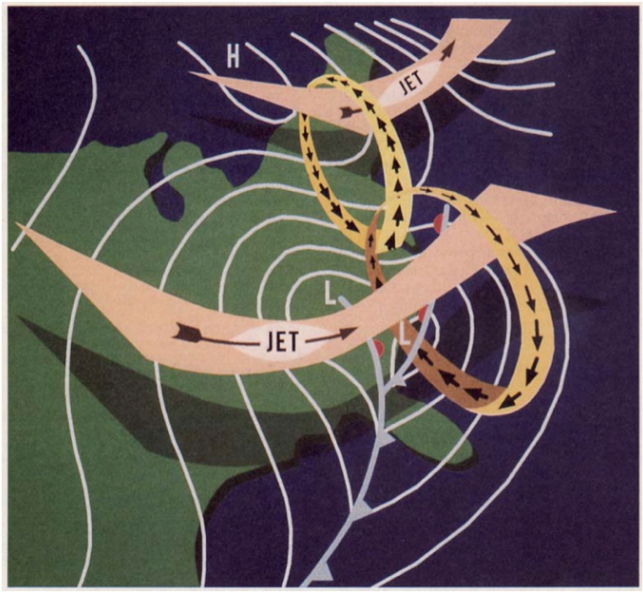

Fig. 1.3. Schematic of dual jet-related circulation patterns during Northeast snowstorms. Circulations are represented by pinwheels, jet streaks are embedded within confluent and diffluent regions, and solid lines are sea level isobars [Fig. 4-17 and adapted caption from Kocin and Uccellini (2004)].

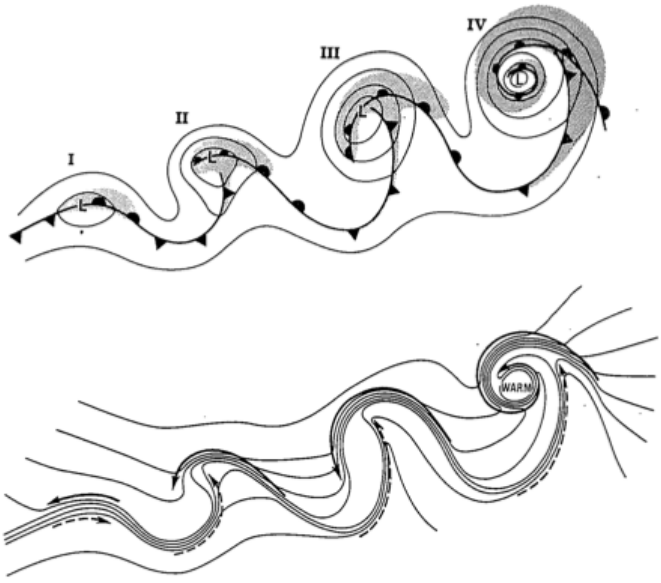

Fig. 1.4. The life cycle of the marine extratropical frontal cyclone: (1) incipient frontal cyclone: (II) frontal fracture; (III) bent-back warm front and frontal T-bone; (IV) warm-core frontal seclusion. Upper: sea-level pressure, solid lines; fronts, bold lines; and cloud signature, shaded. Lower: temperature, solid lines; cold and warm air currents, solid and dashed arrows, respectively [Fig. 10.27 and adapted caption from Shapiro and Keyser (1990)].

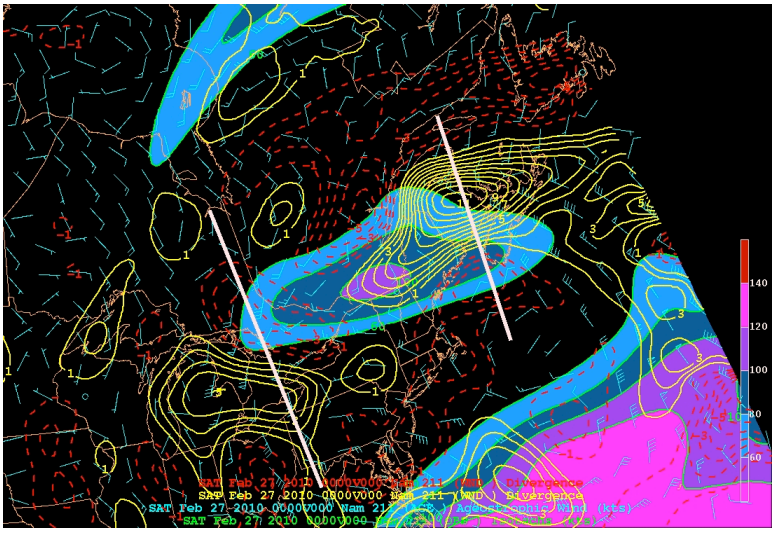

Fig. 1.5. North American Mesoscale Forecast System (NAM) regional analysis of 300-hPa isotachs ≥ 60 kt (green solid/shading), divergence (yellow solid, 10^{-5} s^{-1}), convergence (red dashed, 10^{-5} s^{-1}), and ageostrophic wind (blue barbs, kt), valid at 0000 UTC 27 February 2010. Cross-section axes are shown in white [Fig. 10 and adapted caption from Rochette and Market (2011)]

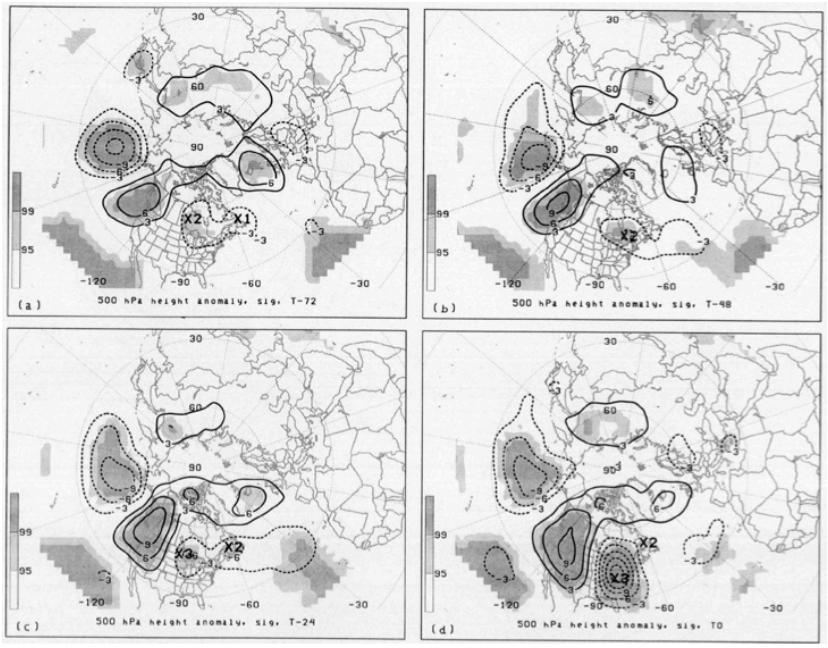

Fig. 1.6. Explosive cyclone composite 500-hPa geopotential height anomaly [contour interval 3 dam, positive (negative) values solid (dashed), zero contour omitted] and statistical significance determined from a two-sided Student's t-test (shading intervals correspond to 95% and 99% confidence limits as shown in legend at left of panels) [Fig. 3 and adapted caption from Lackmann et al. (1996)].

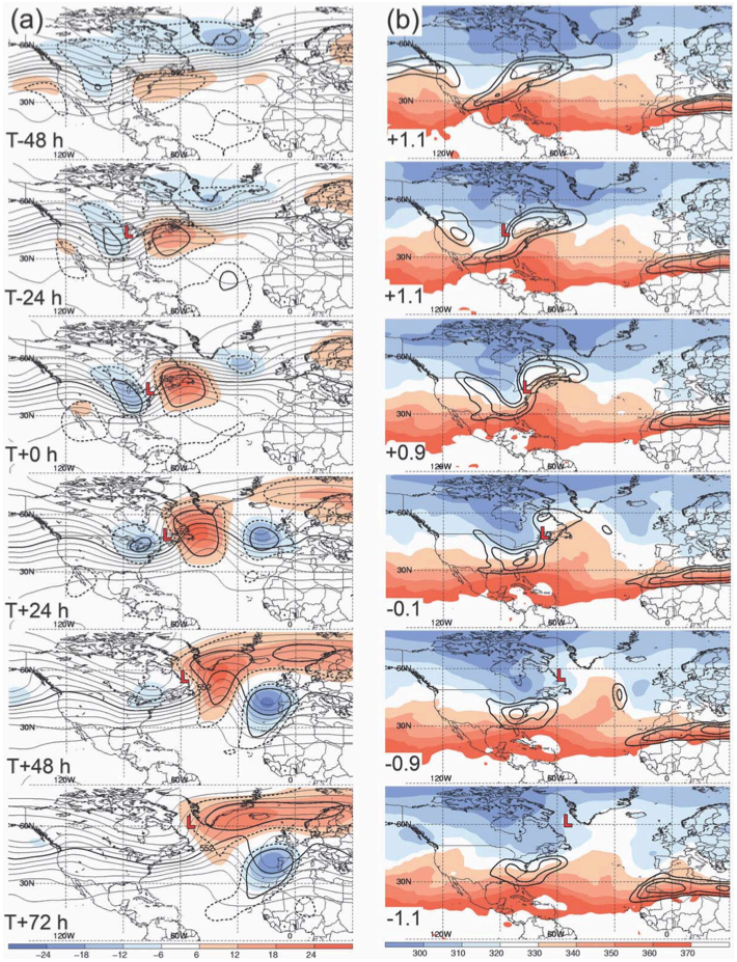

Fig. 1.7. Composite analyses of the five-day period surrounding the onset of a major cool-season NE precipitation event (T+0 h) associated with a NAO^{+} to NAO^{-} transition. Analyses show (a) 500-hPa geopotential height (solid; every 6 dam, with the 552-dam contour shown as a thick line) and departures from climatology (shaded; every 6 dam according to the color bar), with thick dashed (solid) contours denoting statistical significance at the 95% (99%) confidence level; and (b) dynamic tropopause (DT) potential temperature (θ) (shaded; every 10 K according to the color bar) and wind speed (solid; every 5 m s^{-1} beginning at 35 m s^{-1}). The analysis time relative to the onset of the precipitation event is indicated in the bottom- left corner of each analysis in (a), and the composite daily NAO index (SD) is indicated in the bottom-left corner of each analysis in (b). The ‘‘L’’ symbol denotes the position of the key surface low in (a) and (b) [Fig. 3 and adapted caption from Archambault et al. (2010)].

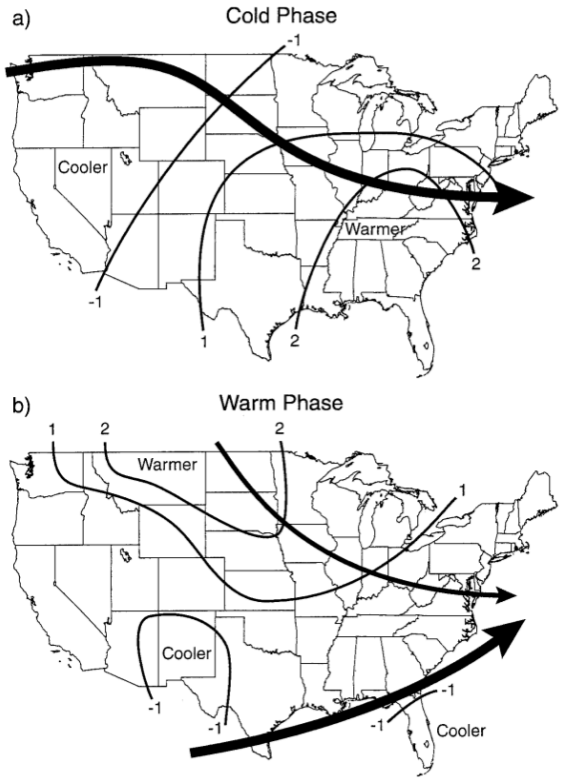

Fig. 1.8. Schematic representation of midwinter surface temperature anomalies (1°C contours with respect to neutral years) and mean 300-hPa jet stream positions during (a) cold and (b) warm ENSO phases. Dominant jets are noted by thick arrows and weaker jets with thin arrows (adapted from Smith et al. 1998). Temperature anomaly patterns are from Sittel (1994) [Fig. 5 and adapted caption from Smith and O'Brien (2001)].

2. Data and Methodology

2.1 Data Sources

In order to determine cases for inclusion in this study, the National Centers for Environmental Prediction–National Center for Atmospheric Research (NCEP–NCAR) reanalysis dataset was utilized spanning the years 1948–2010. The NCEP–NCAR reanalyses are available on a 2.5° × 2.5° grid with 6-h temporal resolution (Kalnay et al. 1996; Kistler et al. 2001), and are located online at http://www.esrl.noaa.gov/psd/. The NCEP–NCAR reanalysis dataset was used to perform a climatological analysis of the identified cyclone events (described below) by gathering data on cyclone location, intensity, 24-h deepening rate and synoptic-scale structure.

Daily AO, NAO and PNA data for each cyclone event was collected from the Climate Prediction Center (CPC) archive, available online at their website http://www.cpc.ncep.noaa.gov/products. ENSO phases for each cyclone event were determined using the CPC's monthly Nino-3.4 sea surface temperature anomalies (SSTA) archive (http://www.cpc.noaa.gov/data/indices/).

Earth- and cyclone-relative composites were developed using the NCEP 24 h daily (1200–1200 UTC) gridded (0.25° x 0.25° resolution) Unified Precipitation Dataset (UPD) and the NCEP–NCAR reanalysis dataset. For a more detailed analysis of the storms chosen for case studies, 1° NCEP Global Forecast System (GFS) analysis data were displayed using the General Meteorological Package (GEMPAK; desJardins et al. 1991). This data was obtained from the in-house data archive at the Department of

Atmospheric and Environmental Sciences at the University at Albany (DAES/UA).

Level III base reflectivity (0.5° elevation angle) data (~1-km horizontal resolution) were gathered from the National Climatic Data Center (NCDC) and displayed using the GDRADR program of GEMPAK. Radiosonde data were obtained from the University of Wyoming archive (http://weather.uwyo.edu/upperair/sounding.html) and hourly METAR reports of surface observations from the U.S. and Canada were obtained from the Iowa State University archive (http://mesonet.agron.iastate.edu/archive/).

The Advanced Research WRF (ARW; Skamarock et al. 2008) model was utilized in the 1–3 January 2010 and 25–27 February 2010 study cases. Information on the WRF Model is available online at http://www.mmm.ucar.edu/wrf/users/. The initial and boundary conditions were derived from 12 km NCEP NAM model analysis by WRF preprocessing. The model was run with two-way nested domains with 12, 4 and 1.33 km grid spacing, using the Thompson microphysics scheme (Thompson et al. 2004) and YSU (Yonsei University; Hong et al. 2004) planetary boundary layer scheme.

2.2 Methodology

2.2.1 Event Identification and Categorization

The first objective was to identify large-scale upper level zonal wind anomalies in the northeastern U.S. spanning as many years as possible, in order to develop a case list of ACEs. Since the NCEP–NCAR reanalysis dataset extends back to 1 January 1948 with 6-h temporal resolution; it was used for this task. A cyclone domain was defined

extending from 37–51°N and 83–60°W (Figure 2.1). This ensured that cyclones that remained well off the coast of the northeastern U.S. were still captured. To be considered an ACE, the following criteria had to be met simultaneously for at least a 12-h period in the domain: (1) a 300-hPa standardized zonal wind anomaly ≤ −3 SD; and (2) a sea level pressure < 1000 hPa. Standardized anomalies of 300-hPa zonal winds were calculated using a method similar to Grumm and Hart (2001). The daily 300-hPa zonal wind was normalized with respect to 30-yr climatology by

$$N = (X - \mu) / \sigma \tag{2.1}$$

where N is the standardized anomaly, X is a parameter value at a given grid point, μ is the 21-day running mean of the given parameter for that grid point, and σ is the grid point 21-day running standard deviation. Using standardized 300-hPa zonal wind anomalies guaranteed that the significance of the anomaly did not change throughout the cool season, despite the magnitude of the anomaly. The above method yielded a total of 86 ACEs, which were then manually inspected to determine if a coherent surface low pressure was present. This subjective analysis eliminated eight cases in which no organized cyclone was present, leaving 78 cases left for further classification (Table 1).

A basis for event categorization came from the 2–3 January and 25–27 February 2010 high impact cyclone events. Both of these events met the criteria to be considered ACEs, and had strikingly similar synoptic scale forcing features. These features included 300-hPa easterly jet streaks north of the cyclone center, and 850-hPa northerly warm air advection northwest of the cyclone center. In an effort to identify ACEs of a similar nature, a subjective classification method was developed. This classification method required the following features to be present at the hour (0000, 0600, 1200 or 1800 UTC)

when the zonal wind anomaly was at a minimum for the event: (1) a 300-hPa easterly jet streak (> 30 m s^{-1}) poleward of the cyclone; and (2) 850-hPa northerly warm air advection on the poleward and western side of the cyclone. Each event was manually inspected to ensure that the primary component of the 300-hPa jet streak core was easterly, and that the primary component of the 850-hPa wind vector associated with warm air advection was northerly (Figure 2.2). These ACEs were referred to as easterly jet streak (EJS) events. Remaining ACEs were classified as either cutoff low or open-wave based on the configuration of the 300-hPa trough at the hour (0000, 0600, 1200 or 1800 UTC) when the zonal wind anomaly was at a minimum for the event. Cutoff low events refer those in which a manual inspection of the 300-hPa geopotential height field revealed a 60-m height rise in all directions from the center of the cutoff circulation. Open-wave events refer to those in which the 300-hPa trough remained open. The goal of this scheme was to classify ACEs in as few categories as possible and yet make meaningful distinctions regarding synoptic-scale cyclone structure.

2.2.2 Event Climatology and Statistics

Once a case list of 78 ACEs was developed, a climatological analysis was performed using data gathered from the NCEP–NCAR reanalysis dataset. For each category of ACE the following was determined:

1) The frequency of event occurrence from a monthly and decadal perspective.
2) The event duration, defined as the amount of time in consecutive 6-h intervals that the surface cyclone (<1000 hPa) remained in the cyclone domain.

3) The minimum sea level pressure and maximum 24-h cyclone deepening rate. These statistics were determined through a manual inspection of sea level pressure data at 6-h intervals.
4) The average daily minimum 300-hPa zonal wind (kt) in the cyclone domain.
5) The average value and trend of the AO, NAO, PNA and ENSO. The trend was defined as the difference in the individual teleconnection value from one week prior to event occurrence and day of event occurrence.

2.2.3 Cyclone Composites

Earth- and cyclone-relative composites were created for all three categories of ACEs using the NCEP–NCAR reanalysis dataset. For each event, the analysis time was defined as the hour (0000, 0600, 1200 or 1800 UTC) when the 300-hPa zonal wind anomaly was at a minimum for the event. The earth-relative composites utilize a five-day lag of 500-hPa geopotential heights and standardized anomalies, and demonstrate the large-scale Rossby wave pattern that is favorable for the development of ACEs. When creating cyclone relative composites, the grid for each cyclone event was centered on the location of the surface cyclone. The grids for each event in a given category were then averaged and centered on the centroid of all cyclone events. The resulting cyclone-relative composites demonstrate the moisture, thermal and kinematic structures associated with ACEs.

A variety of diagnostic fields were calculated and analyzed using GEMPAK. The Q-vector form of the QG omega equation using the geostrophic wind (Eq. 2.2) and the definition of the Q-vector (Eq. 2.3) was applied and plotted, ignoring the $-\frac{R}{p}$ term.

$$\left(\sigma\nabla_p^2 + f_0^2\frac{\partial^2}{\partial p^2}\right)\omega = -2\vec{\nabla}_p \bullet \vec{Q} \tag{2.2}$$

$$\vec{Q} = \begin{pmatrix} \frac{\partial \vec{V}_g}{\partial x} \bullet \vec{\nabla}_p T \\ \frac{\partial \vec{V}_g}{\partial y} \bullet \vec{\nabla}_p T \end{pmatrix} = \begin{pmatrix} Q_1 \\ Q_2 \end{pmatrix} \tag{2.3}$$

This helped facilitate the investigation of QG forcing for ascent in the composites. The results of the composite analysis of ACEs will be presented in chapter 3.

2.2.4 Case Study Analyses

The 2–3 January and 25–27 February 2010 ACEs were chosen as study cases because they caused record snowfall in the northeastern U.S., were poorly forecast by numerical models at lead times greater than 24-h, and are representative of the EJS composites. The case studies will focus on identifying the features responsible for the development and intensification of the surface cyclones, the anomalous track of the surface cyclones, and the forcing mechanisms for heavy snowfall. In both study cases there was significant orographic precipitation enhancement, which led to challenging precipitation forecasts. As a result both cases have been analyzed using ARW simulations to develop a better understanding of the mesoscale phenomena that can develop during EJS events. All diagnostic fields were calculated and displayed using GEMPAK, and

snowfall accumulation maps for the study cases were obtained from the National Operational Hydrologic Remote Sensing Center (NOHRSC, http://www.nohrsc.noaa.gov/).

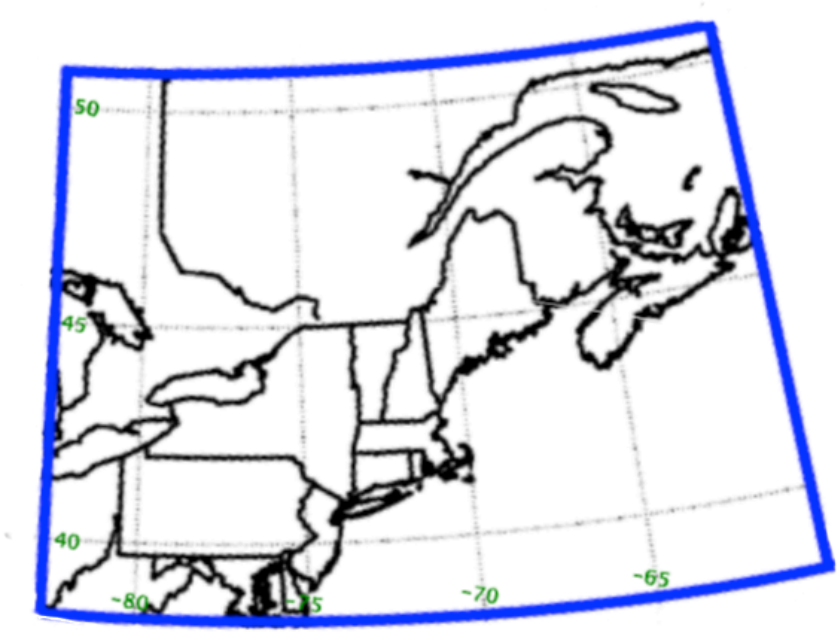

Fig. 2.1. Northeastern U.S. cyclone domain (blue outline).

Table 1. Listing of ACE dates.

Case No.	Cyclone Date	Case No.	Cyclone Date
1	1-Mar-49	40	26-Jan-78
2	12-Mar-49	41	26-Jan-79
3	23-Mar-50	42	16-Nov-81
4	26-Nov-50	43	6-Dec-81
5	29-Nov-50	44	17-Jan-83
6	12-Dec-50	45	12-Mar-83
7	24-Feb-51	46	20-Apr-83
8	4-Apr-51	47	5-Apr-87
9	13-Dec-52	48	29-Apr-88
10	27-Mar-53	49	4-Apr-90
11	31-Mar-53	50	21-Apr-91
12	7-Nov-53	51	6-Jan-92
13	5-Feb-54	52	13-Dec-92
14	16-Oct-55	53	23-Apr-93
15	10-Jan-56	54	21-Dec-93
16	17-Feb-57	55	17-Mar-94
17	9-Mar-57	56	21-Jan-95
18	17-Jan-58	57	15-Nov-95
19	25-Jan-58	58	21-Dec-95
20	3-Feb-58	59	27-Dec-95
21	9-Feb-58	60	21-Nov-96
22	18-Feb-58	61	1-Apr-97
23	21-Mar-58	62	19-Apr-97
24	2-Apr-58	63	6-Dec-97
25	26-Oct-58	64	25-Feb-98
26	29-Nov-61	65	26-Feb-99
27	7-Dec-62	66	12-Mar-99
28	29-Oct-63	67	31-Dec-00
29	31-Jan-66	68	6-Mar-01
30	25-Dec-66	69	5-Apr-04
31	11-Feb-68	70	25-Apr-05
32	6-Nov-69	71	2-Dec-05
33	28-Dec-69	72	16-Apr-07
34	11-Feb-70	73	29-Oct-08
35	27-Jan-71	74	28-Nov-09
36	16-Apr-71	75	3-Jan-10
37	18-Dec-73	76	26-Feb-10
38	4-Apr-75	77	8-Nov-10
39	26-Jan-77	78	6-Dec-10

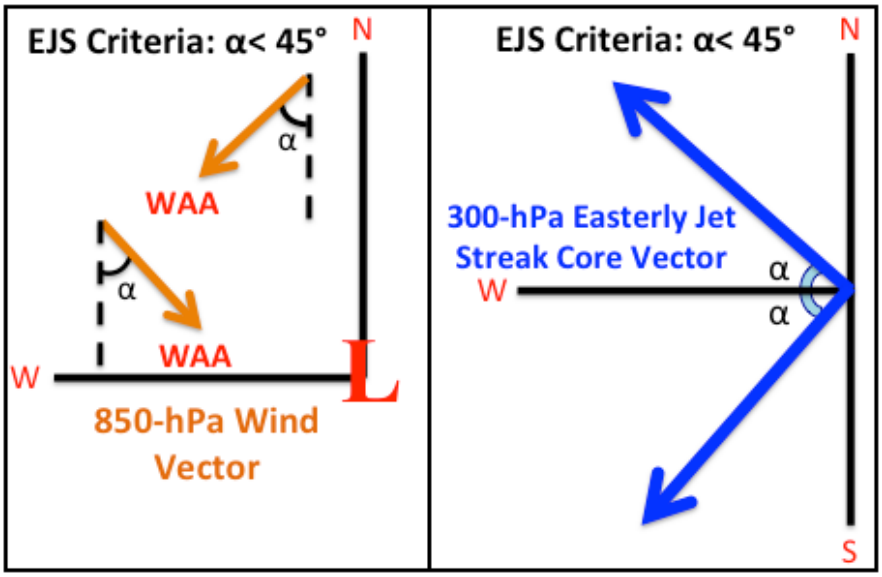

Fig. 2.2. EJS event criteria for orientation of: 850-hPa warm air advection (left) and 300-hPa jet streaks (right). The orange arrows denote 850-hPa wind vectors and the blue arrows denote 300-hPa jet streak core vectors.

3. Results: ACE Overview

3.1 ACE Classification

The classification method discussed in Section 2.2 was applied to the 78 identified ACEs. All events were deemed classifiable and fell into one of three categories: EJS, open wave or cutoff low. These results are summarized in Fig. 3.1.

The EJS category held the most events, with 32 meeting the criteria discussed in Section 2.2. The open wave category contained 25 events and the cutoff low category contained 21 events. Of the 78 ACEs contained in this study, 53 events were associated with a 300-hPa cutoff cyclone, while 25 events remained an open wave in the 300-hPa geopotential height field. An inspection of all events in the EJS category confirmed that every EJS event could also be considered a cutoff low event and contained a closed 300-hPa circulation over the Northeast U.S., making the EJS category a subset of the cutoff low category.

3.2 ACE Climatology and Statistics

3.2.1 Frequency and Characteristics

A decadal analysis of ACE frequency (Fig. 3.2) reveals that the 1950's, 1990's and 2000's saw the most event occurrences, with at least one event per year on average.

The 1960's through the 1980's were minima in ACE frequency with less than one event per year on average. 32% of all ACEs contained in this climatology occurred in the ten-year period from 1949-1959. This is attributable to a prolonged period of large-scale circulation anomalies favorable for the development of ACEs (discussed below in Section 3.2.2). The largest number of EJS and cutoff low events occurred in the active decade of the 1950's, while the most open wave events occurred in the 1990's. From a monthly perspective, ACEs were most common in December and April, with 40% of events occurring during these two months (Fig. 3.3) This statistic reflects the frequent occurrence of Northeast U.S. cutoff lows in the early spring months (e.g., Payer 2010). ACEs were least common in October and November, accounting for only 17% of event occurrences. EJS and cutoff low events were most frequent in the months of December and April, respectively, while an equal number of open wave events occurred in the months of December through April.

The average duration of ACEs in the Northeast U.S. cyclone domain was 38 h ± 5 h, with significant disparities between individual categories of ACEs (Fig. 3.4). EJS events were the longest in duration averaging 46 h ± 3 h in the cyclone domain, while cutoff low events averaged 38 h ± 2 h. Open wave events were the shortest in duration averaging only 30 h ± 2 h. The domain average daily 300-hPa zonal wind minimum was −67 kt for EJS events, −40 kt for cutoff low events and –25 kt for open wave events. Thus, a slow moving surface cyclone associated with an EJS event is consistent with enhanced upper-level easterlies, and a faster moving surface cyclone associated with an open wave event is consistent with weaker upper-level easterlies. The average surface cyclone tracks of all three categories of ACEs are shown in Fig. 3.5. The surface low

associated with EJS and cutoff low events enters the cyclone domain tracking north-northeast, and then turns northwestward around 41° N. The EJS cyclone has a more abrupt westward displacement than the cutoff low cyclone; however, both tend to reduce speed after commencing their westward movement. Both EJS and cutoff low cyclones proceed to drift east-northeastward and exit the cyclone domain. The open wave surface cyclone takes a meridional path, moving at a greater speed than the EJS and cutoff low cyclones, and exits the cyclone domain at approximately the same longitude that it entered. The surface cyclone tracks in Fig. 3.5 are largely a reflection of the upper-level flow configurations associated with ACEs, and will be discussed further in Section 3.3.

ACE intensity varied from a minimum sea level pressure of 955 hPa during an EJS event on 26 January 1978, to 997 hPa during a cutoff low event on 5 April 1987. EJS events were the most intense with an average minimum sea level pressure of 979 hPa, followed by cutoff low events with an average of 985 hPa, and open wave events with an average of 987 hPa (Fig. 3.6). The average maximum 24-h deepening rate of EJS events also exceeded that of cutoff low and open wave events. EJS events deepened an average of 19 hPa in 24 h while cutoff low events deepened 15 hPa and open wave events deepened 14 hPa. Of the 32 EJS events, sixteen met the criterion to be considered extratropical bombs, or cyclones whose central pressure decrease exceeded the critical rate at 45°N of 20 hPa in 24 h (Sanders and Gyakum 1980). Only six cutoff low events and six open wave events met this criterion. This suggests that EJS events may be associated with coupled jet streaks and highly amplified upper-level flow, allowing for enhanced thermal and differential vorticity advection, and subsequently rapid cyclogenesis. A lifecycle primarily over the western North Atlantic Ocean would also

contribute to the rapid intensification of EJS cyclones from a QG perspective, through decreased frictional and increased diabatic effects. The variation of intensification rates by category is likely a result of differences in mean upper-level patterns and resultant dynamical forcing. Section 3.3 will use a composite analysis to analyze the dynamical forcing mechanisms associated with each category of ACEs.

3.2.2 Teleconnection Responses

An analysis of ACE frequency reveals multiple event clusters at various times throughout the 62-y time span. This suggests that certain large-scale flow regimes may be favorable for repeated ACE development. As a result, the AO, NAO, PNA and ENSO were inspected during each ACE to determine if preferred phases exist. The mean daily AO value for all ACEs was −1.1 SD. EJS, open wave, and cutoff low events averaged −1.73 SD, −0.9 SD and −0.66 SD, respectively. A time series of daily AO values from 1950–1979 (Fig. 3.7a) and 1980–2010 (Fig. 3.7b) overlaid with ACE occurrences illustrates event clustering during significantly negative AO periods. For example, the late 1950's saw ten ACEs in a 15-month period during which the AO remained distinctly negative. The negative phase of the AO is associated with high-latitude blocking and anomalously weak mid-latitude westerlies, thus it is to be expected that ACEs will be more frequent when the index is significantly negative. The mean AO trend for all ACEs was −0.68 SD over the one week period prior to event occurrence. The mean trend of EJS, open wave and cutoff low events was −0.93 SD, −0.87 SD and −0.25 SD,

respectively. A first order conclusion suggests that a large-scale regime associated with declining AO values enhances the probability of ACE occurrence.

The mean daily NAO value for all ACEs was −0.45 SD. EJS, open wave and cutoff low events averaged −0.77 SD, −0.16 SD and −0.42 SD, respectively. These results are illustrated in Figure 3.8. The NAO trend for all ACEs averaged −0.41 SD, with EJS, open wave and cutoff low events averaging −0.47, −0.33 and −0.44 SD, respectively. Overall, the NAO index responded similarly to the AO index prior to and during ACEs; however, the magnitude of the response was slightly weaker. The negative phase of the NAO is associated with upper-level ridging over the North Atlantic Ocean and much of Greenland, with troughing over the Northeast U.S. Thus, similarly to the AO, it makes sense that the negative phase of this index is associated with ACE occurrence.

The mean daily PNA value for all ACEs was 0.49 SD, with EJS, open wave and cutoff low events averaging 0.34 SD, 0.64 SD and 0.54 SD, respectively. Figure 3.9 illustrates the distribution of PNA values for all ACEs. The PNA trend for all ACEs averaged +0.26 SD, with EJS, open wave and cutoff low events averaging +0.18 SD, +0.16 SD and +0.43 SD, respectively. A positive PNA trend implies large-scale ridge building over western North America with enhanced troughing over the eastern U.S. In this regime, cyclone development is favored downstream of a long wave trough over the eastern half of the U.S.

The mean monthly sea surface temperature anomalies (SSTAs) in the Niño 3.4 region were used to determine the phase of ENSO during each ACE. The average SSTA

for all ACEs was 0.13°C, with EJS, open wave and cutoff low events averaging 0.17°C, 0.21°C and 0.01°C, respectively. The distribution of SSTAs for all ACEs is shown in Fig. 3.10. These results indicate that EJS and open wave events are more common during weak El Niño regimes, while cutoff low events are more common in a neutral ENSO regime. A weak El Niño regime can favor a more active subtropical jet and storm track across the southeastern U.S., with an increased likelihood of cyclogenesis along the East Coast.

After analyzing the above statistics, it is clear that ACEs are preferred during certain phases of the AO, NAO, PNA, and to a lesser extent ENSO. The favored scenario is one in which the AO and NAO are negative, the PNA is positive and El Niño is weak. The AO displayed the most noteworthy signal overall, and the negative phase of the AO appears to be a necessary precondition for the development of EJS events. This indicates that the most important feature associated with ACE development is anomalous upper-level ridging at high latitudes, indicative of atmospheric blocking. When the PNA is in the positive phase, the likelihood of a cyclogenetic trough over the eastern U.S. increases significantly. The combination of a significantly negative AO/NAO and positive PNA would yield a situation where an eastward moving upper-level trough over the east-central U.S. is more likely to decrease speed and cutoff as it approaches blocking downstream. If an El Niño regime is also present, an active southern stream will increase the possibility of a trough merger and a rapidly intensifying surface cyclone. The trends of the aforementioned teleconnection indices are also rather substantial for a seven-day time period, and may be a useful forecasting tool. The following section will explore the

evolution of upper-level features associated with the aforementioned teleconnection regimes using composite analysis.

3.3 Composite Analyses

3.3.1 Earth-relative Composites

Figures 3.11–3.15 illustrate the evolution of the large-scale features associated with each category of ACE through composites of mean 500-hPa geopotential heights (and standardized anomalies) every 24-h. At t_{-96} , all three categories of ACEs display a 500-hPa Rossby wave pattern characterized by a trough over the eastern Pacific Ocean, a ridge over the western U.S. and a second trough over the central U.S. (Figs. 3.11a–c). The central U.S. trough is later responsible for forcing the composite cyclone as it progresses toward the East Coast. The most significant feature in all ACE composites is a region of anomalously high 500-hPa heights extending from central Canada to southern Greenland (Figs. 3.11a–c). The magnitude of this positive height anomaly is the greatest in the EJS composite with a small region of +.75–1σ values. This preexisting feature indicates the presence of a large-scale blocking regime. The height anomaly pattern present in all ACE composites (Figs. 3.11a–c) is consistent with the negative phase of the AO/NAO, and the positive phase of the PNA.

At $t_{-72,}$ the western U.S. ridge and central U.S. trough become more amplified in all ACE composites (Figs. 3.12a–c). The amplitude of ridging is strongest in the cutoff low and open wave composites, and weakest in the EJS composite. Conversely, the magnitude of ridging in northeast Canada and southern Greenland is the strongest in the EJS composite with a large region of +1–1.25σ values (Fig. 3.12a). In all three composites, a region of negative standardized anomalies is visible across the south-central U.S. in association with a southern stream shortwave trough (Figs. 3.12a–c). The presence of a southern stream trough in phase with a northern stream trough increases the overall amplitude of the longwave trough over central U.S.

At t_{-48}, the eastern U.S. trough begins to take on a negative tilt in all ACE composites, as surface cyclogenesis initiates off the East Coast (Figs. 3.13a–c). Figures 3.13a–c display a surface low pressure (denoted by the red circle) downstream of the cyclogenetic trough in a region characterized by upper-level ageostrophic wind divergence (not shown). Negative standardized anomalies of 1–1.5σ exist in the base of the cyclogenetic trough, indicative of amplification as northern and southern stream shortwaves interact in a trough merger. In the EJS composite, a large region of anomalous (+1.5σ) ridging continues to develop over the Davis Strait (Fig. 3.13a), while less widespread ridging (+1–1.5σ) exists over northeast Canada in the cutoff low and open wave composites (Figs. 3.13b–c). The continued development of downstream ridging in all ACE composites acts to impede the eastward progression of the cyclogenetic trough.

At t_{-24}, a highly amplified, negatively tilted upper-level trough is located over the Northeast U.S. in the EJS and cutoff low composites (Figs. 3.14a–b). The open wave

composite displays a slightly broader, less amplified upper-level trough over the same location (Fig. 3.14c). The surface low has moved poleward, located just off the New Jersey coast in each ACE composite. Forcing for surface cyclogenesis is strongest in the EJS and cutoff low composites (Figs. 3.14a–b), as decreases in the half wavelength indicate strong cyclonic vorticity advection and upper-level divergence (not shown). In the cutoff low and open wave composites (Figs. 3.14b–c), a broad ridge (+1σ) is in place across the western U.S., while a slightly weaker ridge exists in the EJS composite (Fig 3.14a). However, the EJS composite displays a highly anomalous upper-level ridge (+2σ) over northeast Canada (Fig. 3.14a), positioned further west than in the cutoff low and open wave composites (Figs. 3.14b–c). The strengthening of positive height anomalies over northeast Canada indicates the continued development of upper-level blocking, and a declining AO/NAO. In the EJS composite, a well-defined geopotential height anomaly dipole is also in place over eastern North America, indicating enhanced geostrophic easterly flow on the northern flank of the negative anomaly over northern New England (Fig. 3.14a). This dipole is not as pronounced in the cutoff low and open wave composites where the ridge axis is further east over the Canadian Maritime Provinces (Figs. 3.14b–c).

At t_0, the EJS and cutoff low composites exhibit a closed upper-level circulation over the Northeast U.S. (Figs. 3.15a–b), while the open wave composite remains an open wave in the 500-hPa geopotential height field (Fig. 3.15c). In all ACE composites, a region of anomalously low heights (−2.5–3σ) is centered at the base of the longwave trough, just off the U.S. East Coast. The development of closed lows in the EJS and cutoff low composites is reminiscent of the LC2 scenario (Thorncroft et al. 1993), in

which a negatively tilted trough wraps up cyclonically, remaining poleward of the main belt of westerlies. The surface low is nearly vertically stacked in the EJS and cutoff low composites (Figs. 3.15a–b), indicating a cyclone in the later stages of its lifecycle. The westward movement of the EJS and cutoff low surface cyclones (previously discussed in Section 3.2) coincides with cutoff low development in Figs. 3.15a–b, indicating that the surface low is pulled westward as the strongest forcing becomes concentrated near the center of the upper-level circulation. In the EJS and cutoff low composites (Figs. 3.15a–b), the presence of a high amplitude ridge (+2.5σ) downstream of the Northeast U.S. is likely the primary forcing mechanism for cutoff low development. In the open wave composite (Fig. 3.15c), ridging is weaker and further east allowing the trough to progress eastward and remain open. The EJS composite displays a height anomaly pattern indicative of a strongly negative AO/NAO regime, while the cutoff low and open wave composites display a height anomaly pattern indicative of a strong positive PNA regime, confirming the results of Section 3.2.

3.3.2 Cyclone-relative Composites

At t_0, the EJS composite 500-hPa geopotential height field displays a deep closed low centered over southern New England, embedded in a negatively tilted upper-level trough (Fig. 3.16a). The surface cyclone is located under the northeast side of the closed 500-hPa low, just poleward of a 500-hPa vorticity maximum. This indicates that the cyclone is in the later stages of development and is likely occluded in nature. A 100 kt

upper-level westerly jet streak is located on the southern flank of the closed upper-level low, while a 60 kt upper-level easterly jet streak is located over northern New England on the northern flank of the closed low (Fig. 3.16a). The surface low is located in the poleward exit region of the westerly jet streak where upper-level divergence is favored. Northern New York and northwest New England are situated under the equatorward exit region of the easterly jet streak in a region favorable for QG forcing for ascent. A high precipitable water (PWAT) axis is oriented from southeast to northwest, wrapping cyclonically around the surface low, indicating moisture transport inland from the Atlantic Ocean (Fig. 3.16a). The intersection of a high PWAT axis with a region of deep-layer warm air advection-driven ascent indicates the potential for heavy precipitation to the northwest of the cyclone center over northern New York and New England.

An EJS composite of 700-hPa equivalent potential temperature (θ_e) at t_0 reveals a ridge axis oriented from east to west across southern Quebec (Fig. 3.16b). This indicates an area referred to as the trowal (**tro**ugh of **w**arm air **al**oft; Penner 1955) where the crest of warm air aloft is located, and where QG forcing for ascent is favored (e.g., Martin 1999). The trowal is typically found in the northern and northwestern quadrants of developed cyclones, as seen in Fig. 3.16b. The presence of this feature suggests that wrap-around clouds and precipitation will be prominent to the northwest of the cyclone center. Within the θ_e ridge, a region of northeasterly 850-hPa warm air advection is found over northern New England and southern Quebec (Fig. 3.16b). Northeasterly warm air advection acts to cyclonically rotate the thermal ridge, reverse the low-level baroclinity (allowing for upper-level easterly jet streak development previously discussed in Fig. 3.16a), and enhance QG forcing for ascent by the Laplacian of temperature advection.

Low-level northwesterly winds in the northwest quadrant of the cyclone (Fig. 3.16b), coupled with near-saturation in the 925-850 hPa layer (not shown), suggests the possibility of significant orographic precipitation enhancement in mountains of New York and Vermont (e.g., St. Jean and Sisson 2004).

Figure 3.16c illustrates the 700-hPa QG forcing associated with EJS events at t_0. Warm colors are indicative of Q-vector convergence and QG forcing for ascent, while cold colors indicate Q-vector divergence and forcing for subsidence. The strongest QG forcing for ascent is located to the northwest of the surface cyclone over northern New York and Southern Quebec, as previously inferred. This is a region associated with strong 850-hPa warm air advection, beneath the equatorward exit region of a 300-hPa easterly jet streak. Fig. 3.16c also displays Q-vectors, which represent the rate of change of the vector potential temperature gradient along a geostrophic trajectory. Keyser et al. (1992) performed a natural-coordinate partitioning of Q-vectors into along (Q_s) and across (Q_n) isentrope components, which physically represent the magnitude and rotational components of QG frontogenesis (e.g., Martin 1999). Thus, a large amount of information can be gathered by analyzing the orientation of Q-vectors with respect to the horizontal potential temperature gradient. In the region of maximum Q-vector convergence, Q-vectors are primarily aligned parallel to the isentropes (Fig. 3.16c) indicating the weak magnitude of frontogenesis (Q_n) in this region. However, this implies that the rotational component of QG frontogenesis plays a large role and must be the main contributor to QG forcing for ascent. Since Q-vectors are directed along isentropes in the downstream direction over northern New York and New England, it is inferred that the Q_s contribution is rotating isotherms cyclonically and creating a thermal ridge in the

horizontal. The trowal axis, as previously identified in Fig. 3.16b, is located just to the north of the maximum in Q-vector convergence. This indicates that the majority of QG forcing for ascent associated with EJS events occurs in close proximity to the trowal, in the northwest quadrant of the cyclone.

At t_0, the 500-hPa geopotential height field associated with cutoff low events is similar to that of EJS events; however, the cutoff circulation is located further southwest and is slightly weaker (Fig. 3.17a). The composite surface cyclone is located favorably for continued intensification, just downstream of a 500-hPa vorticity maximum in a region of inferred differential cyclonic absolute vorticity advection (not shown). A cyclonically curved 300-hPa jet streak is positioned at the base of the upper-level trough, with the surface cyclone situated beneath the poleward exit region (Fig. 3.17a). The location of the poleward jet exit region favors deep-layer ascent across much of eastern New York and New England through a thermally indirect vertical circulation. A second, weaker jet streak is located near the downstream ridge axis, with the ascending branch of a thermally direct circulation located over northeast Maine and Atlantic Canada. A high PWAT corridor is located over northern New England, directed from southeast to northwest in the warm sector of the cyclone (Fig. 3.17a). This bears great similarity to the EJS composite (Fig. 3.16a); however, the PWAT corridor is now further west and more robust. Widespread precipitation is favored in northern New York and New England where a large region of inferred QG forcing for ascent intersects the axis of high PWAT.

At t_0, the cutoff low composite reveals a thermal ridge in the 700-hPa θ_e field extending from Nova Scotia northwestward into southern Quebec (Fig. 3.17b). Like in the EJS composite, this feature indicates the trowal region at the nose of the warm sector

where parcels undergo moist, cyclonic ascent. The orientation of the thermal ridge suggests that the cutoff low surface cyclone is not as "wrapped up" or occluded as in the EJS composite, but still maintains a bent-back warm frontal zone. A region of maximum 850-hPa warm air advection is centered over northern Maine, with widespread northeasterly warm air advection further west over northern New York and southern Quebec (Fig. 3.17b). These areas are collocated with a high PWAT corridor in the poleward exit region of an upper-level jet streak, and are prone to strong QG forcing for ascent. To the northwest of the composite cyclone, the 850-hPa winds are from the northwest in a region of weak low-level warm air advection (Fig. 3.17b). The 925-850 hPa layer is also near saturation across much of this region (not shown), introducing the potential for lake and orographic enhanced precipitation.

A plot of 700-hPa QG forcing associated with the cutoff low composite at t_0 is displayed in Fig. 3.17c. The greatest QG forcing for ascent occurs in a zone just west of the strongest low-level warm air advection, in the poleward jet-exit region. In comparison to the EJS composite, the cutoff low composite displays a larger area of stronger forcing to the north of the cyclone center. This area is collocated with the trowal as previously identified in Fig. 3.17b, implying significant lift is occurring at the nose of the warm sector. Q-vectors are of the greatest magnitude across northern New York and New England, and are oriented downstream along isentropes, converging at the trowal axis (Fig. 3.17c). This suggests that rotational frontogenesis (Q_s) is the primary component responsible for the QG forcing for ascent in this region. It also suggests that development of the trowal is being aided by Q_s convergence as isentropes rotate, creating a thermal ridge near the axis of maximum convergence. Precipitation in the western portion of the

trowal is not likely to be of a banded nature due to a lack of traditional frontogenesis. However, further north and east across southern Quebec, Q-vectors of a lesser magnitude are oriented across isentropes toward warmer air implying weak low- to mid-level frontogenesis along a bent-back warm front.

Fig. 3.18a displays the 500-hPa geopotential height field associated with the open wave composite at t_0. In contrast to the EJS and cutoff low composites, the negatively tilted upper-level trough over the Northeast U.S. is primarily open in this composite, with only one closed 534 dam contour across southern New York. Downstream of the 500-hPa trough axis, forcing for ascent is favored in a region of inferred differential cyclonic absolute vorticity advection over northeastern New England (Fig. 3.18a). The poleward exit region of a cyclonically curved 300-hPa jet streak coincides with the equatorward entrance region of an anticyclonically curved 300-hPa jet streak over this same geographic area. As a result, the surface low is likely to intensify over northeastern New England as it tracks into this region of enhanced ascent. A high PWAT corridor is also located to the east of the surface cyclone, oriented from southeast to northwest across eastern New England (Fig. 3.18a). The combination of strong forcing for upward vertical motion and abundant moisture northeast of the cyclone center indicates the potential for a heavy precipitation event.

An open wave composite plot of 700-hPa θ_e at t_0 is shown in Fig. 3.18b. A distinct thermal ridge is oriented identically to the PWAT corridor previously identified in Fig. 3.18a. This signifies the warm sector of the cyclone where large-scale ascent is favored. Similar to the PWAT corridor, the θ_e ridge does not extend significantly around the poleward and western side of the surface low, indicating that the trowal is not fully

developed. This differs from the EJS and cutoff low composites (Figs. 3.16b and 3.17b) where the θ_e axis extends northwest of the cyclone center. The foregoing observations suggest that the open wave composite surface cyclone is still in the developing stages and has not begun the occlusion process. The location of the strongest warm air advection associated with open wave events is concentrated to the northeast of cyclone center, just east of the developing trowal axis (Fig. 3.18b). The magnitude of the warm air advection indicates strong isentropic lift and QG forcing for ascent by the Laplacian of temperature advection. To the west of the surface cyclone, a region of northerly 850-hPa winds creates a scenario favorable for lake-enhanced precipitation.

Figure 3.18c displays 700-hPa Q-vectors and QG forcing associated with open wave events at t_0. QG forcing for ascent is present over a large region north and east of the surface cyclone, and the magnitude of the forcing is markedly stronger than in the EJS and cutoff low composites (Figs. 3.16c and 3.17c). This is likely the result of several previously mentioned forcing features including: 1) dual jet streaks providing enhanced ascent in the poleward exit region of the southern jet streak and the equatorward entrance region of the northern jet streak, 2) cyclonic differential absolute vorticity advection downstream of the upper-level trough axis, and 3) strong low-level warm air advection in the warm sector of the developing cyclone. Across southeastern Quebec, Q-vectors are directed across isentropes toward warmer air (Fig. 3.18c) and thus imply low- to mid-level frontogenesis beneath the equatorward entrance region of the northern jet streak in the warm frontal zone. Across eastern New England, Q-vectors are directed along isentropes (Fig. 3.18c) indicating the presence of rotational frontogenesis (Q_s), albeit weaker than in EJS and cutoff low composites (Figs 3.16c and 3.17c). This accounts for

the lack of a wrap-around 700-hPa θ_e ridge and well-defined trowal in the northwest quadrant of the cyclone.

The composite precipitation distribution in the 24-h period following t_0 is shown for all three categories of ACEs in Figs. 3.19a–c. The heaviest precipitation associated with EJS events occurs northwest of the surface cyclone from northeast New York to southwest Maine (Fig. 3.19a). This area is located in the trowal region where QG forcing for ascent was previously identified. Maxima in precipitation are collocated with the high terrain of the Green and White Mountains of Vermont and New Hampshire, suggesting orographic forcing plays a significant role in the total precipitation distribution. The heaviest precipitation associated with cutoff low events is also found to the northwest of the cyclone over northern New York and Vermont, extending into southern Quebec (Fig. 3.19b). This area is located in a region of strong warm air advection at the nose of the PWAT corridor previously identified. Heavy precipitation also extends across much of east-central New York indicating significant wrap-around precipitation in association with the trowal. Open wave events have a precipitation maximum further northeast across southwestern Maine and northeast New Hampshire (Fig. 3.19c). This region is characterized by strong QG forcing for ascent and is in the center of a high PWAT corridor. The majority of precipitation is located to the north and northeast of the cyclone center, which is consistent with a less developed trowal. The composite precipitation distributions for all three categories of ACEs correspond well with the diagnosed areas of enhanced forcing for ascent.

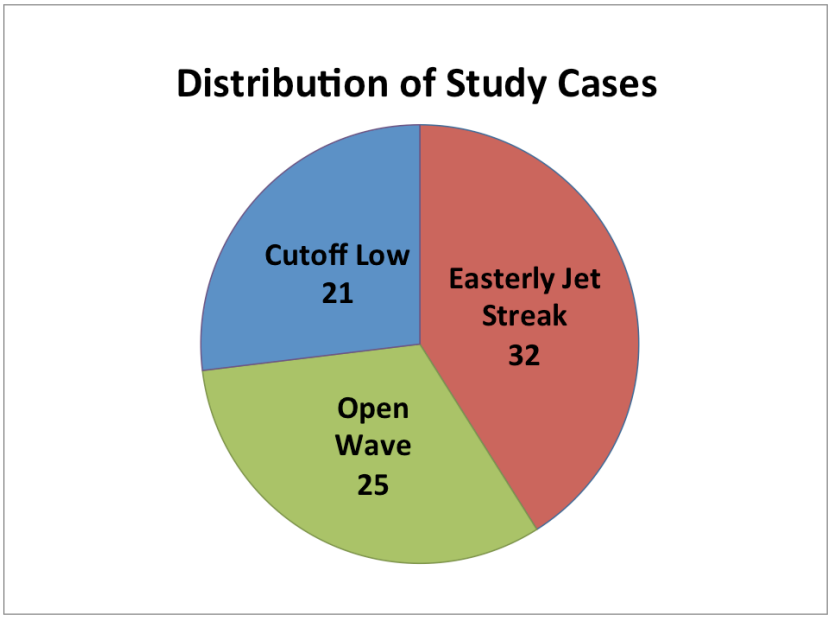

Fig. 3.1. Distribution of ACEs by category.

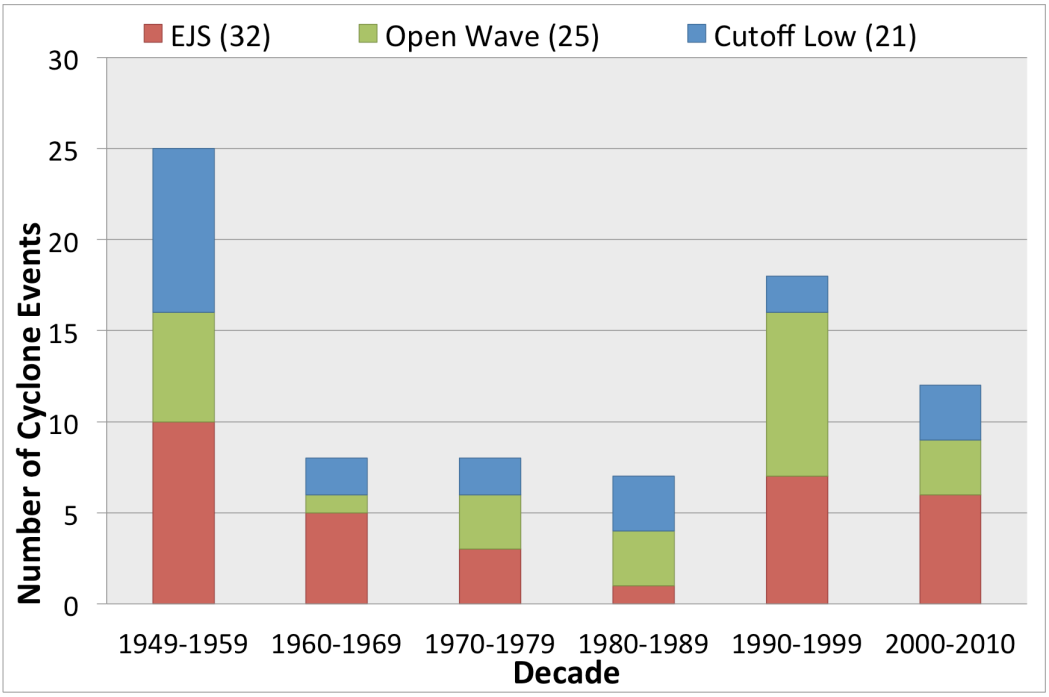

Fig. 3.2. Frequency of ACEs by decade. The red bars denote EJS events, the green bars denote open wave events, and the blue bars denote cutoff low events.

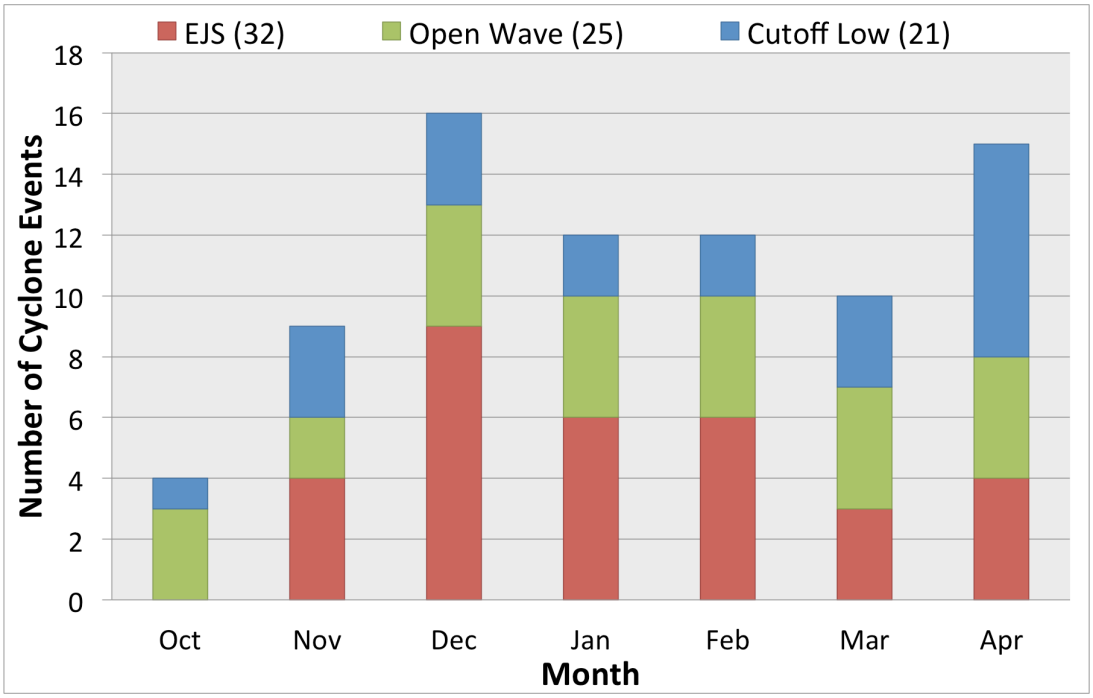

Fig. 3.3. Frequency of ACEs by month. The red bars denote EJS events, the green bars denote open wave events, and the blue bars denote cutoff low events.

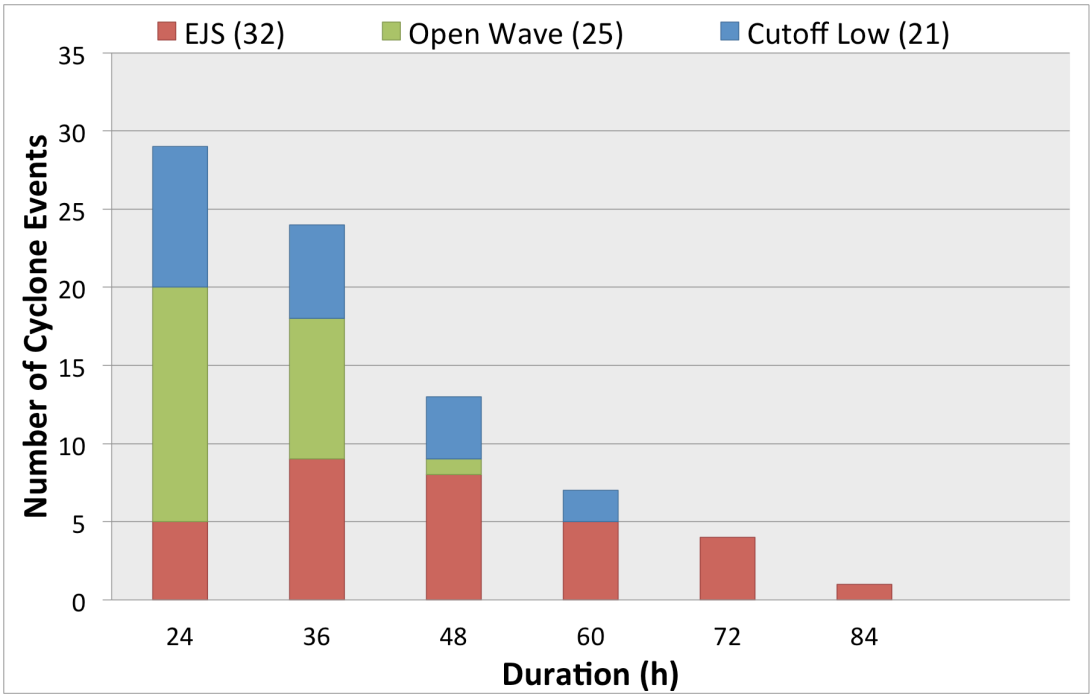

Fig. 3.4. Histogram of the duration of all ACEs from 1948–2010. The red bars denote EJS events, the green bars denote open wave events, and the blue bars denote cutoff low events.

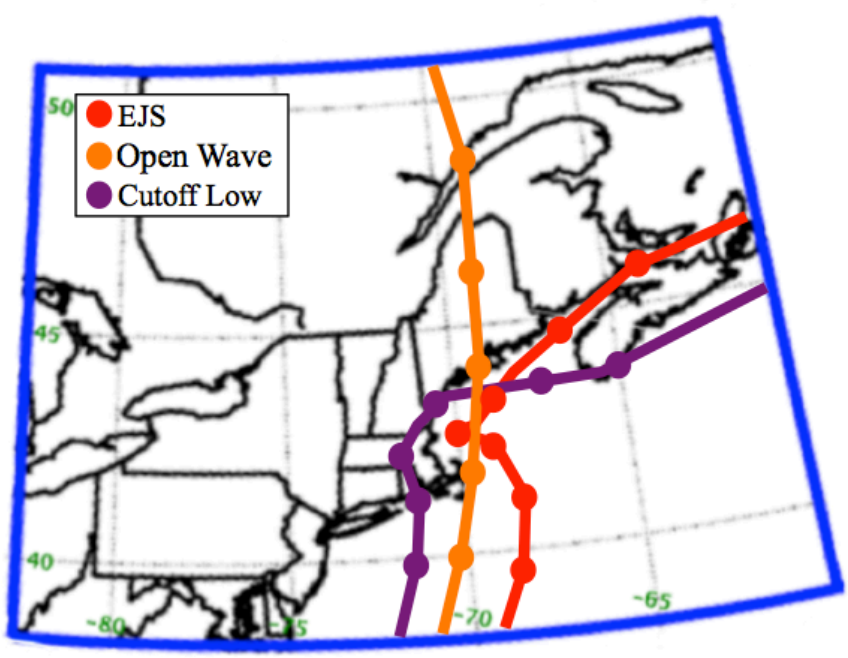

Fig. 3.5. Composite surface cyclone tracks for each category of ACE based upon the location of the composite cyclone center at six-hour intervals.

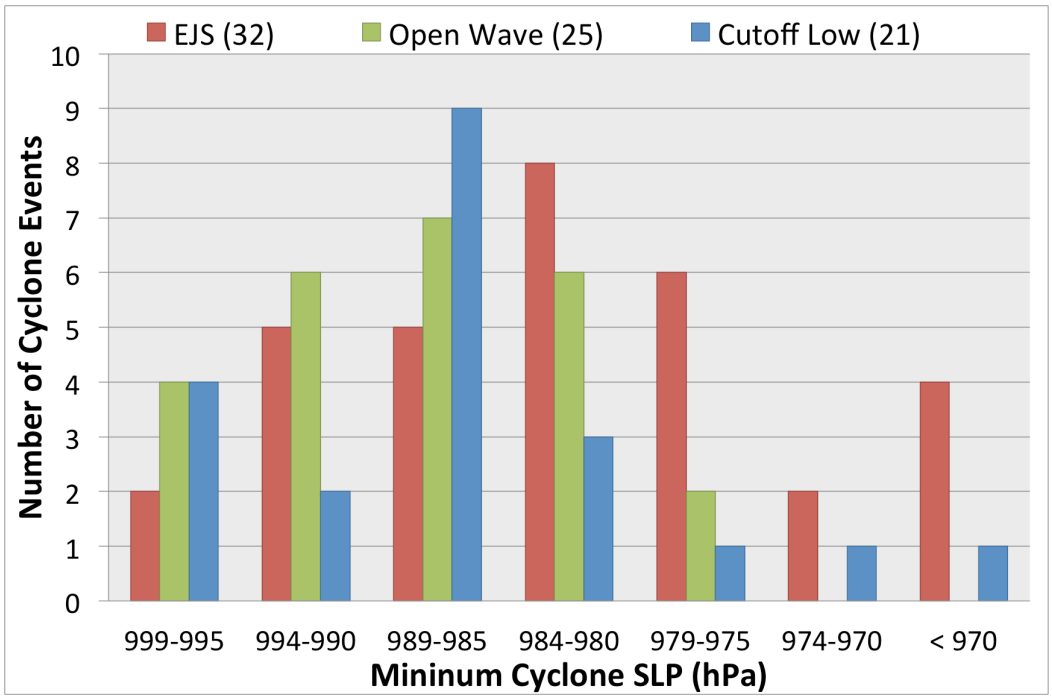

Fig. 3.6. Histogram of the minimum cyclone SLP for all ACEs. The red bars denote EJS events, the green bars denote open wave events, and the blue bars denote cutoff low events.

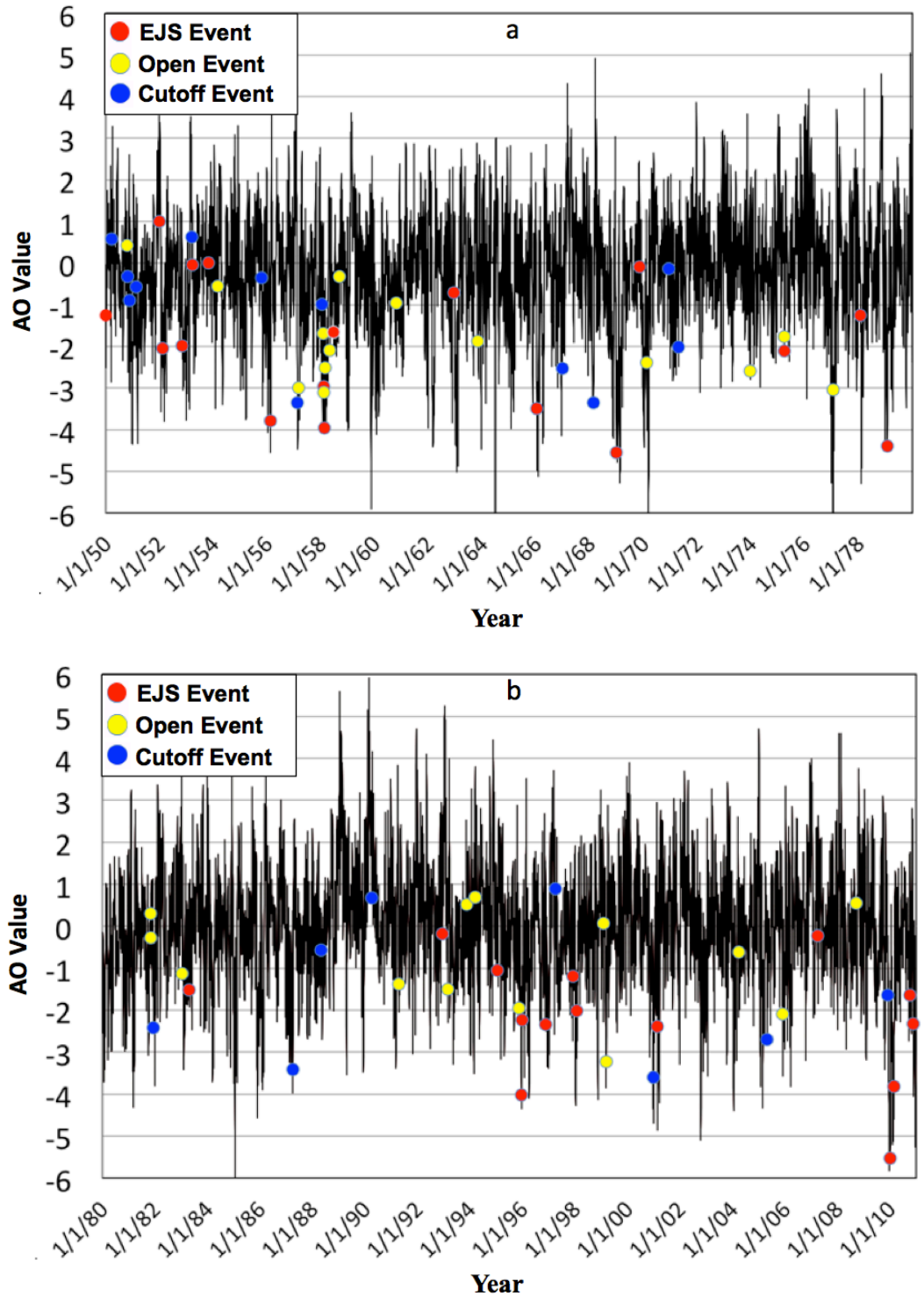

Fig. 3.7. Time series of AO values from 1950–1979 (a) and 1980–2010 (b). The red, yellow and blue circles indicate the occurrence of EJS, open wave and cutoff low events, respectively.

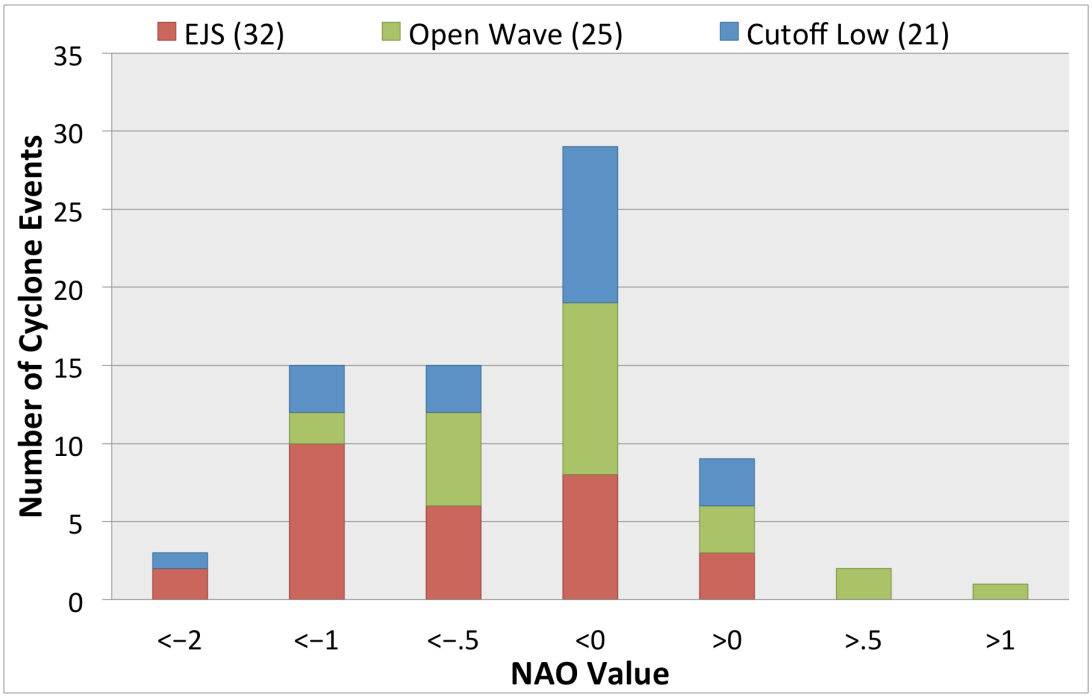

Fig. 3.8. Distribution of NAO values for all ACEs. The red bars denote EJS events, the green bars denote open wave events, and the blue bars denote cutoff low events.

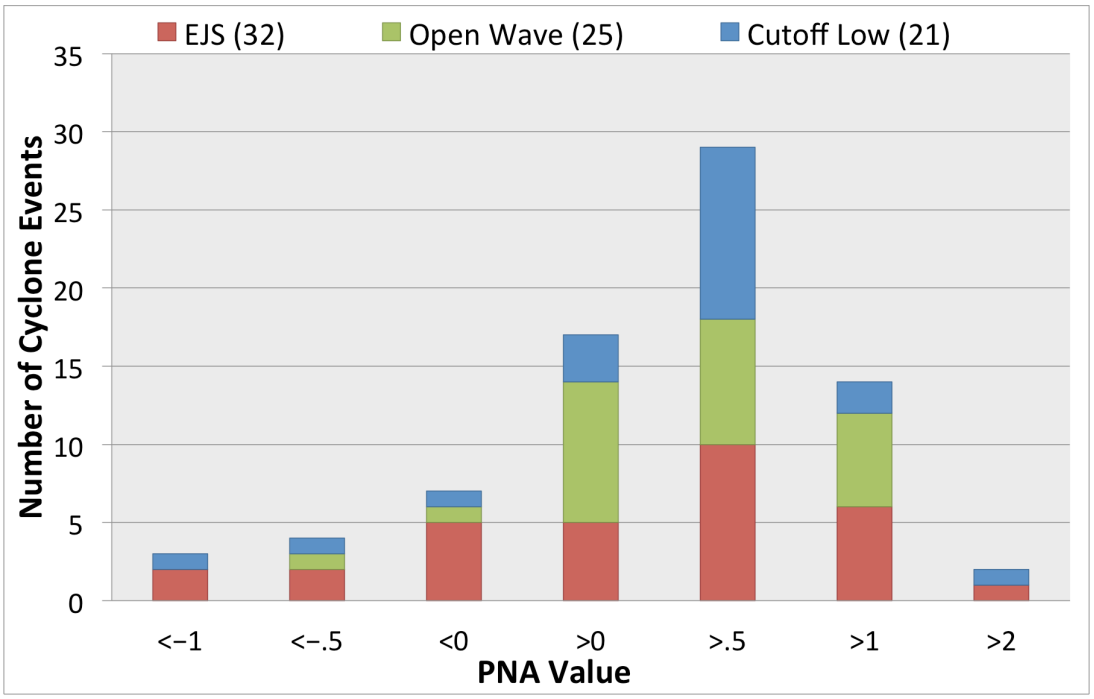

Fig. 3.9. As in Fig. 3.8, except for PNA values.

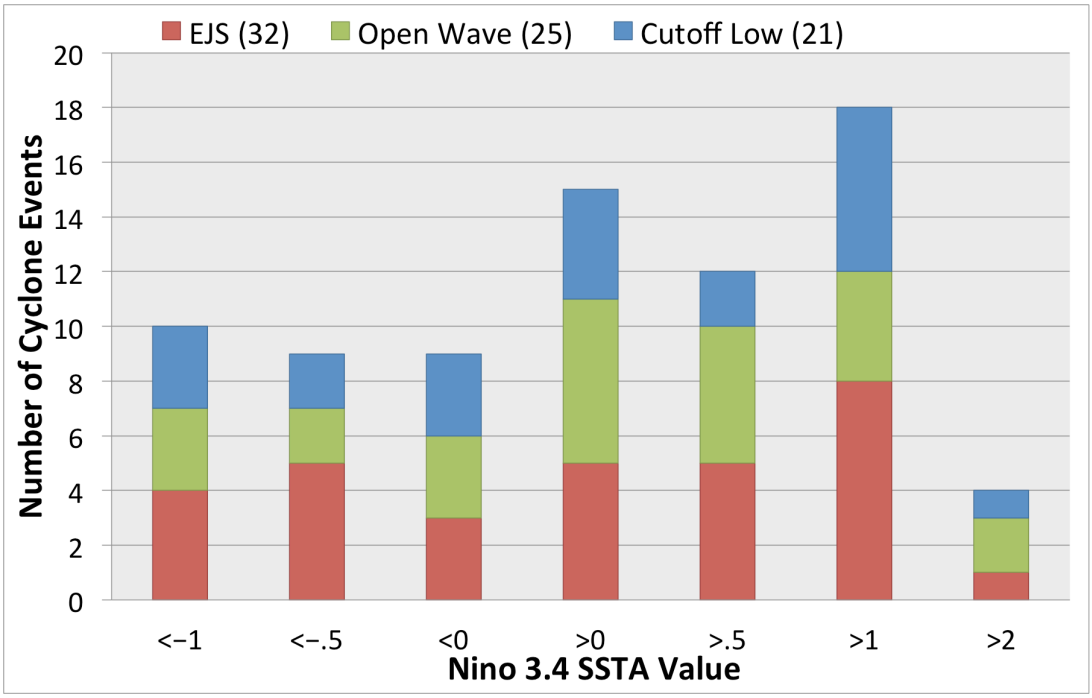

Fig. 3.10. As in Fig. 3.8, except for Niño 3.4 SSTA values.

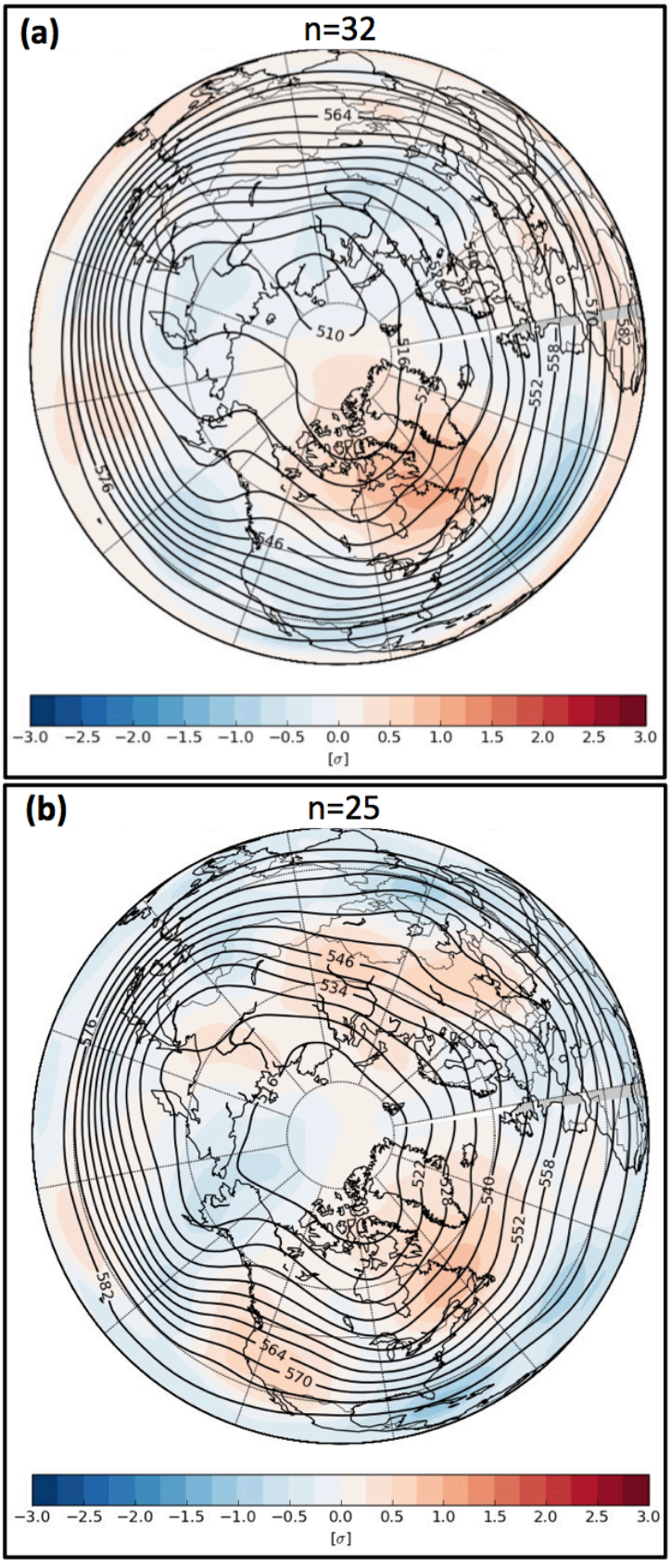
(a)
n=32
564
510
516
552
558
576
546
−3.0 −2.5 −2.0 −1.5 −1.0 −0.5 0.0 0.5 1.0 1.5 2.0 2.5 3.0
[σ]
(b)
n=25
546
534
516
528
540
552
558
582
564
570
−3.0 −2.5 −2.0 −1.5 −1.0 −0.5 0.0 0.5 1.0 1.5 2.0 2.5 3.0
[σ]

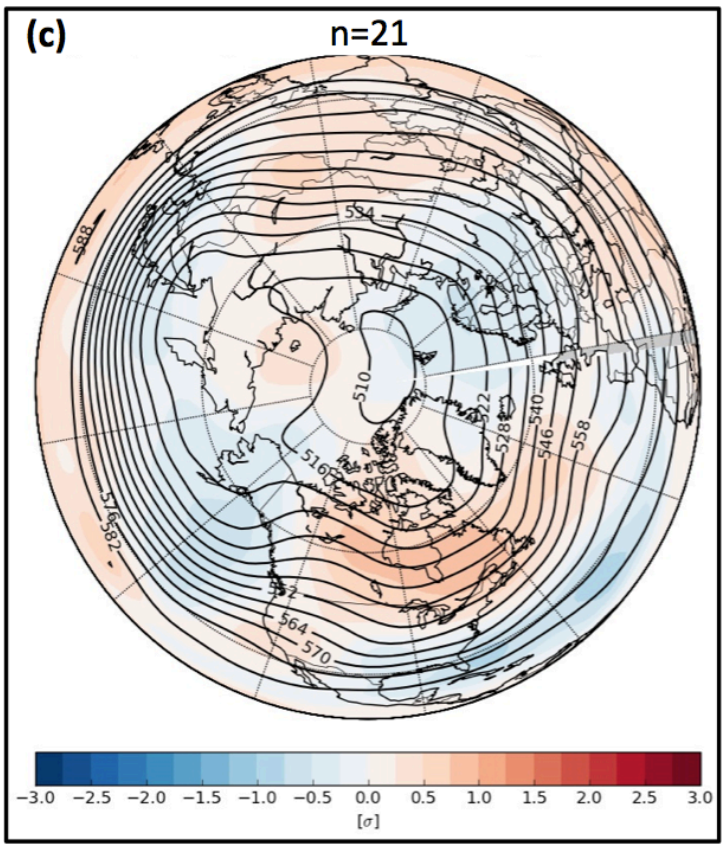

Fig. 3.11. Composite 500-hPa geopotential height (contoured every 6 dam) and standardized anomalies (shaded every .25σ) at t_{-96} for EJS events (a), cutoff low events (b), and open wave events (c).

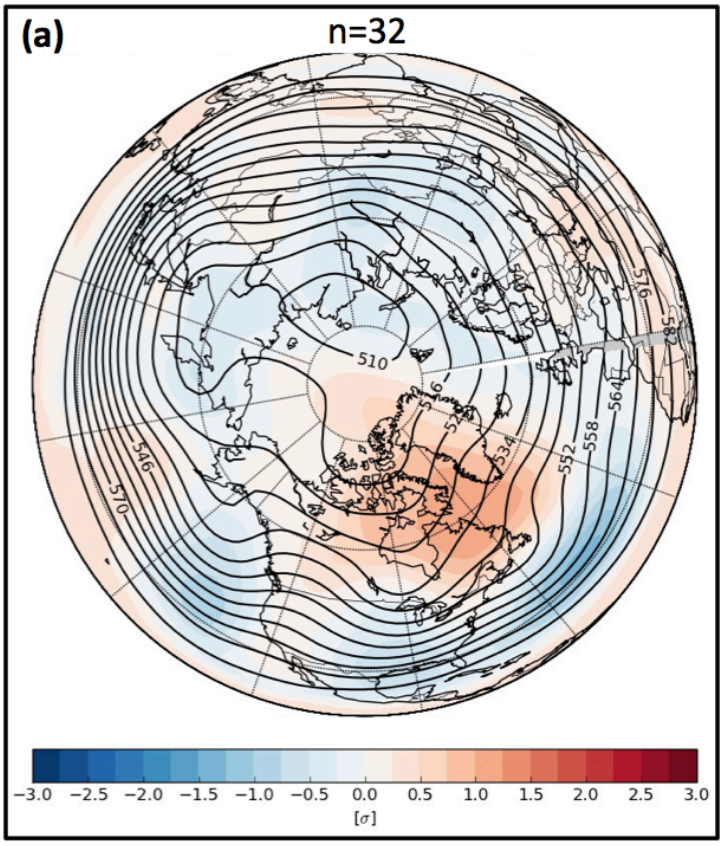
(a)
n=32
510
516
534
552
558
564
546
570
−3.0 −2.5 −2.0 −1.5 −1.0 −0.5 0.0 0.5 1.0 1.5 2.0 2.5 3.0
[σ]

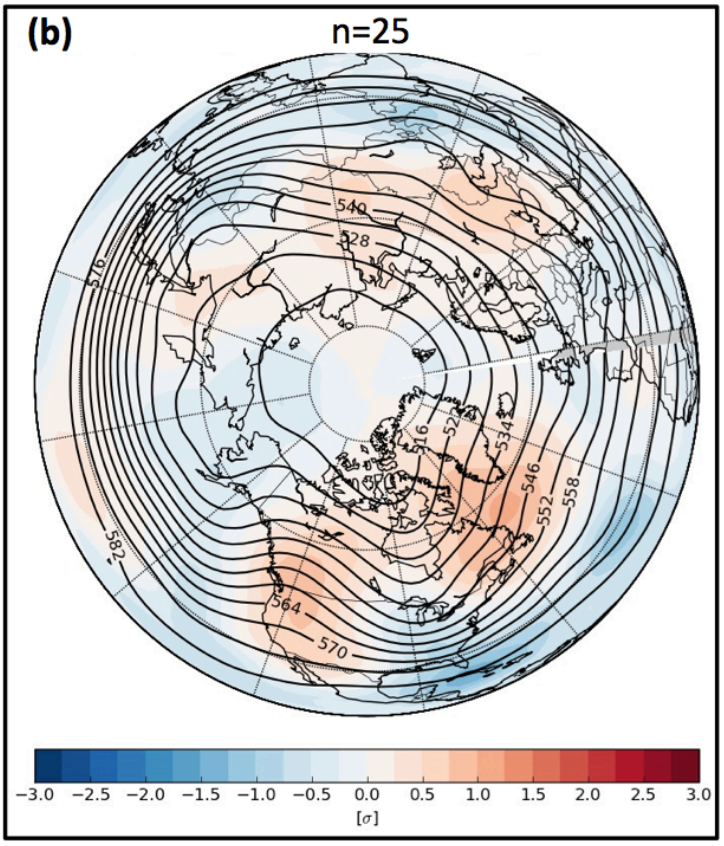
(b)
n=25
540
528
516
534
546
552
558
564
570
−3.0 −2.5 −2.0 −1.5 −1.0 −0.5 0.0 0.5 1.0 1.5 2.0 2.5 3.0
[σ]

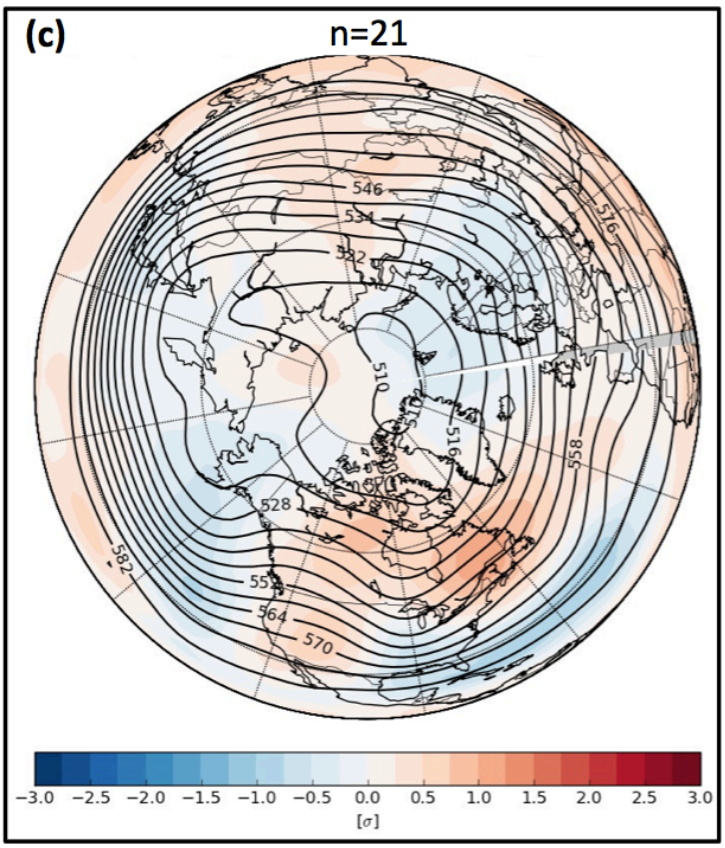

Fig. 3.12. As in Fig. 3.11, except at t_{-72}.

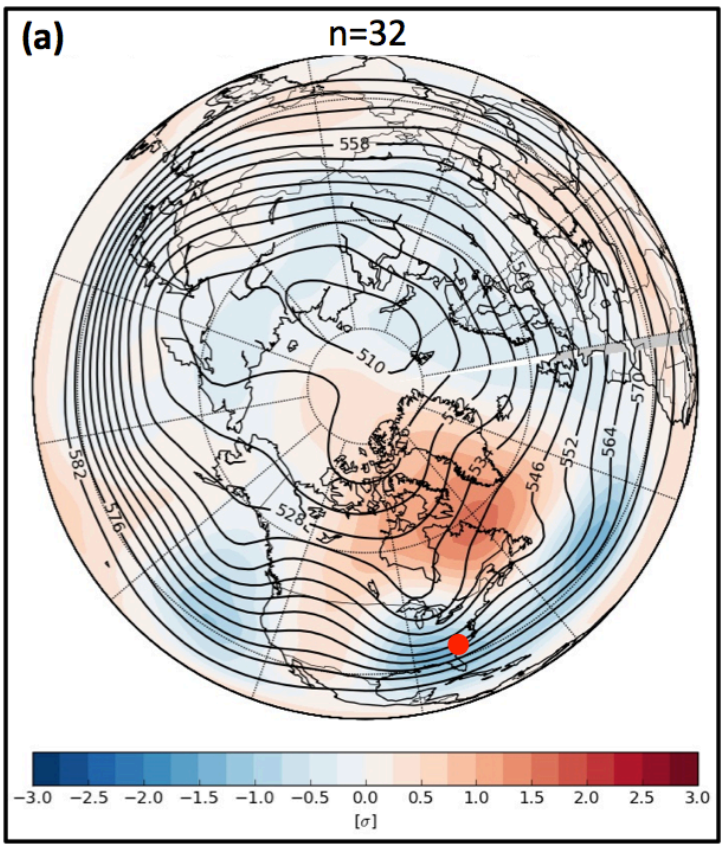
(a)
n=32
558
510
570
582
516
528
534
546
552
564
−3.0 −2.5 −2.0 −1.5 −1.0 −0.5 0.0 0.5 1.0 1.5 2.0 2.5 3.0
[σ]

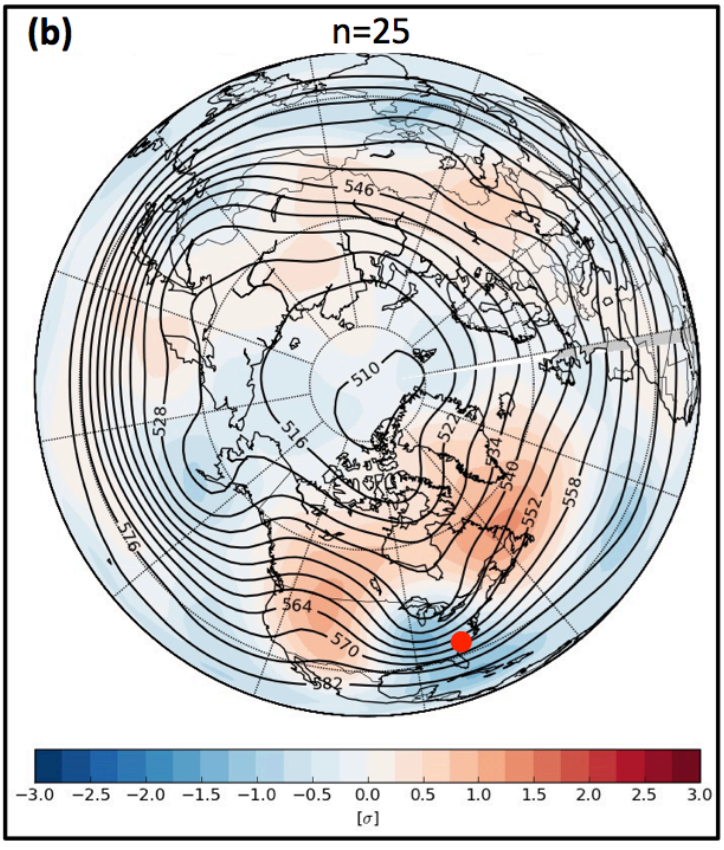
(b)
n=25
546
510
528
516
522
534
540
552
558
576
564
570
582
−3.0 −2.5 −2.0 −1.5 −1.0 −0.5 0.0 0.5 1.0 1.5 2.0 2.5 3.0
[σ]

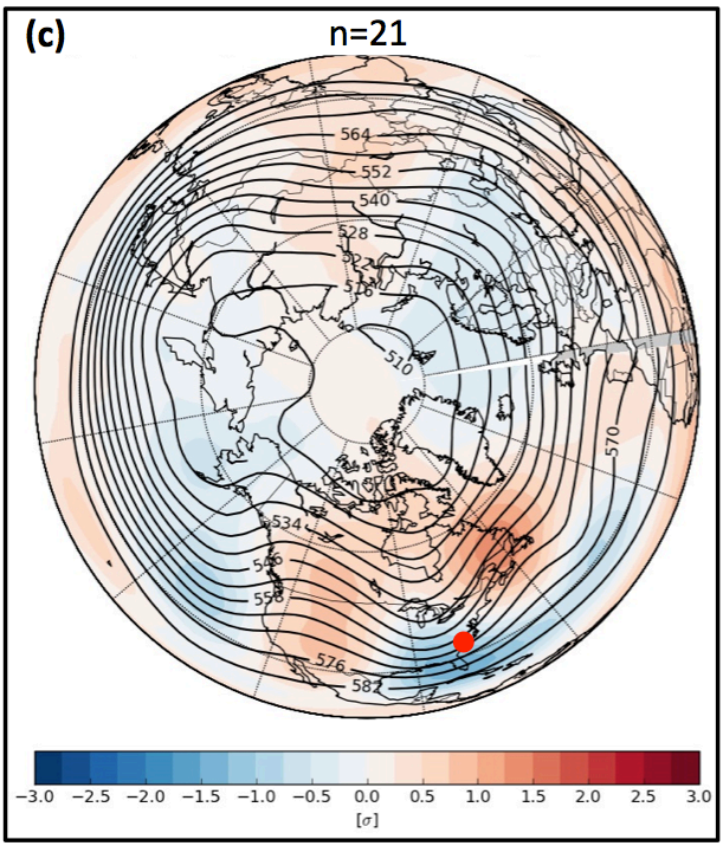

Fig. 3.13. Composite 500-hPa geopotential height (contoured every 6 dam) and standardized anomalies (shaded every .25σ) at t_{-48} for EJS events (a), cutoff low events (b), and open wave events (c). Red circle denotes the location of the surface cyclone (<1000 hPa).

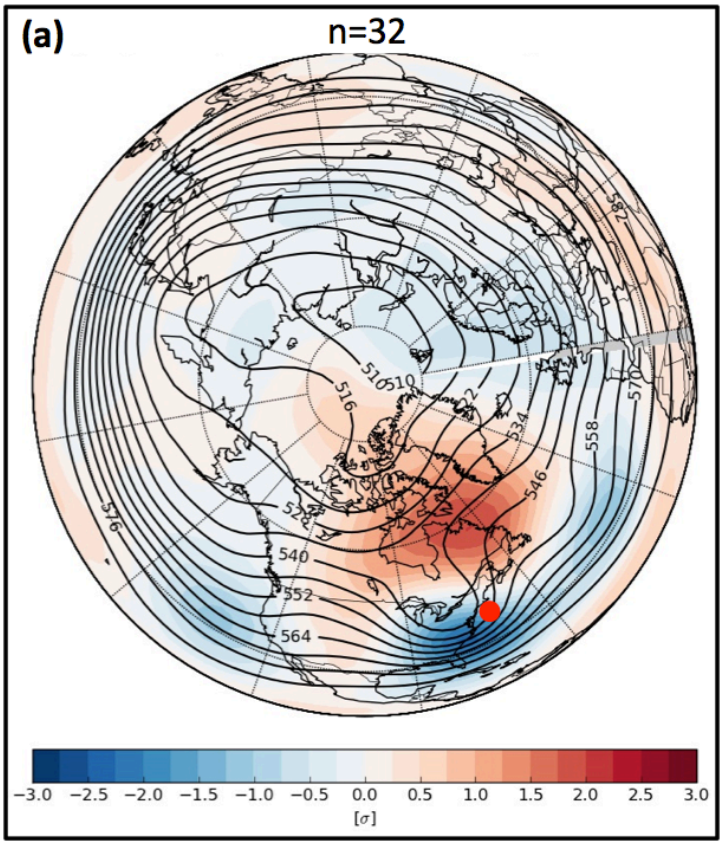
(a)
n=32
510
516
522
528
534
540
546
552
558
564
570
576
582
−3.0 −2.5 −2.0 −1.5 −1.0 −0.5 0.0 0.5 1.0 1.5 2.0 2.5 3.0
[σ]

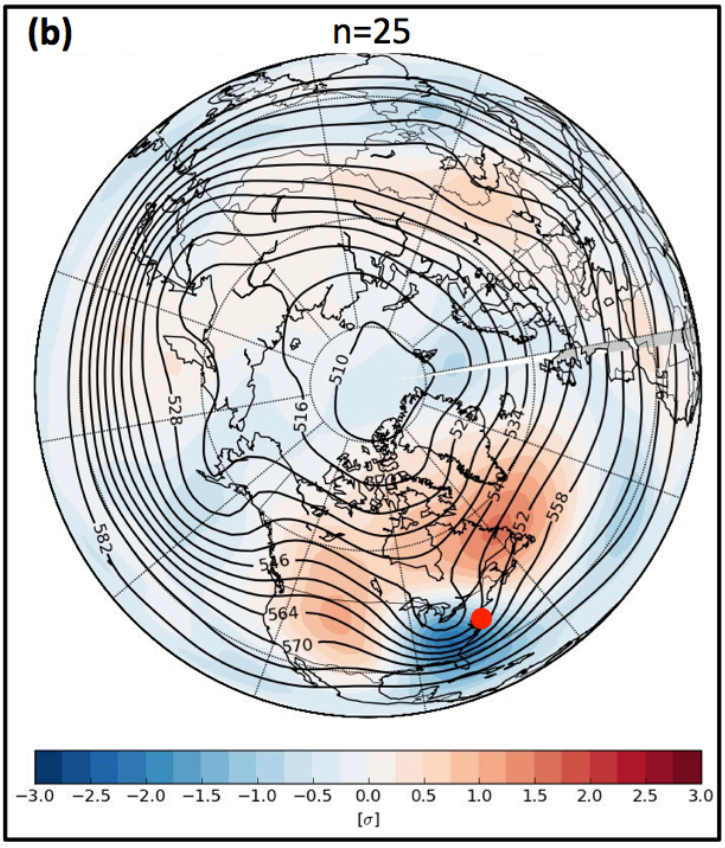
(b)
n=25
510
516
522
528
534
540
546
552
558
564
570
576
582
−3.0 −2.5 −2.0 −1.5 −1.0 −0.5 0.0 0.5 1.0 1.5 2.0 2.5 3.0
[σ]

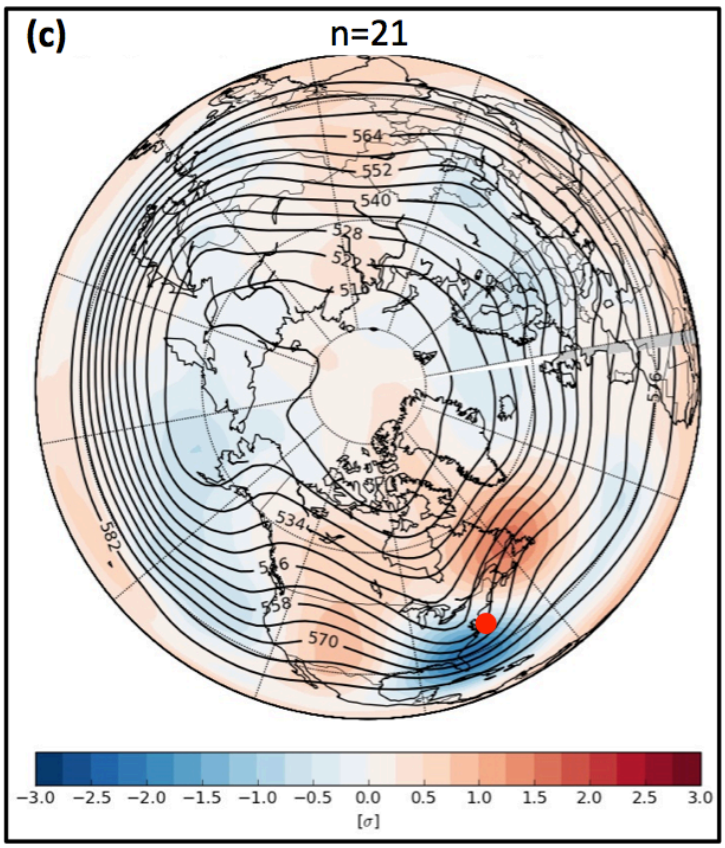

Fig. 3.14. As in Fig. 3.13, except at t_{-24}.

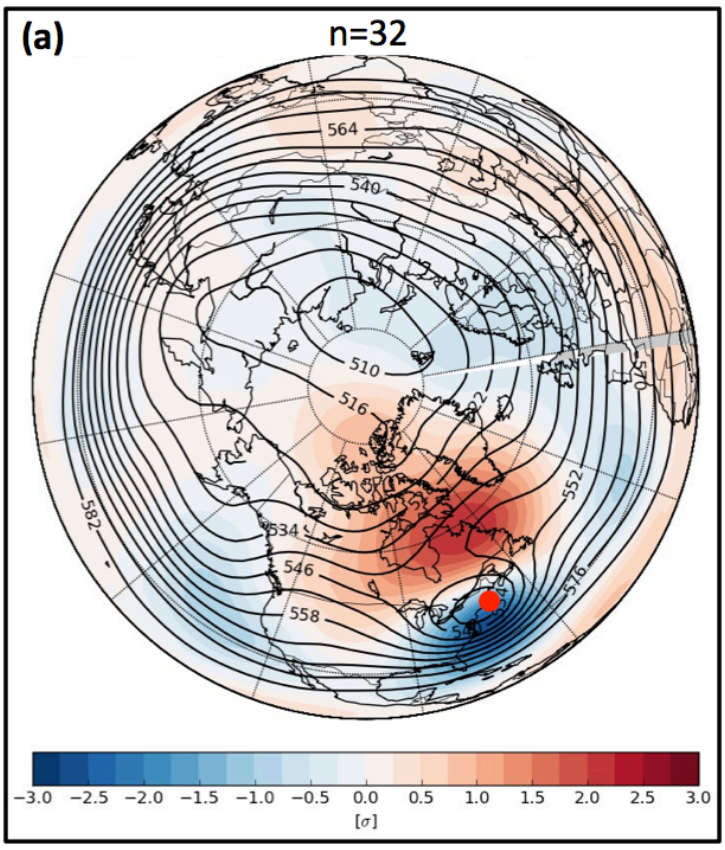
(a)
n=32
564
540
510
516
582
534
546
558
552
576
−3.0 −2.5 −2.0 −1.5 −1.0 −0.5 0.0 0.5 1.0 1.5 2.0 2.5 3.0
[σ]

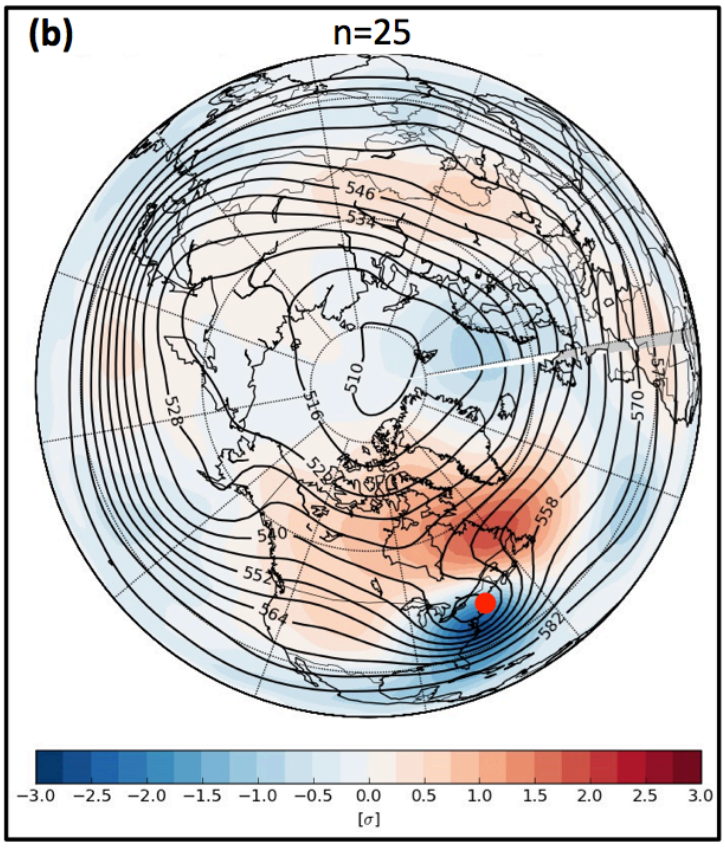
(b)
n=25
546
534
510
516
528
540
552
564
558
570
582
−3.0 −2.5 −2.0 −1.5 −1.0 −0.5 0.0 0.5 1.0 1.5 2.0 2.5 3.0
[σ]

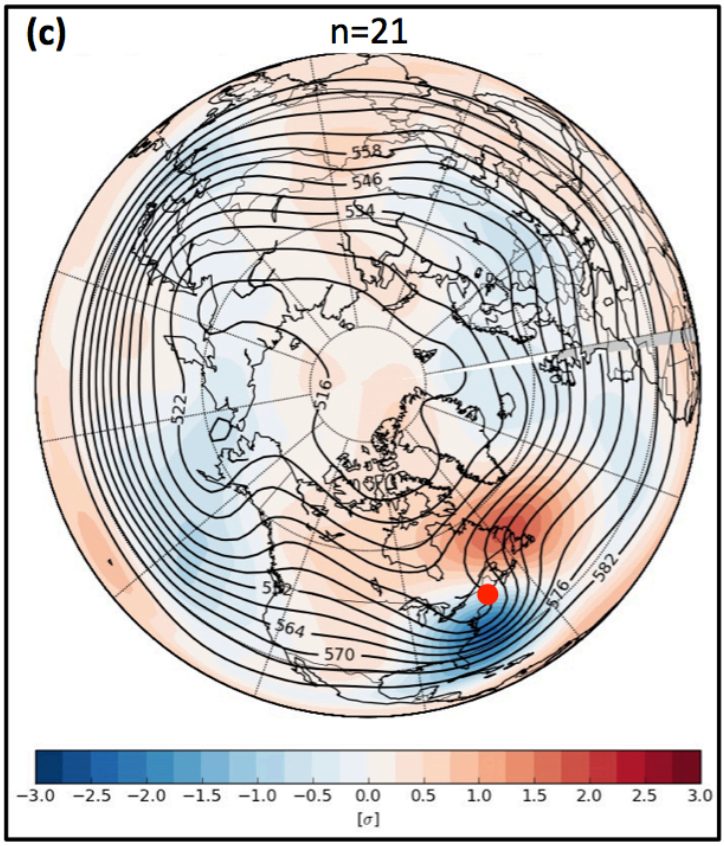

Fig. 3.15. As in Fig. 3.13, except at t_0.

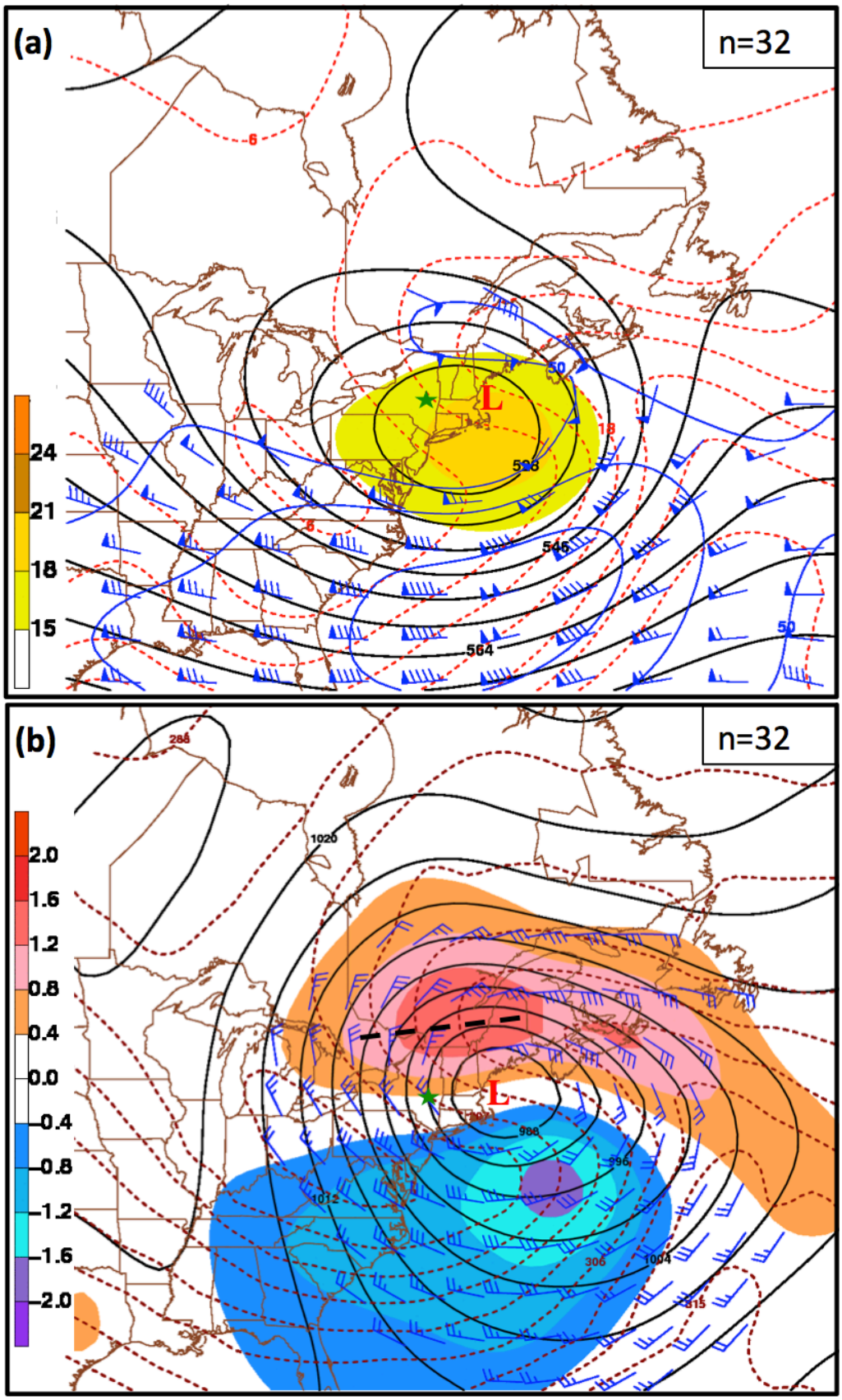
(a)
n=32
L
24
21
18
15
(b)
n=32
L
2.0
1.6
1.2
0.8
0.4
0.0
-0.4
-0.8
-1.2
-1.6
-2.0

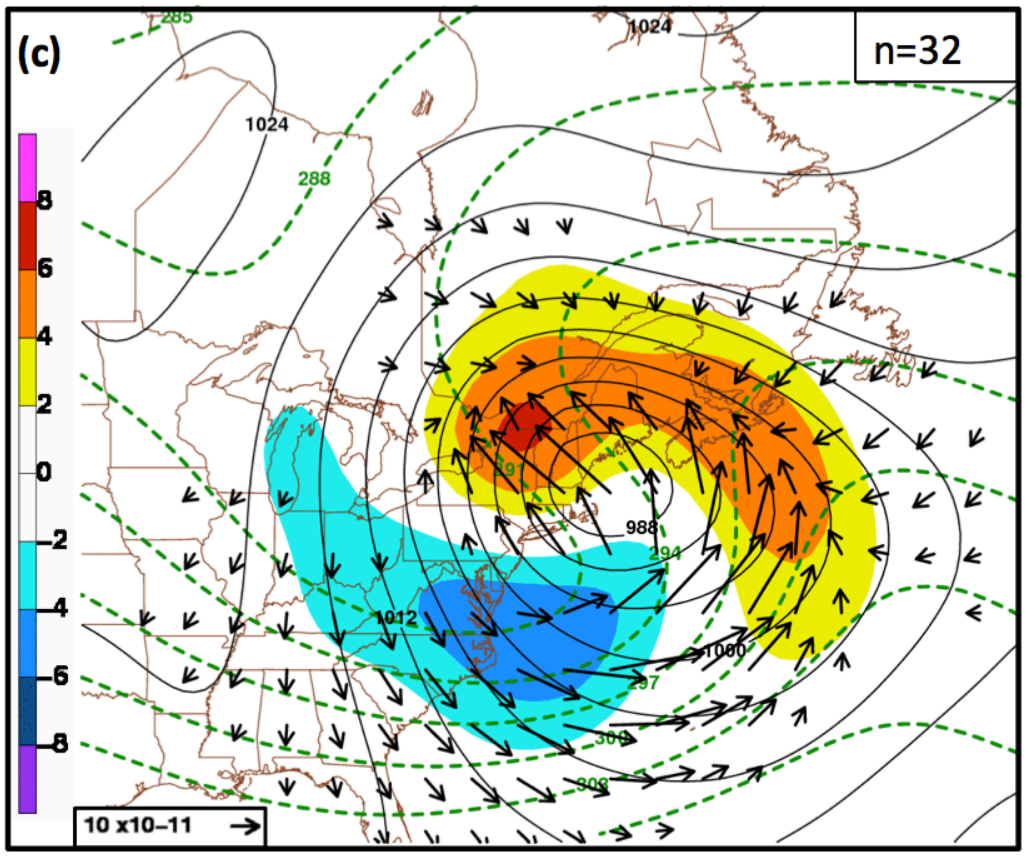

Fig. 3.16. EJS category composite (n=32). (a) 500-hPa geo. height (dam, black contours) and abs. vort (10^{-5} s^{-1}, shaded), 300-hPa wind (kt, barbs), and PWAT (mm, red dashed). The green star denotes the approximate location of Albany, NY and the blue contours outline regions of 300-hPa wind greater than 50, 70 and 90 kt; (b) 850-hPa temp. advection (K h^{-1}, shaded), mean sea level pressure (hPa, black contours), 700-hPa equivalent potential temperature (K, red dashed), and 850-hPa wind (kt, barbs). The dashed black line denotes the trowal axis and the red L denotes the surface cyclone center; (c) mean sea level pressure (hPa, black contours), 700-hPa potential temperature (K, green dashed), Q-vectors (arrows, 10^{-11} K m^{-1} s^{-1}), and Q-vector convergence (10^{-12} Pa m^{-2} s^{-1}, shaded).

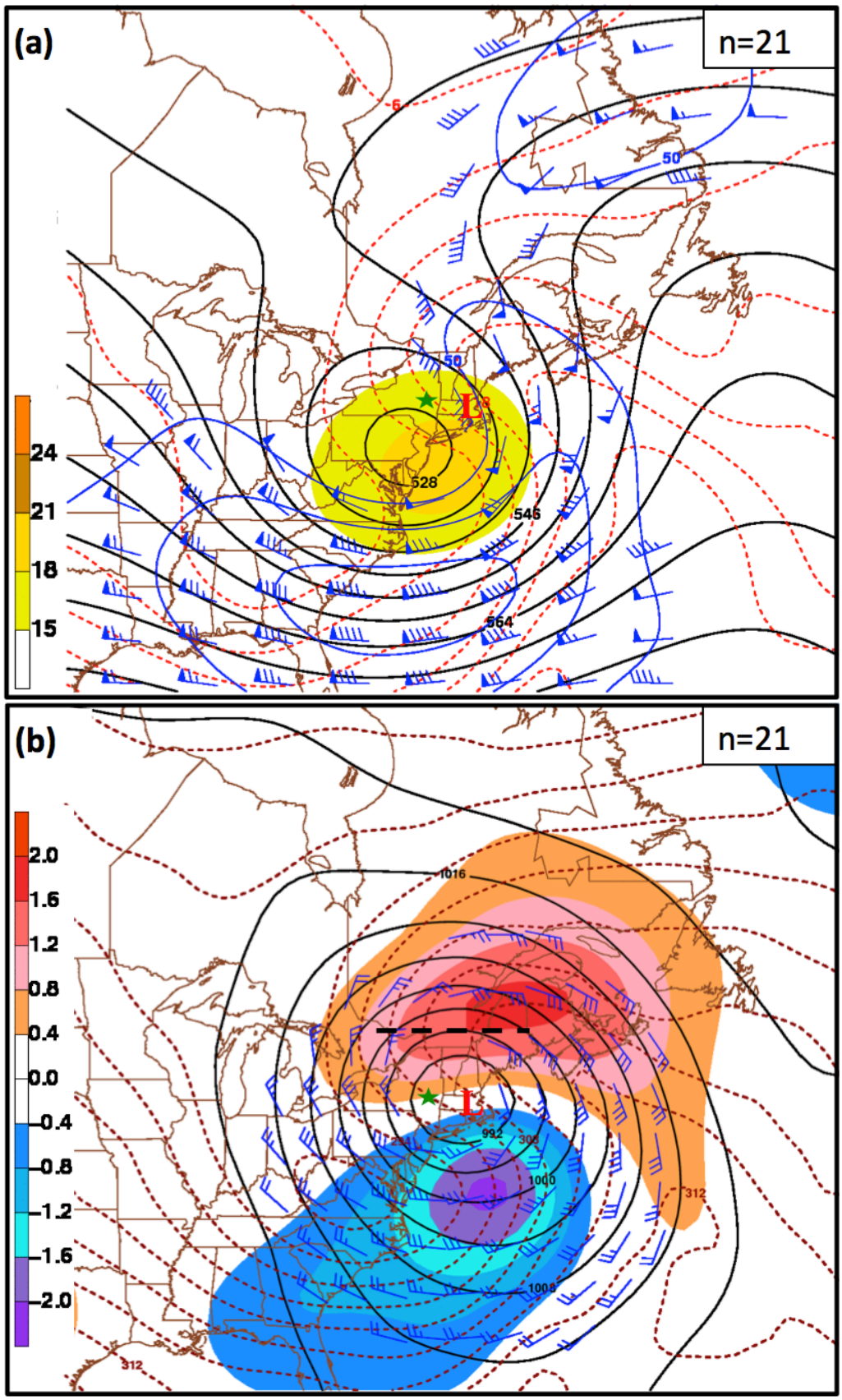
(a)
n=21
6
50
50
L
528
546
564
24
21
18
15
(b)
n=21
2.0
1.6
1.2
0.8
0.4
0.0
-0.4
-0.8
-1.2
-1.6
-2.0
1016
L
992
1000
1008
312
312

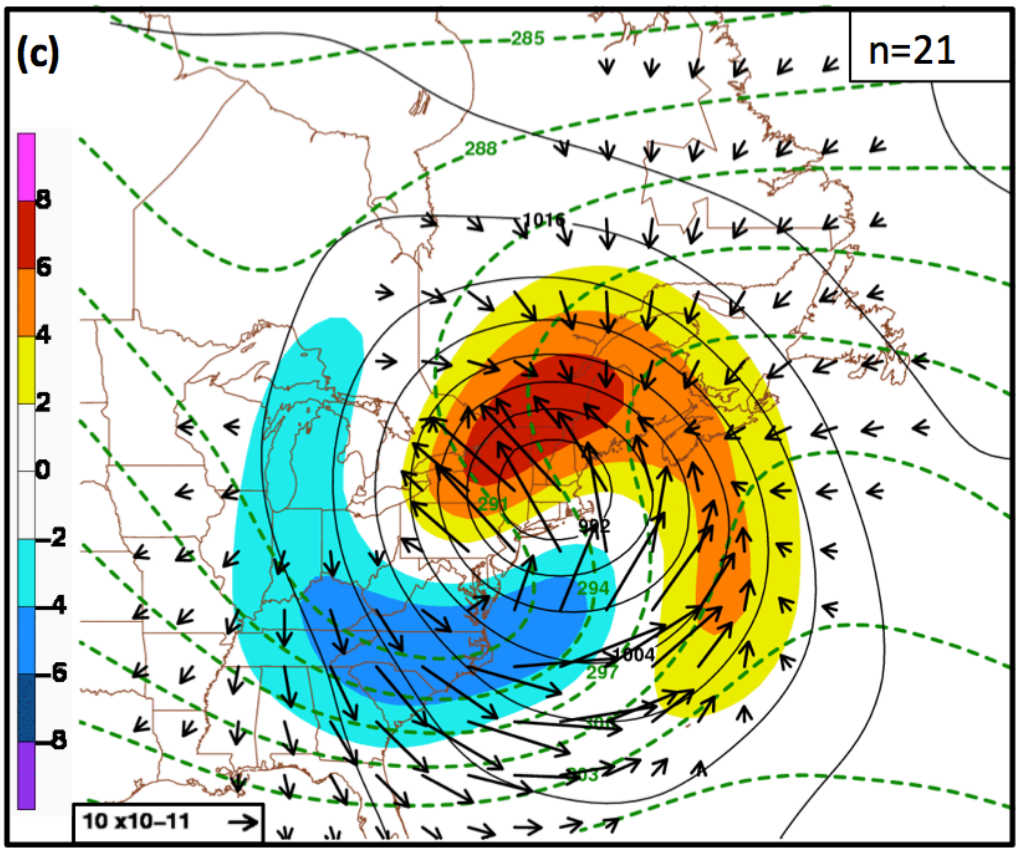

Fig. 3.17. As in Fig. 3.16, except for the cutoff low category composite (n=21).

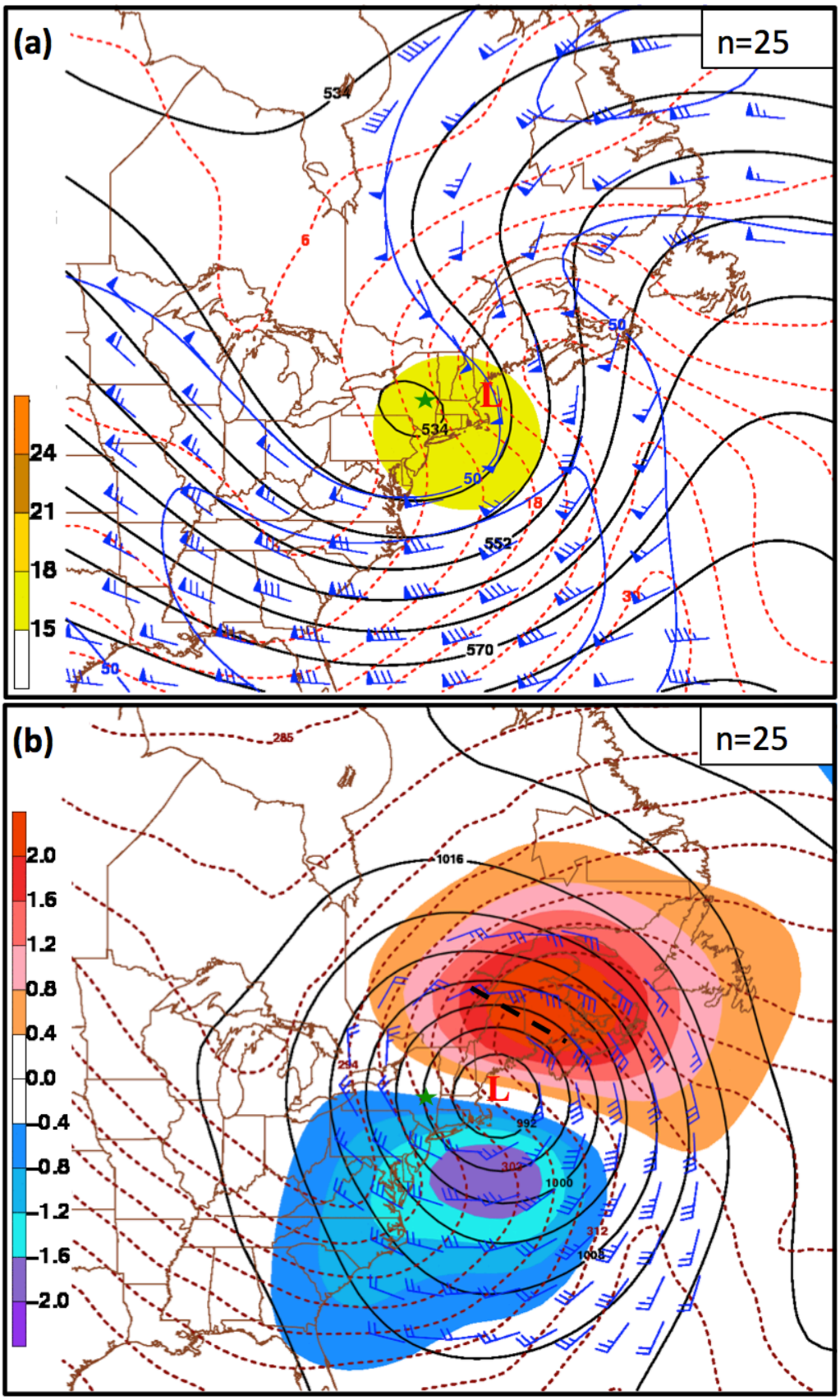
(a)
n=25
534
6
L
534
50
18
552
570
24
21
18
15
(b)
n=25
285
1016
L
294
992
1000
312
1008
2.0
1.6
1.2
0.8
0.4
0.0
-0.4
-0.8
-1.2
-1.6
-2.0

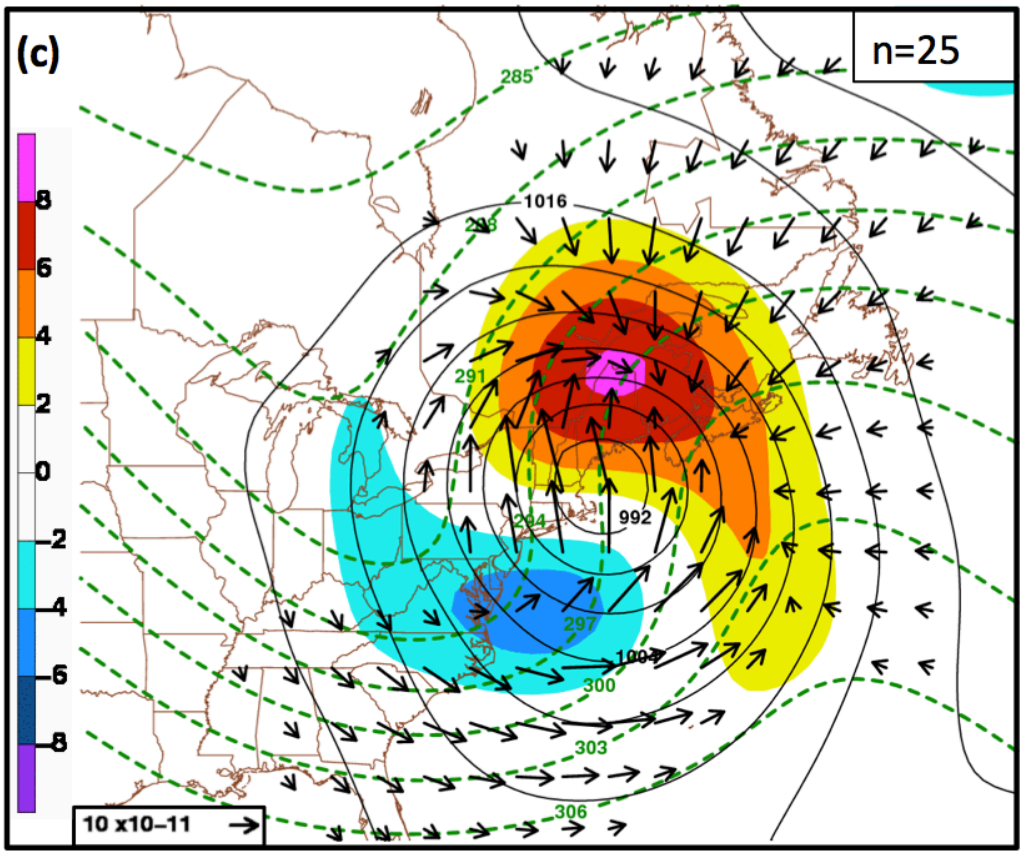

Fig. 3.18. As in Fig. 3.16, except for the open wave category composite (n=25).

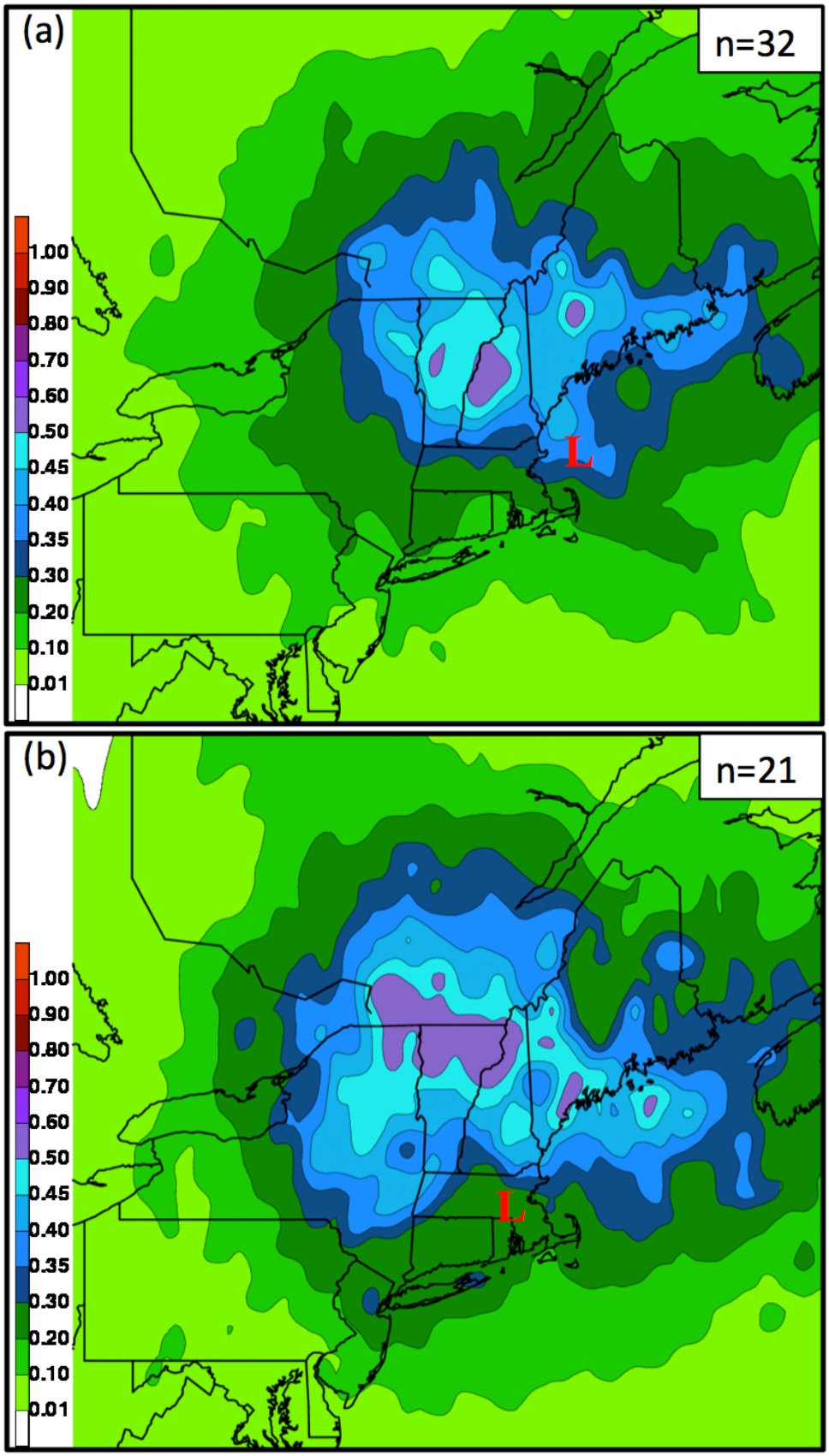
(a)
n=32
1.00
0.90
0.80
0.70
0.60
0.50
0.45
0.40
0.35
0.30
0.20
0.10
0.01
L
(b)
n=21
1.00
0.90
0.80
0.70
0.60
0.50
0.45
0.40
0.35
0.30
0.20
0.10
0.01
L

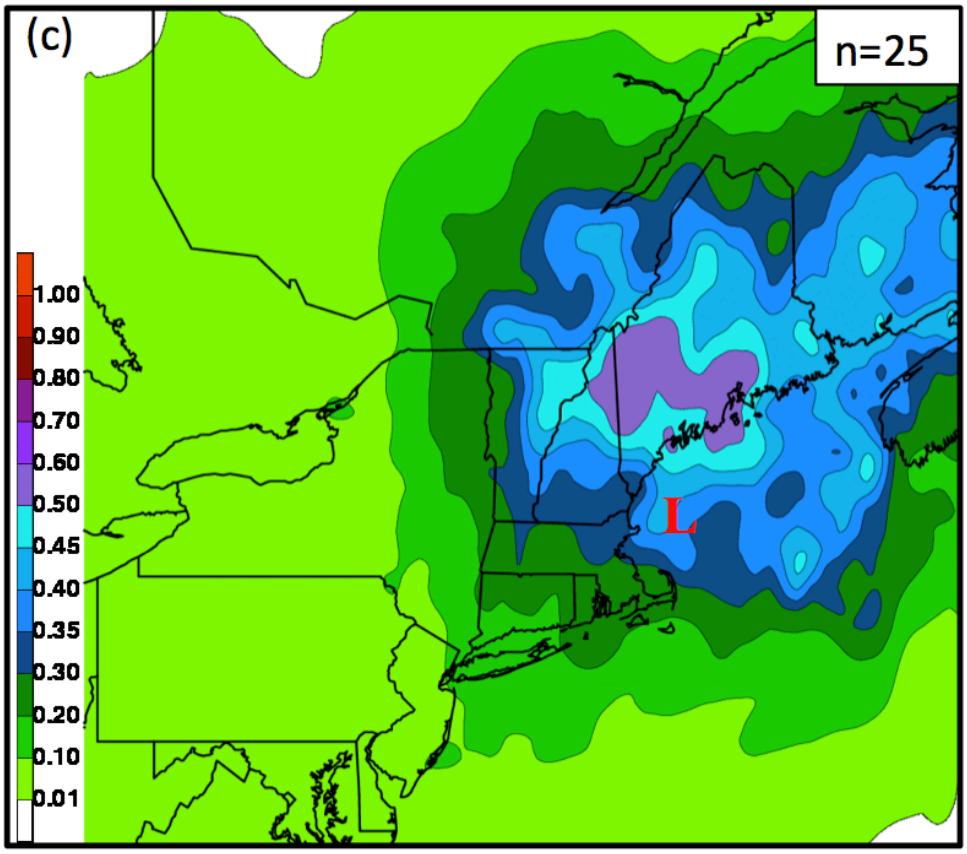

Fig. 3.19. Composite precipitation (in, shaded) in the 24-h period following t_0 for (a) EJS events, (b) cutoff low events, and (c) open wave events. Red L denotes the location of the surface cyclone at t_0.

4. Results: Case Studies of Two High Impact EJS Events

4.1 2–3 January 2010 EJS Event

4.1.1 Event Overview

The 2–3 January 2010 EJS event impacted the Northeast U.S. with a widespread, long duration snowfall extending from Pennsylvania to Maine (Fig. 4.1). The primary surface cyclone reached a minimum sea level pressure of 966 hPa in the Gulf of Maine after deepening 34 hPa in 24 h, leading to strong winds and blizzard-like conditions across much of the Northeast U.S. The heaviest snow fell in Vermont's Champlain Valley where Burlington, VT received 85 cm, making it the greatest single storm snowfall total on record. Snow fell for a long duration at many Northeast U.S. locations including Burlington, VT, where a continuous 35 h snowfall caused numerous travel delays. The presence of strong spatial gradients in the total snowfall distribution (Fig. 4.1) indicates that topographical forcing likely played a crucial role during this event. In particular, high terrain locations along and in the lee of the Green Mountain spine received far less snowfall than valley locations on the windward side.

4.1.2 Large-scale Evolution

Numerical models showed considerable variability in forecasting various meteorological fields during the period leading up to 03 January 2010. Figures 4.2a–d display the evolution of the Global Ensemble Forecast System (GEFS) 500-hPa height

mean and spread, and sea level pressure mean and spread valid at 0000 UTC 3 January. The 72-h GEFS 500-hPa height distribution (Fig. 4.2a) displays a cutoff low located off the New England coast, a well-defined anticyclone centered over Greenland, and a secondary cutoff low over the central North Atlantic Ocean. Considerable phase and amplitude uncertainty exists regarding the cutoff low off the New England coast, while primarily phase uncertainty exists in regard to the blocking anticyclone. The S-shaped pattern of the spread from the cyclone off New England to the blocking anticyclone over Greenland suggests that some ensemble members are displaying diabatically enhanced ridging downstream of the intensifying cyclone. The 72-h mean sea level pressure forecast (Fig. 4.2b) depicts a sub-980 hPa surface low southeast of Nova Scotia, with a 1036 hPa surface high located over central Canada. A 8–10 hPa spread exists to the northwest and southeast of the surface low indicating significant disagreement among ensemble members regarding the surface low track, and to a lesser degree, intensity. The 48-h 500-hPa height forecast (Fig. 4.2c) displays slightly less phase uncertainty concerning the cutoff low over New England; however, more significant phase uncertainty exists regarding the diabatically enhanced North Atlantic ridging. The 48-h mean sea level pressure forecast (Fig. 4.2d) exhibits a much deeper, sub-972 hPa surface low with more substantial spread (10–12 hPa) to the west of the surface low. The increase in spread indicates increasing disagreement among ensemble members concerning cyclone track, despite decreasing forecast lead-time. At the time of the event, operational forecasters also noted the sizeable variability of numerical model precipitation forecasts leading up to the cyclone (e.g., Stuart 2010a).

Figures 4.3a–d illustrate the evolution of the large-scale upper-level circulation through dynamic tropopause (1.5-PVU surface; DT) potential temperature (θ) analyses from 1200 UTC 31 December 2009 to 1200 UTC 03 January 2010. At 1200 UTC 31 December (Fig. 4.3a), a large region of high DT θ is evident across Greenland and the North Atlantic Ocean (denoted by red arrow in Fig. 4.3a), indicative of an elevated tropopause and a large-scale upper-level ridge. Over central North America, several regions of low DT θ (denoted by red circles in Fig. 4.3a) indicate multiple shortwave troughs embedded in a split flow regime, downstream of a western U.S. ridge. At 1200 UTC 01 January (Fig. 4.3b), a northern stream shortwave trough approaches the western Great Lakes region as a southern stream shortwave trough tracks across the northern Gulf Coast states. At 1200 UTC 02 January (Fig. 4.3c), the northern and southern streams merge as multiple regions of low DT θ amalgamate over the Northeast U.S., while a region of high DT θ downstream (denoted by the red arrow in Fig. 4.3c) begins to move poleward. At 1200 UTC 03 January (Fig. 4.3d), a DT θ hook (analogous to a PV hook) is evident over the Northeast U.S. (denoted by the red arrow in Fig. 4.3d) as a cyclonic wave breaking event unfolds in response to a stationary upper-level block over the high latitude North Atlantic Ocean. A reversal of the meridional PV gradient over eastern North America implies strong upper-level easterly flow across northern New England, poleward of an intense surface cyclone (not shown) at the tip of the PV hook.

Figures 4.4a–d display the evolution of 1000-500-hPa thickness, 1000-hPa geopotential height and 700-hPa geostrophic temperature advection from 1200 UTC 02 January to 0600 UTC 03 January. The track of the surface low nicely follows regions of 700-hPa geostrophic warm air advection throughout the period, confirming the usefulness

of the Sutcliffe–Petterssen development theory (Sutcliffe 1947; Sutcliffe and Forsdyke 1950; Petterssen 1956). Initially, the strongest warm air advection is located to the northeast of the 1000-hPa geopotential height minimum, leading to a northeastward track of the surface low (Figs. 4.4a–b). As the cyclone "wraps up", the strongest warm air advection becomes concentrated to the west-northwest of the 1000-hPa geopotential height minimum, leading to a west-northwestward track of the surface low from 0000–0600 UTC (Figs. 4.4c–d).

Coupled 300-hPa jet streaks are evident when the surface cyclone initially tracks northeastward at 1200 UTC 2 January (Fig. 4.5a). From 1200–1800 UTC 2 January (Figs. 4.5a–b), the surface cyclone deepens from 980 hPa to 972 hPa as strong forcing for cyclogenesis is present beneath the poleward exit region of the southern jet streak. From 1800 UTC 2 January–0000 UTC 3 January (Figs. 4.5b–c), the surface low is favorably located downstream of a 1000–500-hPa thickness trough in a region of inferred cyclonic thermal vorticity advection by the 1000–500-hPa thermal wind over the cyclone center, which likely contributed to further deepening. During this time period the surface cyclone tracks northwestward, while a region of easterly flow aloft begins to develop to the northwest of the surface cyclone (Figs. 4.5b–c). From 0000–0600 UTC 3 January (Figs. 4.5c–d), the surface low continues to track westward into the Gulf of Maine while a 90 kt easterly jet streak becomes established poleward of the surface cyclone.

4.1.3 Synoptic-scale Features

Figure 4.6a illustrates the aforementioned 90 kt 300-hPa easterly jet streak at 0600 UTC 03 January. The jet streak is situated on the northern flank of the upper-level cutoff circulation, with the equatorward exit region and strongest upper-level divergence located over southeast Quebec and northern New England. A cross-section extending from central Quebec to central Long Island (Fig. 4.6b) reveals an area of upward vertical velocities beneath the equatorward jet exit region, indicating large-scale upward motion in the ascending branch of a thermally indirect vertical circulation. Burlington, VT (denoted by the green star in Figs. 4.6a–b) is located beneath the region of strong upward vertical motion and is in a favorable location for synoptically enhanced precipitation.

Directly beneath the equatorward jet exit region exists a large zone of northerly 850-hPa warm air advection over northern Vermont, northern New York and southern Quebec (Fig. 4.7a). The low-level baroclinicity is increased in these regions (with warm air to the north) and it is inferred that the Laplacian of warm air advection is maximized in this region, contributing to broad QG forcing for ascent. Interestingly, an area of northwesterly 925-hPa cold air advection exists over much of northern New England (Fig. 4.7b), indicating a complex differential thermal advection pattern. A direct result of near surface cold air advection beneath low- to mid-level warm air advection is a distinct inversion around 900-hPa, seen in 0000 UTC 03 January soundings from Maniwaki, QC and Albany, NY (Figs. 4.8a–b).

At 0600 UTC 03 January, the entirety of northern Vermont is located in an area of near saturation based on the low-level relative humidity (Fig. 4.9). Thus, moist low-level northwesterly flow directed orthogonal to the Green Mountain spine favors significant orographic precipitation enhancement (e.g., St. Jean and Sisson 2004). A well-defined

trowal axis (indicated by the black dashed curve) is also apparent at 0600 UTC 03 January, detectable by a 700-hPa θ_e ridge extending towards northern New England (Fig. 4.9) where the strongest low-to mid-level warm air advection is present. The trowal airstream is typically characterized by large-scale, moist, cyclonic ascent, manifesting itself as wrap-around precipitation to the northwest of the surface cyclone (e.g., Martin 1999). The advection of 700-hPa θ_e by the 700-hPa wind suggests that the trowal axis will continue to rotate southwestward toward New York and Vermont, contributing to prolonged precipitation over these regions. A portion of the trowal is collocated with a region of 500-hPa cyclonic absolute vorticity advection over northern Vermont and southern Quebec (Fig. 4.10), likely as a result of vorticity lobes rotating around the closed upper-level low. Both the trowal and the strongest 500-hPa cyclonic vorticity advection are located beneath the equatorward jet exit region (Fig. 4.10), implying that strong QG forcing for ascent is present to the northwest of the surface cyclone. A high precipitable water corridor is directed from the northwest Atlantic Ocean inland toward southeast Quebec, extending cyclonically around the upper-level low as a result of deep easterly flow. The combination of strong forcing for ascent with a moisture channel inland from the Atlantic Ocean likely led to a widespread snowfall across the region.

The total QG forcing from a Q-vector perspective is seen at 0600 UTC 03 January in Figure 4.11. As previously inferred from Figures 4.6–4.10, the strongest forcing for ascent is located to the northwest of the surface cyclone, extending from southeast Quebec into northeast New England. The trowal axis is nearly collocated with the maximum in Q-vector convergence, indicating that large-scale QG forcing for ascent is occurring in the occluded quadrant of the cyclone. Weaker forcing for ascent exists

across northern New York and Vermont, likely a result of low-level warm air advection beneath the equatorward jet exit region of the easterly jet streak. In the region of maximum forcing, Q-vectors are primarily aligned along isentropes, suggesting that the convergence of Q_s is the primary forcing component of the Q-vector and is acting to rotate isentropes into a thermal ridge. Further west across southwest Quebec and northern New York, Q-vectors are directed across isentropes toward warmer air indicating low- to mid-level frontogenesis along a severely bent-back warm front. Areas of central Vermont that received heavy snowfall totals are located just south of the strongest QG forcing for ascent, indicating that mesoscale forcing for ascent was likely ongoing.

4.1.4 Mesoscale Features

Radar (Fig. 4.12a) and surface observations (Fig. 4.12b) at 0400 UTC 03 January depict a large area of high reflectivity values (15–35 dBZ) across Maine, New Hampshire and far eastern Massachusetts falling as light to moderate snow. This precipitation is likely the result of a combination of the previously mentioned forcing mechanisms simultaneously occurring to the northwest of the surface cyclone. However, in the Champlain Valley of northern Vermont, far eastern New York, and downwind of Lake Ontario, high reflectivity values (20–30 dBZ) are present well ahead of the primary region of precipitation, indicating lake- and terrain-induced ascent. A meridionally oriented, narrow band of heavy snowfall across the Champlain Valley of northern Vermont (Fig. 4.12a) is partially responsible for producing 85 cm of snowfall in Burlington, VT, with only 5–10 cm 20–30 mi to the east. This indicates that the band

remained stationary for the majority of the event, possibly as a result of persistent moist, northwesterly upslope flow interacting with unusually high low-level stability (strong 900-hPa inversion; Fig. 4.8).

From 0400–0700 UTC 03 January, the region of large-scale ascent and precipitation continues to push southwestward, enhancing reflectivity values over the Champlain Valley (Fig. 4.12c) and ultimately contributing to 25 cm of snowfall at Burlington, VT during the 3 h period (not shown). Surface observations from 0400 and 0700 UTC 03 January across southern Quebec and northern New York reveal primarily westerly and southwesterly winds, while persistent northwesterly winds continue at Burlington, VT (Fig. 4.12b, d). This suggests that the low-level flow may be channeling down the cone shaped Champlain Valley, gaining moisture from Lake Champlain and converging in the vicinity of Burlington, VT (e.g., Payer 2010).

Results from a 1.33 km resolution WRF simulation are shown in Figures 4.13–4.15, and are used to investigate the mechanisms that allowed for the persistence of the heavy snow band in the Champlain Valley. A model forecast sounding for Burlington, VT valid at 1800 UTC 02 January reveals a saturated layer from the near-surface–800-hPa level, with low-level northwesterly winds veering to easterly above 500-hPa (Fig. 4.13a). An isothermal layer is present from 850–700-hPa, indicating modest stability, likely as a result of increasing warm air advection from the north. The 10-m wind field at 1800 UTC 02 January across southern Quebec (Fig. 4.13b) displays westerly winds turning down the Champlain Valley and becoming primarily northwesterly in the vicinity of Burlington, VT. Speed convergence is evident just to the east of Burlington, VT (blue circle) as the flow decelerates along the windward slopes of the mountain spine, ascends

over the peaks, and accelerates down the leeward slopes (Fig. 4.13b). A cross-section taken in the direction of the low-level flow (A to A′ in Fig. 4.13b) confirms that the cross-barrier wind decelerates slightly at the surface, but remains nearly constant around 925-hPa while flowing up and over the ridge tops (Fig. 4.13c). Near surface θ_e contours begin to slope upward just east of Burlington, VT (blue circle) and become steeply sloped directly along the windward slopes of the Green Mountain spine (Fig. 4.13c). This suggests that air parcels (traveling along θ_e surfaces) arrive from the northwest and undergo rapid ascent close to the ridge crest, leading to a persistent region of heavy precipitation just to the east of Burlington, VT. This model depiction fails to explain the observed prolonged heavy snow band over Burlington, VT and surrounding valley regions; however, the model forecast 12 h later displays a vastly different scenario.

At 0600 UTC 03 January, the model forecast sounding for Burlington, VT reveals a strong inversion around 925-hPa, with nearly saturated air from the surface to 500-hPa in a large region favorable for dendritic growth (Fig. 4.14a). This forecast sounding more closely matches the observed soundings from Maniwaki, QC and Albany, NY previously seen in Fig. 4.8. The 10-m wind field depicts northwesterly flow in the northern Champlain Valley, decelerating significantly and turning northerly (parallel to the mountain spine) before reaching the Green Mountain barrier. An analysis of the cross-barrier wind in the along-flow direction (Fig. 4.14c) confirms that the flow orthogonal to the mountain spine decelerates from 30–40 kt just west of Burlington, VT, to less than 5 kt just east of Burlington, VT. θ_e surfaces collocated with the region of greatest flow deceleration slope steeply upwards, indicating strong ascent in the valley region well upwind of the Green Mountain spine. Along and just east of the ridge crest, θ_e surfaces

plunge downward as the flow rapidly accelerates, indicating strong subsidence. This model depiction is able to explain the persistence of an intense snow band over Burlington, VT, primarily as a result of orographically blocked upslope flow in a near-saturated low-level environment. The presence of a strong low-level inversion and increased stability effectively prevents the low-level flow from directly traversing the Green Mountain barrier, and forces convergence and upward vertical motion well upwind of the windward slopes (e.g., Sisson et al. 2010).

Figures 4.15a–b display the model precipitation forecast over northern Vermont for the 18-h period prior to and after low-level inversion development. Before the inversion is in place, the heaviest precipitation is located along the windward slopes of the Green Mountains (Fig. 4.15a), consistent with steeply sloped θ_e surfaces and ascent in that region. This represents the "typical" upslope snowfall precipitation distribution that occurs in the absence of strong low-level stability. After the inversion has developed and the low-level stability has significantly increased, the heaviest precipitation falls upwind of the mountains, at valley locations below 180 m (600 ft). This depiction more accurately represents the observed snowfall distribution from 2–3 January 2010, suggesting that the model simulation developed the low-level inversion much later than it occurred in reality. This case demonstrates how slight changes in low-level stratification can significantly alter the low-level flow and resulting precipitation distribution during northwesterly flow snowfall events in northern Vermont.

4.2 25–27 February 2010 EJS Event

4.2.1 Event Overview

The 25–27 February 2010 EJS event also produced heavy snowfall totals from Pennsylvania to Maine, with large gradients in snowfall over very short distances (Fig. 4.16). Hunter Mountain in the eastern Catskill Mountain range received 48 in (122 cm) of snowfall, while just 10 mi to the east, the Hudson River Valley received primarily light rain. Oddly enough, New York City and parts of western Long Island received over 20 in (51 cm) of snowfall (Fig. 4.16). A variable snowfall of this nature suggests that orographic forcing likely enhanced snowfall in the high elevations, while tight thermal gradients led to extreme variations in precipitation type. Snowfall lasted for more than 48 h in the Catskill Mountains, making it the longest duration event in the Albany National Weather Service county warning area since December 1992 (Stuart 2010b). The surface low associated with the event reached a minimum sea level pressure of 972 hPa over southeast Connecticut after deepening 28 hPa in a 24 h period, leading to 50-70 kt wind gusts over southern Vermont (not shown).

4.2.2 Large-scale Evolution

The GEFS displayed varying sea level pressure and 500-hPa height forecasts at lead times of 72 and 48 h, as seen in Figures 4.17a–d. The GEFS 72 h forecast of 500-hPa height and spread (Fig. 4.17a), valid at 0600 UTC 26 February 2010, displays a closed 500-hPa low centered off the Mid-Atlantic coast with a highly amplified ridge downstream across the western North Atlantic. The greatest uncertainty is associated with the phase of the cutoff low, indicated by significant spread surrounding the majority of

the closed circulation (Fig. 4.17a). The GEFS 72 h forecast of the sea-level pressure reveals a 988 hPa surface low just southeast of Nantucket, MA (beneath the northeast flank of the upper-level low), with a spread of 10–12 hPa to the southwest of the low center (Fig. 4.17b).

An analysis of the 48-h forecast 500-hPa height and sea level pressure fields (Figs. 4.17c,d) reveals important differences from the 72-h forecast. The 500-hPa cutoff low and downstream ridge are located further west with a greater negative tilt, leading to a surface low that is centered over central Massachusetts, several hundred miles northwest of the 72-h forecast location. A mean sea level pressure spread of 6–8 hPa is still present to the west of the surface low in the 48-h forecast, indicating continued disagreement among ensemble members regarding the westward extent of the surface low. The lack of consensus in regard to the cyclone track led to challenging precipitation forecasts within 48 h of heavy snowfall development (e.g., Stuart 2010b).

Figures 4.18a–d display the evolution of the upper-level circulation over North America from 1200 UTC 23 February to 1200 UTC 26 February. At 1200 UTC 23 February, a large-scale northern stream trough axis (denoted by a red circle in Fig. 4.18a) is located across the upper Midwest with a positively tilted southern stream shortwave trough (denoted by a red circle in Fig. 4.18a) exiting the four corners region. High amplitude ridging (increased DT θ) is apparent on the upstream and downstream sides of the large-scale trough, creating a highly amplified, meridional flow pattern across much of the contiguous U.S. High DT θ air extends into the high-latitudes of the North Atlantic with DT winds indicating a large-scale blocking anticyclone is in place (denoted by the arrow in Fig. 4.18a).

Moving forward to 1200 UTC 24 February, the northern stream trough advances eastward toward the central Great Lakes, while the southern stream shortwave trough approaches the Gulf Coast, maintaining a positive tilt (Fig. 4.18b). A strong interaction between the northern and southern stream troughs occurs over the Mid-Atlantic at 1200 UTC 25 February as a trough merger takes place allowing the large-scale trough to tilt negatively (Fig. 4.18c). A large reservoir of low DT θ (high PV) air is in place from the Mid-Atlantic to the Great Lakes, while further east a stream of high DT θ air becomes established in the downstream ridge axis (denoted by the red arrow in Fig. 4.18c). As time progresses, the large-scale block over the high-latitude North Atlantic remains quasi-stationary, forcing the upper-level trough to cutoff over the Northeast U.S. and a cyclonic wave breaking event to occur at 1200 UTC 26 February (denoted by the red arrow in Fig. 4.18d). High DT θ air is apparent wrapping around the poleward and western side of the cutoff circulation, reversing the meridional PV gradient and leading to strong upper-level easterly flow across northern New England.

The surface cyclone took a position several hundred miles off the coast of the Carolinas at 1200 UTC 25 February (Fig. 4.19a), downstream of the large-scale upper-level trough. Initially, the strongest 700-hPa geostrophic warm air advection is located east-northeast of the 1000-hPa geopotential height minimum (Fig. 4.19a), and the surface cyclone subsequently progresses northeastward to a position well off the East Coast at 1800 UTC 25 February (Fig. 4.19b). A meridionally elongated 1000-hPa geopotential height minimum is present at 1800 UTC 25 February, with 700-hPa geostrophic warm air advection surrounding the northern and eastern sides of the cyclone (Fig. 4.19b). The cyclone proceeds to move due north over Nantucket, MA by 0000 UTC 26 February as

strong warm air advection develops to the west-northwest of the cyclone (Fig. 4.19c), suggesting that a westward jog in track will occur. This is confirmed at 0600 UTC 26 February as the cyclone moves westward to a position over southern Connecticut (Fig. 4.19d). The unusual surface cyclone track is likely a product of the aforementioned quasi-stationary upper-level cutoff circulation and the amplified mid-level temperature advection pattern.

Forcing for ascent beneath the poleward exit region of an intense (130+ kt) 300-hPa jet streak off the Southeast U.S. coast likely contributed to the organization of the surface low at 1200 UTC 25 February (Fig. 4.20a). Rapid intensification of the surface low is apparent from 1800 UTC 25 February to 0600 UTC 26 February (Figs. 4.20b–d) as the cyclone progresses downstream of a negatively tilted 1000–500-hPa thickness trough, positioned favorably for cyclonic thermal vorticity advection by the 1000–500-hPa thermal wind over the cyclone center. A thickness ridge begins to wrap around the poleward side of the surface cyclone in Figures 4.20c–d, indicative of strong warm air advection throughout the low- to mid-levels. A region of easterly flow aloft (70–90 kt) appears over eastern Maine at 0600 UTC 26 February, to the northeast of the surface cyclone. This represents a response to the poleward displacement of warm air (thickness ridge) and the equatorward displacement of cold air (thickness trough). The developing easterly jet streak has significant implications for synoptic-scale forcing across parts of the Northeast U.S.

4.2.3 Synoptic-Scale Features

Figure 4.21a illustrates a developing region of easterly flow at 300-hPa extending from the Gulf of Maine westward towards the eastern Great Lakes at 0600 UTC 26 February. A 90 kt southeasterly wind maximum exists over the Gulf of Maine with a secondary maximum of 70 kt over western New York. The strongest upper-level divergence is located over northeast Pennsylvania and southern New York in a region of slightly weaker easterly flow between the two jet streaks (Fig. 4.21a). A cross section taken through this region, along the axis of heaviest precipitation at 0600 UTC 26 February (not shown), displays a fairly complex kinematic structure. A 60 kt easterly wind maximum is located around 250-hPa with winds increasing to 80 kt in the 800–700-hPa layer located above the eastern Catskill Mountain region (denoted by the green star in Fig. 4.21b). An area of upward vertical motion in the 850–700-hPa layer is nearly collocated with the low-level jet axis, while a tilted region of upward vertical motion extends throughout the mid-troposphere toward the upper-level jet core (Fig. 4.21b). This suggests that significant orographic lift is occurring beneath the equatorward jet exit region along the eastern Catskill Mountains, in conjunction with deep-layer ascent along and just south of a developing easterly jet core.

An analysis of 850-hPa winds, temperature and temperature advection at 0600 UTC 26 February displays a zonally oriented band of northerly warm air advection extending from western New England to the eastern Great Lakes (Fig. 4.22a). The warm air advection axis is located along and just south of the region of easterly flow aloft, and it is inferred that the Laplacian of warm air advection is maximized across this region and contributes to broad QG forcing for ascent. Across southeastern New England, a large area of anomalous southerly and southeasterly cold air advection is present, likely

enhancing subsidence behind the surface cold front (Fig. 4.22a). Southerly cold air advection is also evident at 925-hPa over southeastern New England, with a thermal trough stretching from west to east along the southern coast of New England (Fig. 4.22b).

In Figs. 4.22a–b, a distinct tongue of warm air is visible wrapping cyclonically around the low-level circulation, effectively denoting the trowal axis as further depicted by the dashed black line in Figure 4.23. QG forcing for ascent is favored along the trowal axis as well as to the north and west where a secondary θ_e ridge is present. A strong 700-hPa θ_e gradient exists across southern New England as a thermal ridge extends to the northwest of the surface cyclone, while a thermal trough extends to the southeast (Fig. 4.23). A region of decreased low-level relative humidity is coincident with a 700-hPa θ_e trough across eastern New England (Fig. 4.23), indicating a mid-level dry slot wrapping around the eastern quadrant of the cyclone.

At 0600 UTC 26 February, a deep, closed 500-hPa low is centered just off the New Jersey coast, embedded in a negatively tilted large-scale trough (Fig. 4.24). A high moisture corridor extends around the eastern and northern periphery of the closed low, directed towards the region of heaviest precipitation (not shown). Several areas of 500-hPa cyclonic absolute vorticity advection are present across central New York and eastern New England (Fig. 4.24), implying QG forcing for ascent. First, over eastern New England, a region of cyclonic absolute vorticity advection is collocated with the left exit region of a 300-hPa jet streak (Fig. 4.24), likely contributing to heavy rain in the warm sector just northwest of the impinging dry slot. Second, over central New York, a cyclonic absolute vorticity advection maximum intersects the axis of high precipitable

water (Fig. 4.24), indicating a favorable environment for heavy snowfall on the cold side of the low-level frontal zone.

The total QG forcing from a Q-vector perspective at 0600 UTC 26 February illustrates two distinct areas of forcing for ascent: one over central New York and another extending from the northwest Atlantic toward eastern Maine (Fig. 4.25). Of particular interest is the westernmost region of positive forcing, which is likely a result of northerly warm air advection along and northwest of the trowal axis, as well as strong differential vorticity advection. The orientation of the Q-vectors along the isentropes in the region of greatest convergence (positive forcing) suggests that Q_s is the primary forcing component, and that strong low-level frontogenesis and distinct banded precipitation is unlikely (Fig. 4.25). This also implies continued cyclonic rotation of isentropes in the region, leading to a more pronounced thermal ridge and more well defined trowal axis. Looking back at Figure 4.16, the heaviest snowfall totals are located primarily to the northwest of the cyclone center, emphasizing the significance of synoptic-scale forcing mechanisms in the trowal airstream, despite a lack of traditional QG frontogenesis.

4.2.4 Mesoscale Features

At 0000 UTC 26 February, the surface low began to retrograde westward toward Long Island while continuing to deepen below 980 hPa. A stationary front is visible to the northwest of the cyclone center in Figure 4.26a, extending from eastern Long Island northwestward toward the upper Hudson Valley. Critical thickness contours and the 0°C isotherm at 850-hPa (and the surface) are oriented along the stationary front, indicating

the approximate rain/snow line (Fig. 4.26b). This boundary is aligned with the Hudson Valley at 0000 UTC 26 February and remains quasi-stationary as the event unfolds. The quasi-stationary aspect of the thermal pattern suggests that the topography of eastern New York may be acting to reinforce the stationary front by operating as a barrier against the low-level flow.

Results from a WRF simulation seen in Figs. 4.27a–b further illustrate the thermal boundary at 850-hPa (Fig. 4.27a) and the surface (Fig. 4.27b) at 0600 UTC 26 February. A clear wind shift exists along the front at both levels (Figs. 4.27a–b), separating warm, moist easterly and northeasterly flow from cold, dry northerly and northwesterly flow. Easterly and northeasterly upslope flow is present along the eastern slopes of the Catskill Mountains, likely contributing to the enhanced precipitation observed in this area. The strongest surface temperature gradients and wind direction shifts are located along New York's Mohawk and Hudson River Valleys, confirming that flow channeling is playing a significant role in impeding the progression of warm air at low-levels.

Model soundings from Albany and Potter Hollow, NY are seen in Figs. 4.28a–b, the locations of which are denoted by the red circles in Figure 4.27b (Albany, NY is the easternmost circle). The sounding from Albany, NY (100 m elevation) indicates a surface temperature 1–2°C above freezing, decreasing to 0°C around 900 hPa and remaining isothermal. Twenty miles to the southwest at Potter Hollow, NY (500 m elevation) the surface temperature is 1–2°C below freezing and remains primarily isothermal until 800-hPa. Potter Hollow, NY is located just west (cold side) of the north-south thermal boundary and received 39 in (99 cm) of snow during the event, while Albany, NY is located just east of the boundary and received only 5 in (13 cm) of snow. A slight but

significant difference in the direction of the low-level flow (approximately 30°) exists between the two locations and is likely partially responsible for the disparity in thermal profiles and snowfall totals.

A base reflectivity image from 0600 UTC 26 February reveals a large region of heavy precipitation across all of New York and New England, with several areas of 35–45 dBZ returns (Fig. 4.29a). A north-south oriented band of 35–45 dBZ is located along and just east of the Hudson River, extending from Albany, NY southward (Fig. 4.29a). This is likely a manifestation of the "bright band" phenomenon, indicative of melting snowflakes at various elevations, and the approximate rain/snow line. To the west (Potter Hollow, NY) and south (New York City, NY) of this "bright band" precipitation is likely falling as heavy snow, with rain to the east (Albany, NY) of the band (Fig. 4.29b). Surface observations at 0600 UTC 26 February confirm that while Albany, NY is reporting light rain with a temperature of 3°C, Newburgh, NY and New York City, NY are reporting moderate snow with temperatures of 0°C and −1°C, respectively (Fig. 4.29b). This unusual meridional temperature gradient is a result of northerly warm air advection across the upper Hudson Valley and northwesterly cold air advection across the lower Hudson Valley (Figure 4.27b).

The total WRF derived precipitation distribution (Fig. 4.30a) closely matches the observed precipitation distribution (Fig. 4.16), and further highlights the significance of orographic precipitation enhancement during the event. Across eastern New York, maxima in precipitation are collocated with the high terrain of the Catskill and Helderberg Mountains, with minima along the Hudson River Valley. The aforementioned thermal boundary seen in Figs. 4.27a–b is collocated with this strong precipitation

gradient (Fig. 4.30a), such that regions of heavier precipitation received primarily snow, while regions of lighter precipitation received primarily rain.

A cross-section taken in the direction of the low-level flow at 0600 UTC 26 February (from A to A´ in Figure 4.30a) can be seen in Figure 4.30b. Surfaces of constant θ_e slope upward in the direction of the flow moving from the Hudson Valley westward toward the Catskill Mountains, with a maximum in upward vertical motion along the eastern slopes of the Catskill Mountains. Sustained upward vertical motion along the eastern slopes of the Catskill and Helderberg Mountains may have helped reinforce the thermal gradient in this region through adiabatic cooling associated with rapid low-level ascent. Decreases in the cross-barrier wind along and west of the Catskill Mountains are indicative of a significant wind shift associated with the aforementioned stationary frontal boundary. These results indicate that the presence of anomalous mesoscale precipitation and temperature boundaries were likely tied to the terrain of the surrounding area, and led to drastic changes in sensible weather over very short distances.

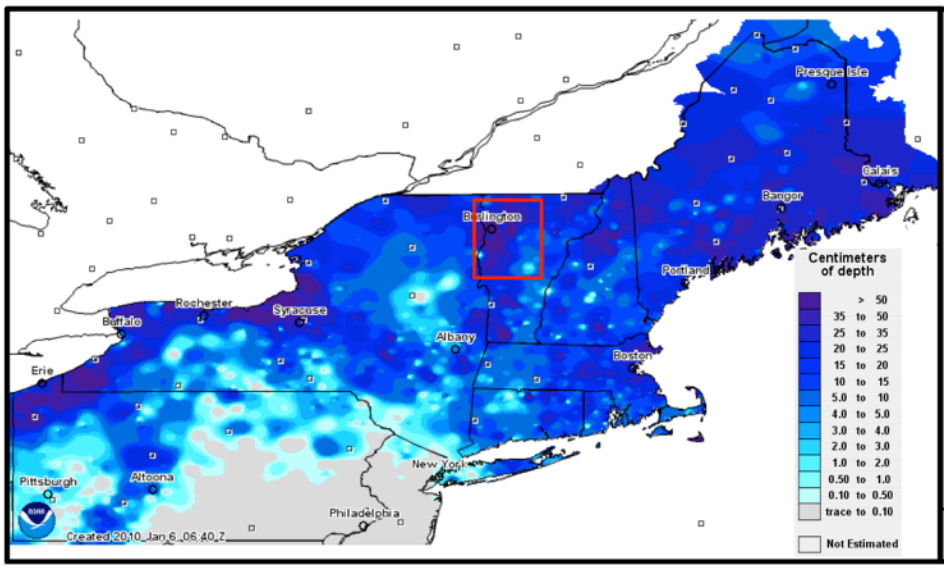

Fig. 4.1. 48-h snowfall accumulation (cm) ending at 0000 UTC 04 January 2010. Red box highlights the snowfall gradient in the vicinity of Burlington, VT.

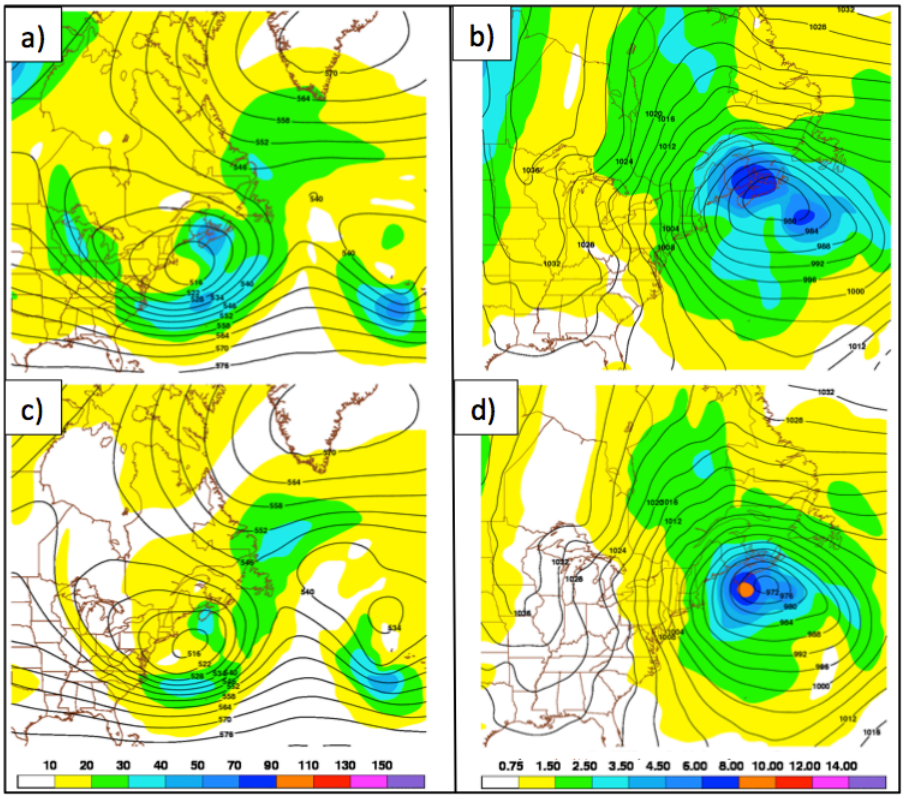

Fig. 4.2. NCEP Global Ensemble Forecast System (GEFS) initialized at (a,b) 0000 UTC 31 December 2009 and (c,d) 0000 UTC 01 January 2010, valid at 0000 UTC 03 January 2010. Left panels show ensemble mean 500-hPa height (dam, contours) and spread (dam, shaded). Right panels show mean sea level pressure (hPa, contours) and spread (hPa, shaded).

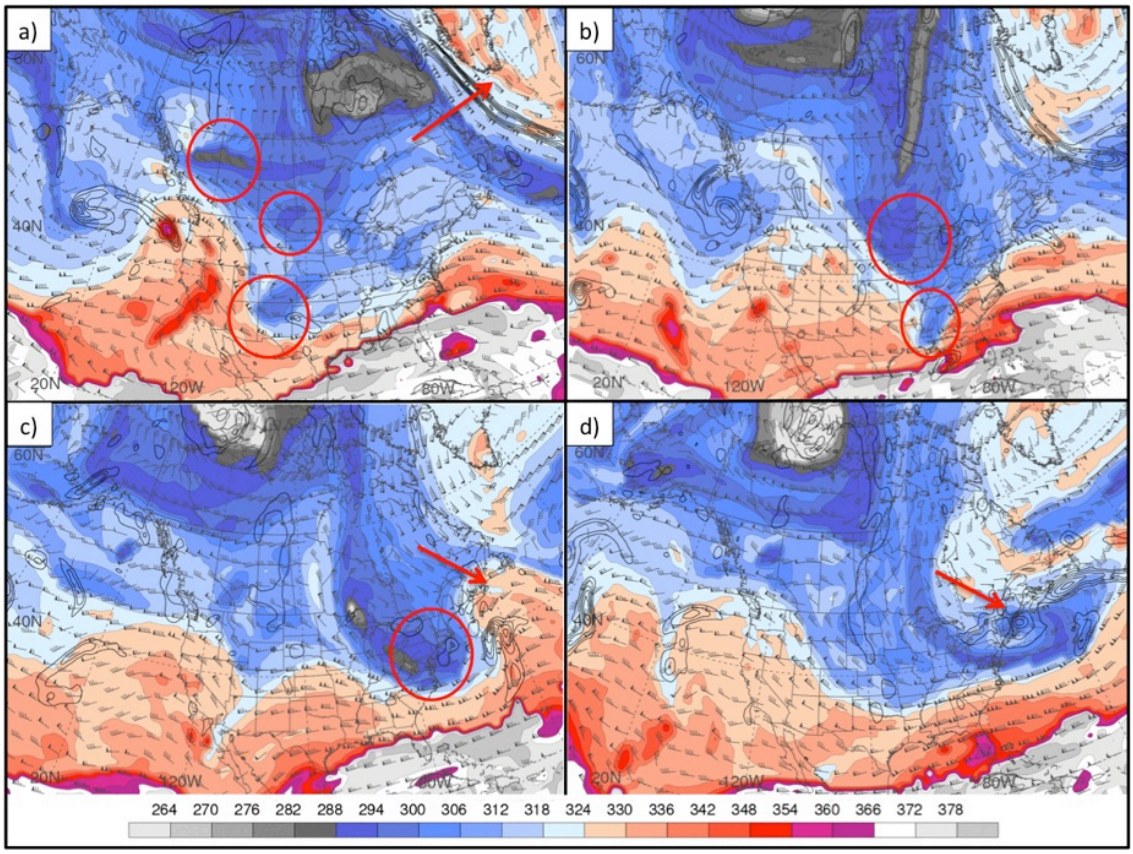

Fig. 4.3. GFS DT (1.5-PVU surface) potential temperature (K, shaded) and wind speed (kt, barbs), and 925-850-hPa layer averaged cyclonic relative vorticity (black contours every 0.5 x 10^{-4} s^{-1}) at (a) 1200 UTC 31 December 2009, (b) 1200 UTC 01 January 2010, (c) 1200 UTC 02 January 2010, and (d) 1200 UTC 03 January 2010. Red circles and arrows indicate the location of key features (Images courtesy of Heather Archambault, available online at http://www.met.nps.edu/~hmarcham/).

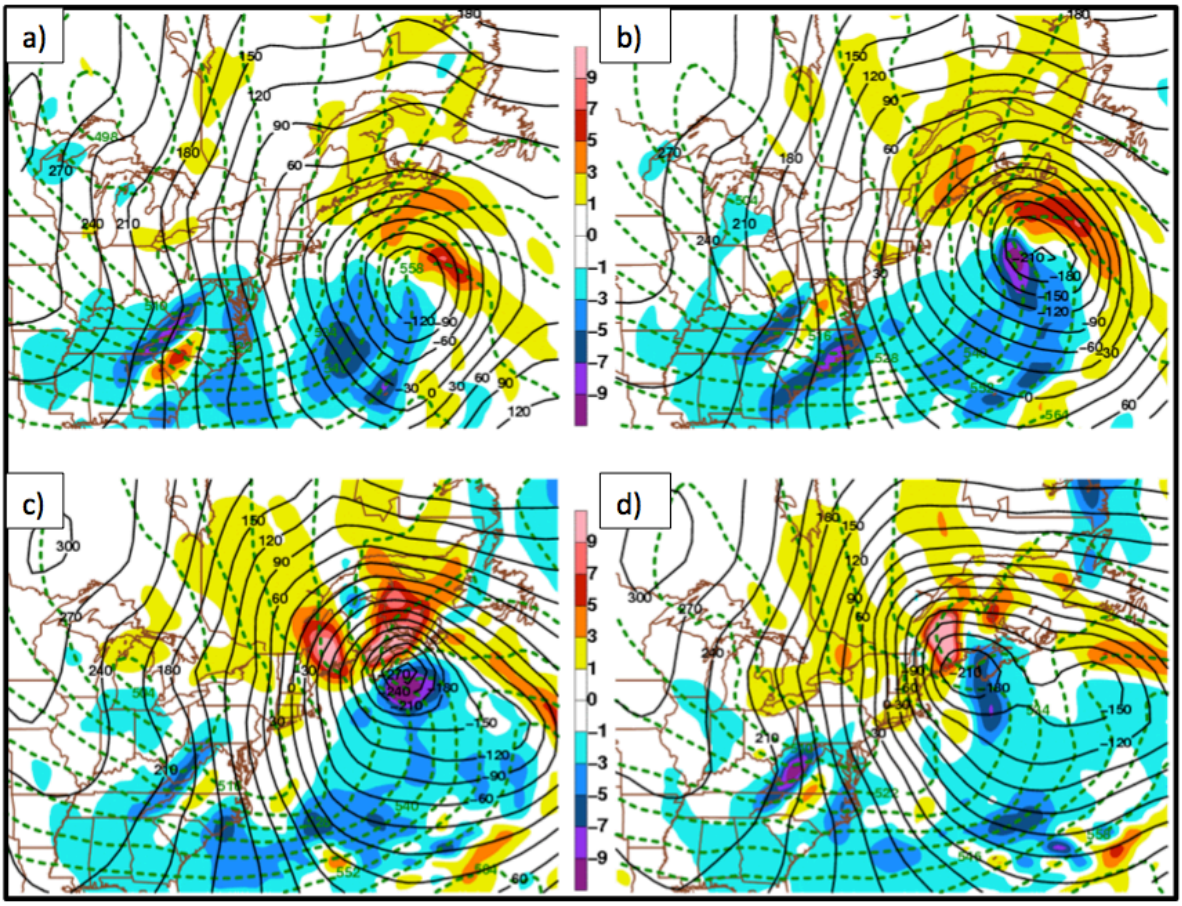

Fig. 4.4. Horizontal Laplacian of 700-hPa geostrophic temperature advection (K (6 h) $^{-1}$, shaded), 1000–500-hPa thickness (dam, green contours), and 1000-hPa geopotential height (dam, black contours) at (a) 1200 UTC 02 January 2010, (b) 1800 UTC 02 January 2010, (c) 0000 UTC 03 January 2010, and (d) 0600 UTC 03 January 2010.

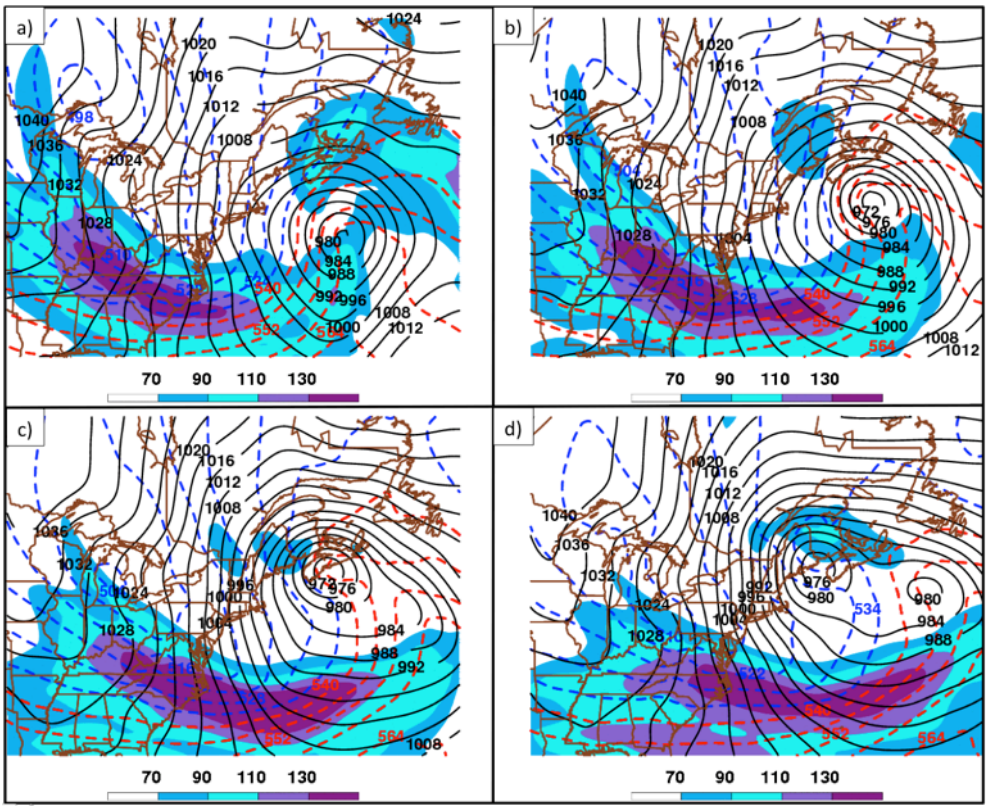

Fig. 4.5. 300-hPa wind speed (kt, shaded), 1000–500-hPa thickness (dam, dashed contours), and mean sea level pressure (hPa, solid contours) at (a) 1200 UTC 02 January 2010, (b) 1800 UTC 02 January 2010, (c) 0000 UTC 03 January 2010, and (d) 0600 UTC 03 January 2010.

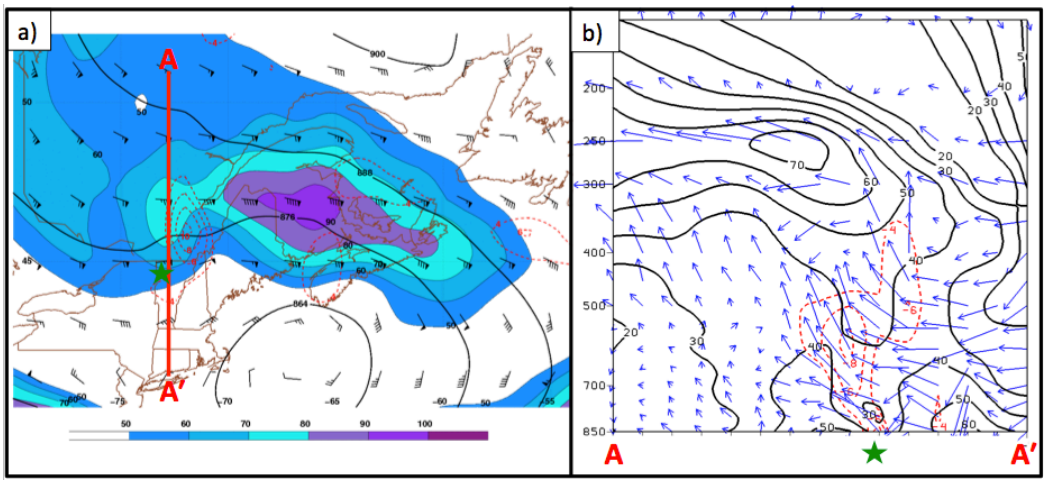

Fig. 4.6. (a) 300-hPa height (dam, solid contours), wind speed (kt, shaded; barbs), and divergence (x 10^{-5} s^{-1}, dashed contours) at 0600 UTC 03 January 2010. (b) Cross-section from A to A´ displaying wind speed (kt, black contours), omega (μb s^{-1}, red contours), and the ageostrophic circulation (kt, arrows) at 0600 UTC 03 January 2010. The green star represents the approximate location of Burlington, VT.

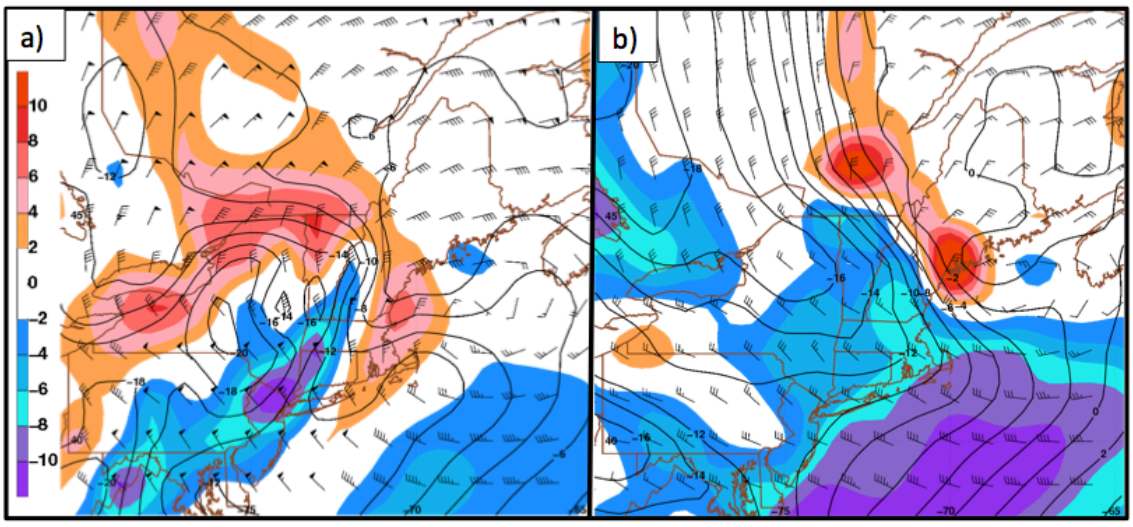

Fig. 4.7. (a) 850-hPa temperature advection (K (6 h) $^{-1}$, shaded), temperature (°C, black contours), and wind speed (kt, barbs) at 0600 UTC 03 January 2010. (b) 925-hPa temperature advection (K (6 h) $^{-1}$, shaded), temperature (°C, black contours), and wind speed (kt, barbs) at 0600 UTC 03 January 2010.

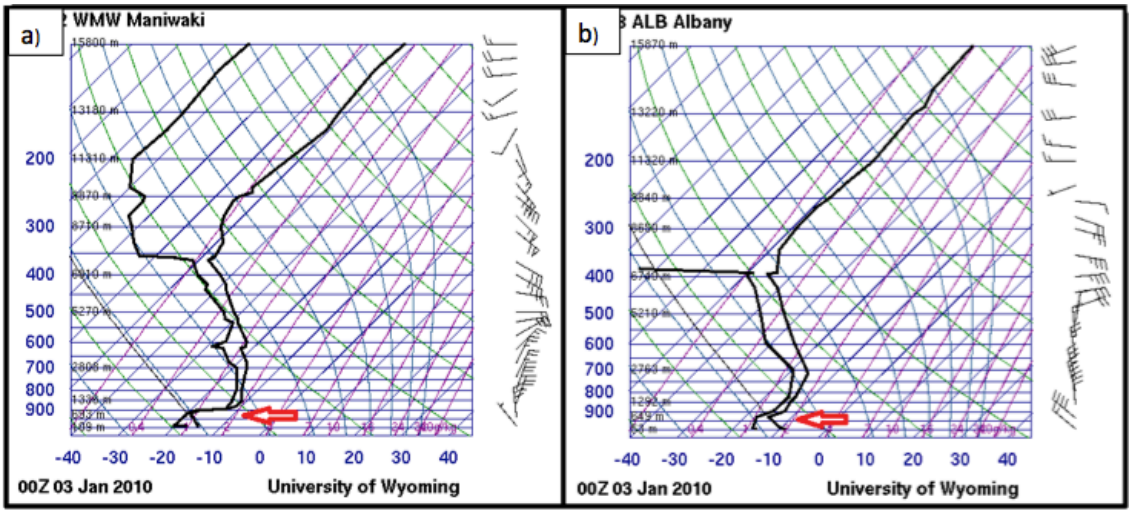

Fig. 4.8. Soundings from (a) Maniwaki, QC (WMW) and (b) Albany, NY (ALB) at 0000 UTC 03 January 2010. Red arrows highlight low-level inversions.

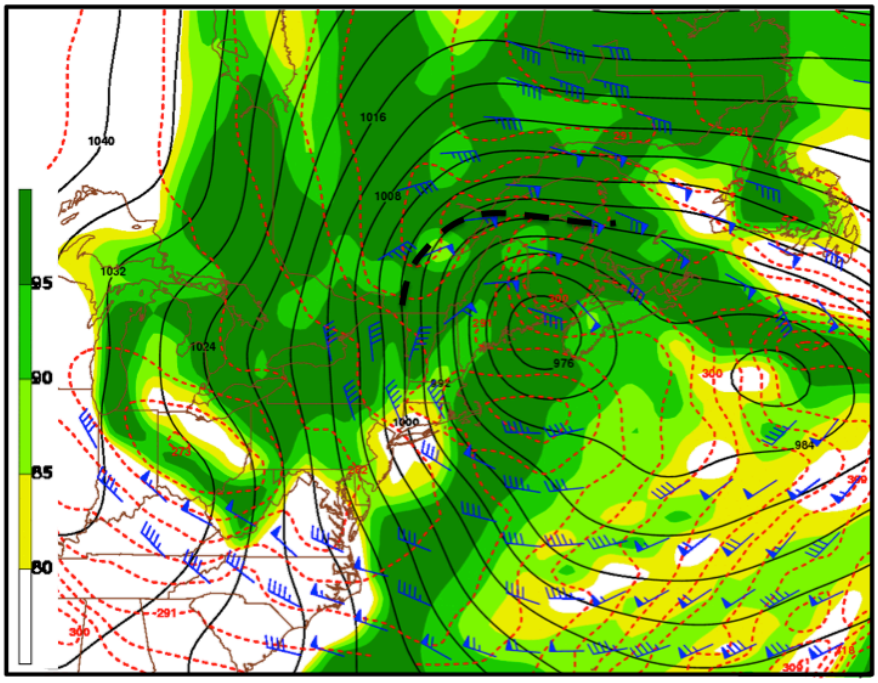

Fig. 4.9. Mean sea level pressure (hPa, solid black contours), 700-hPa equivalent potential temperature (K, red contours), winds (kt, barbs greater than 40 kt), and 925–850-hPa layer average relative humidity (%, shaded) at 0600 UTC 03 January 2010. Black dashed curve represents the approximate location of the trowal axis.

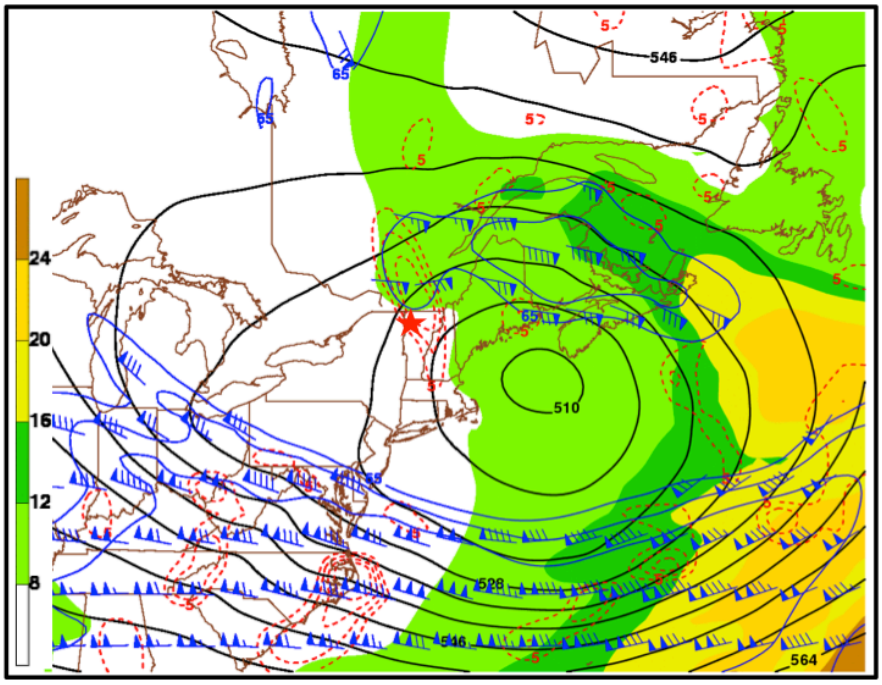

Fig. 4.10. 300-hPa wind speed (kt, barbs greater than 60 kt), 500-hPa geopotential height (dam, black contours), cyclonic absolute vorticity advection (x 10^{-5} s^{-1} (3 h)$^{-1}$, red contours), and precipitable water (mm, shaded) at 0600 UTC 03 January 2010.

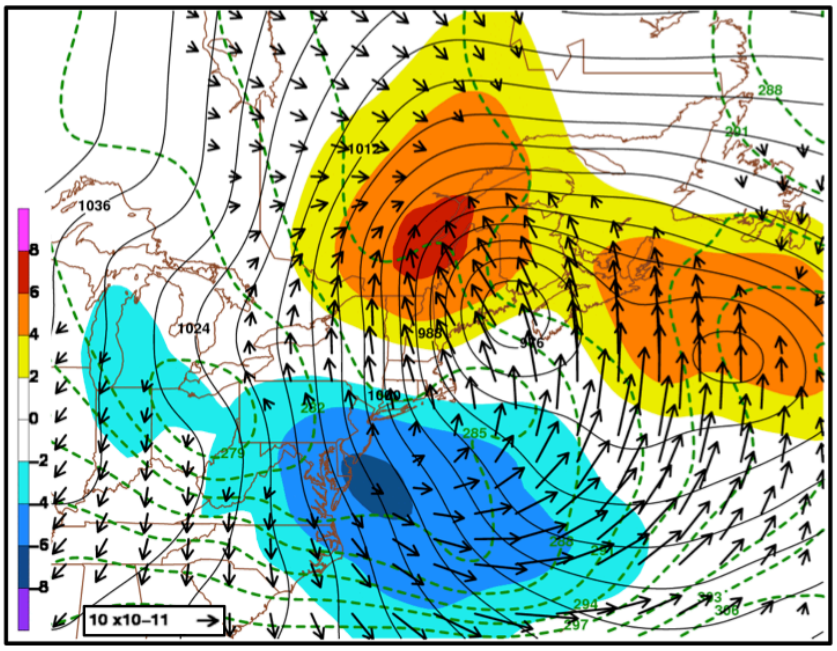

Fig. 4.11. Mean sea level pressure (hPa, black contours), 700-hPa potential temperature (K, green contours), Q-vectors (10^{-11} K m^{-1} s^{-1}, arrows), and Q-vector divergence ($\times 10^{-16}$ K m^{-2} s^{-1}, shaded) at 0600 UTC 03 January 2010.

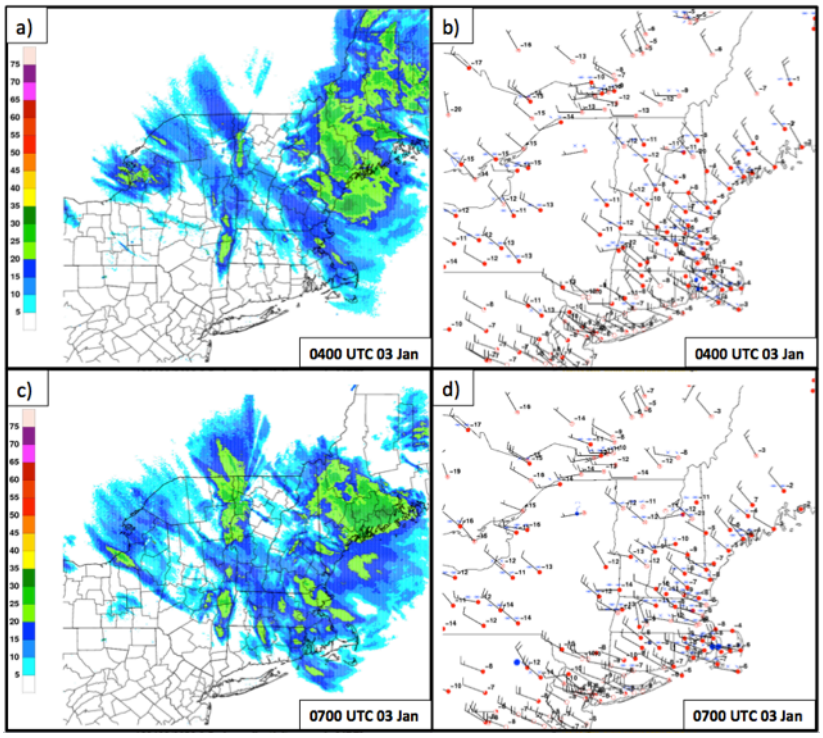

Fig. 4.12. Base reflectivity mosaic (a, c) and surface observations (b, d) at 0400 UTC 03 January 2010 (top panels) and 0700 UTC 03 January 2010 (bottom panels).

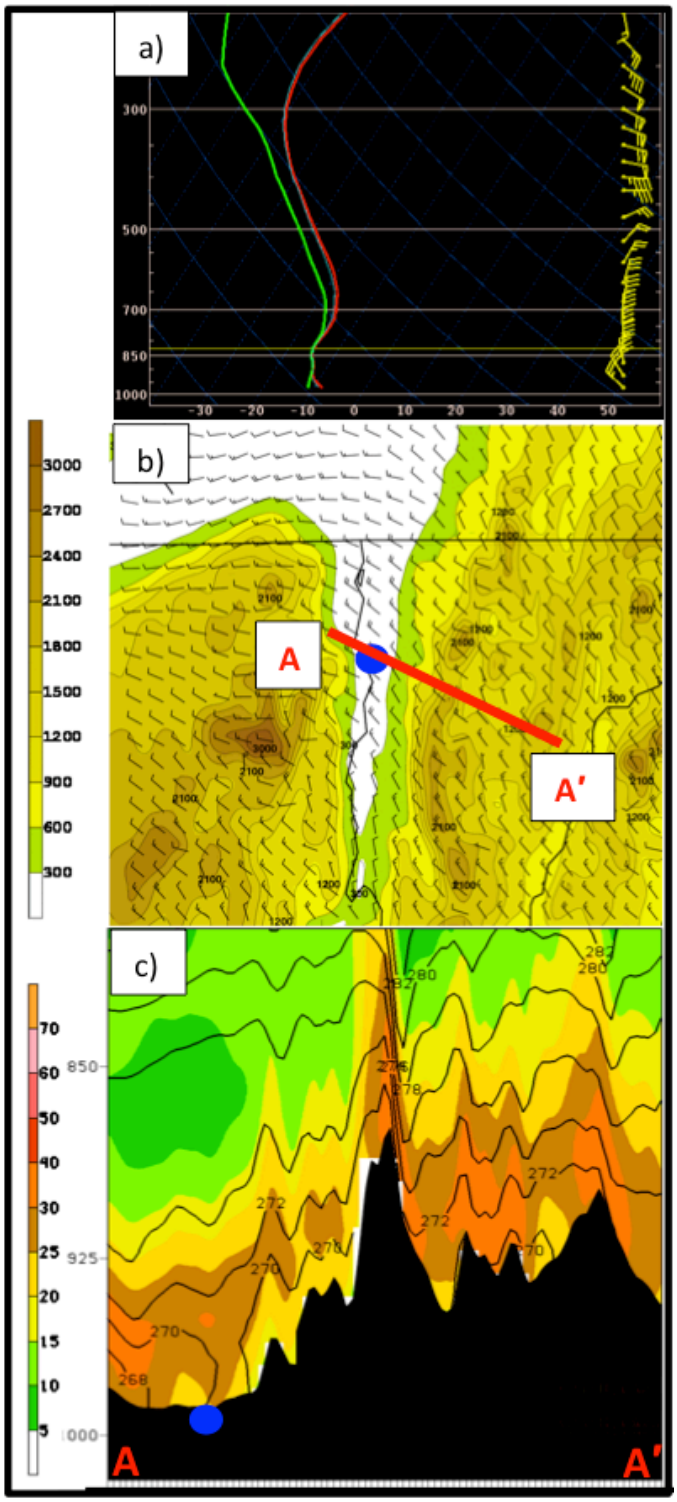

Fig. 4.13. WRF forecast (a) skew-T log P sounding for Burlington, VT, (b) 10 m wind (kt, barbs) and topography (ft, shaded), and (c) equivalent potential temperature (K, black contours) and cross barrier wind speed (kt, shaded) valid at 1800 UTC 02 January 2010. Blue circle denotes the approximate location of Burlington, VT, and the red line denotes the location of the cross-section in (c).

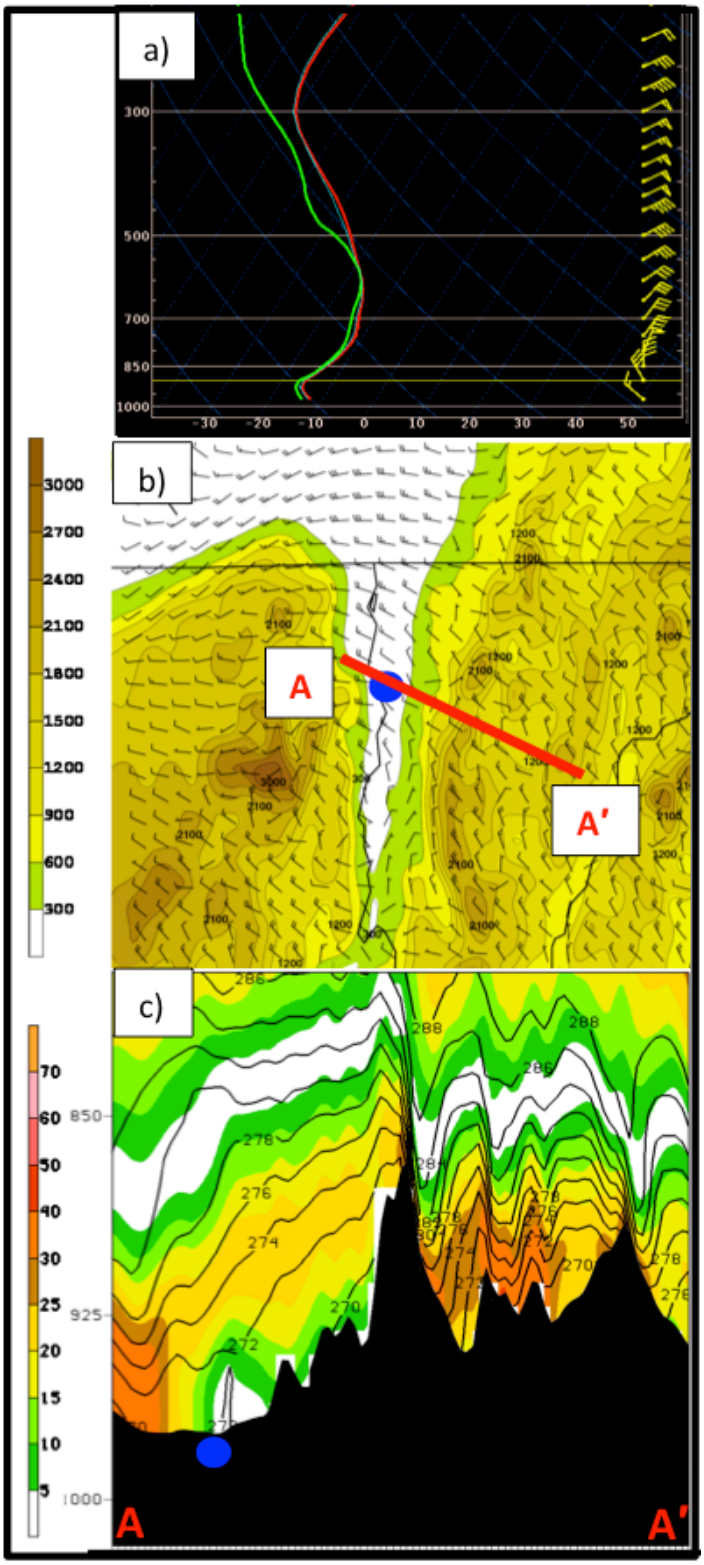

Fig. 4.14. As in Fig. 4.13, except at 0600 UTC 03 January 2010.

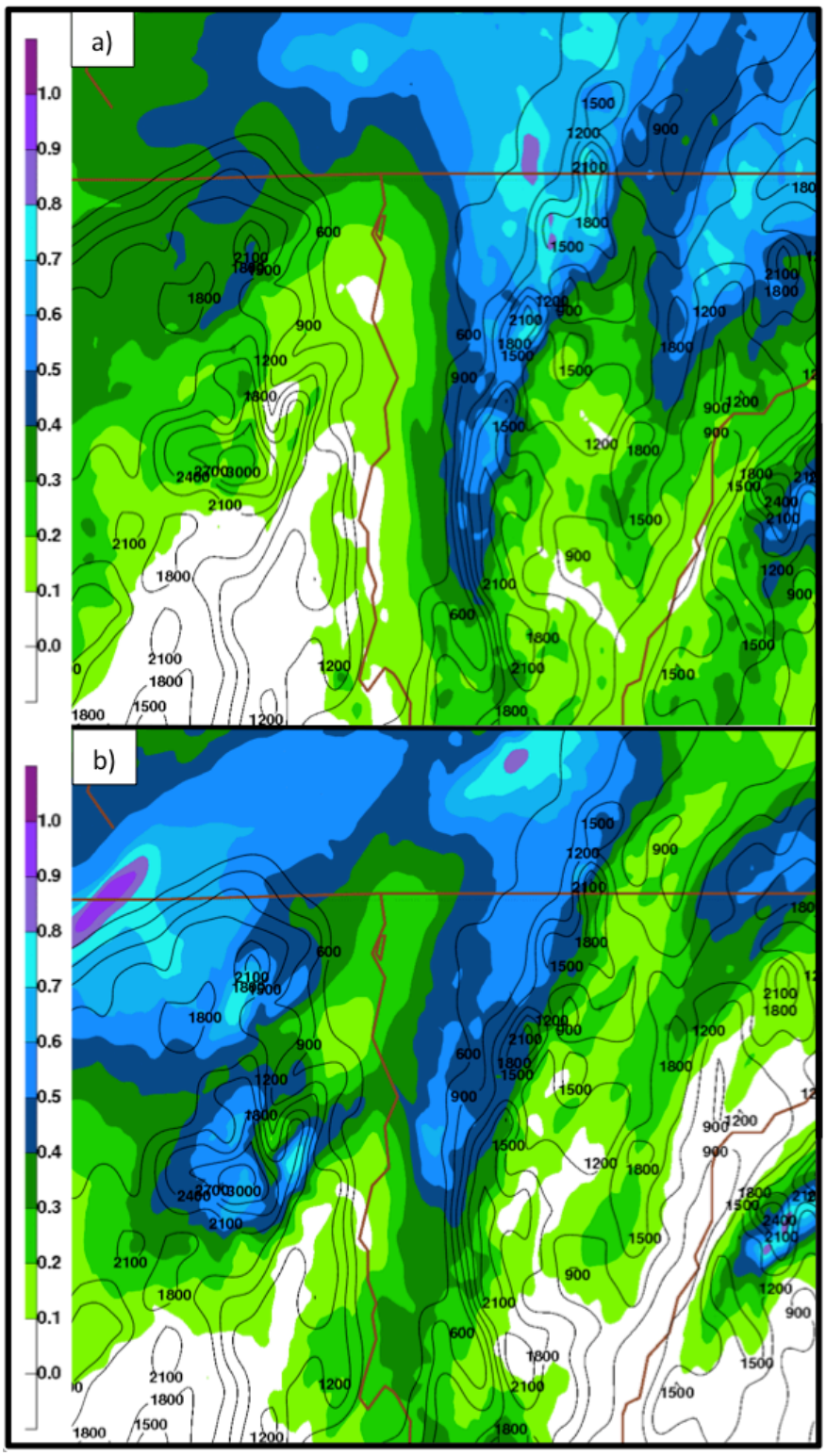

Fig. 4.15. 18-h forecast precipitation (in, shaded) and topography (ft, contours) ending at (a) 0000 UTC 03 January 2010, and (b) 1800 UTC 03 January 2010.

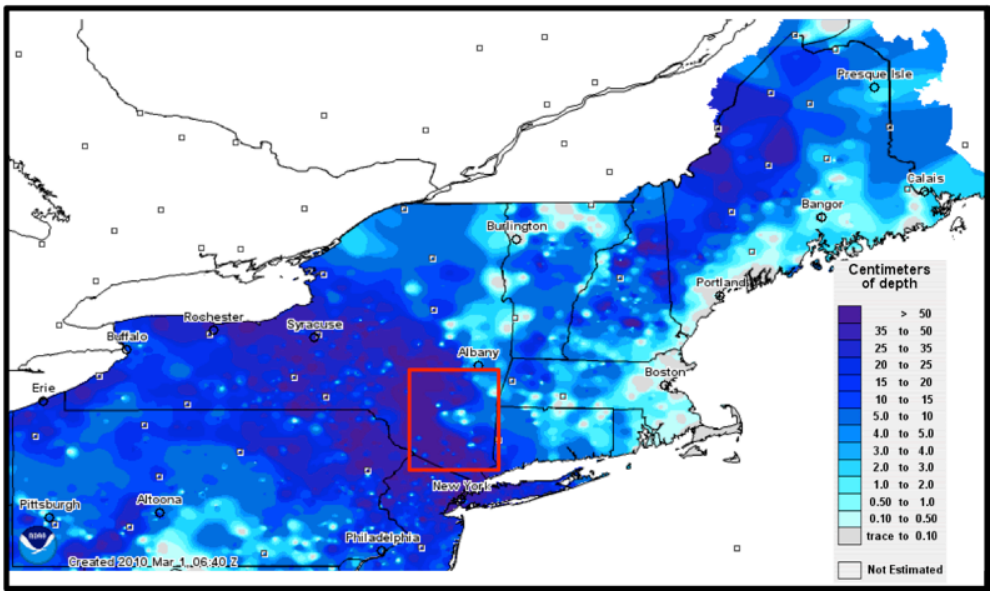

Fig. 4.16. As in Fig. 4.1, except ending at 0000 UTC 27 February 2010. Red box highlights the snowfall gradient in the vicinity of the Hudson Valley.

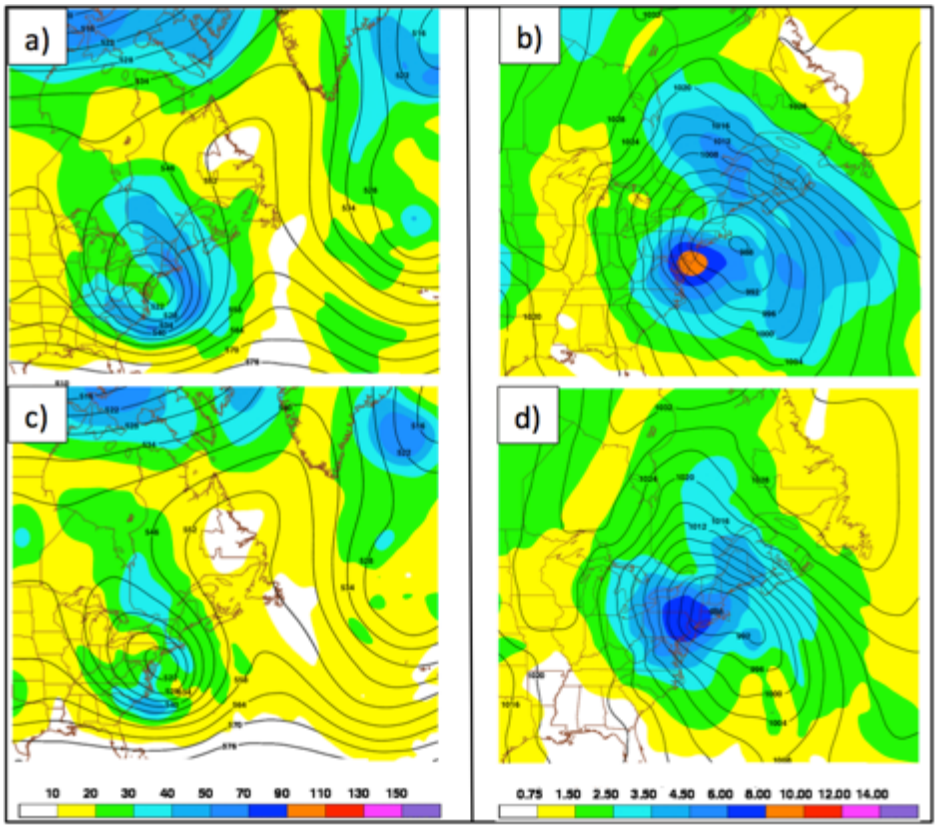

Fig. 4.17. As in Fig. 4.2, except valid at 0000 UTC 26 February 2010 and initialized at (a, b) 0000 UTC 23 February 2010, and (c, d) 0000 UTC 24 February 2010.

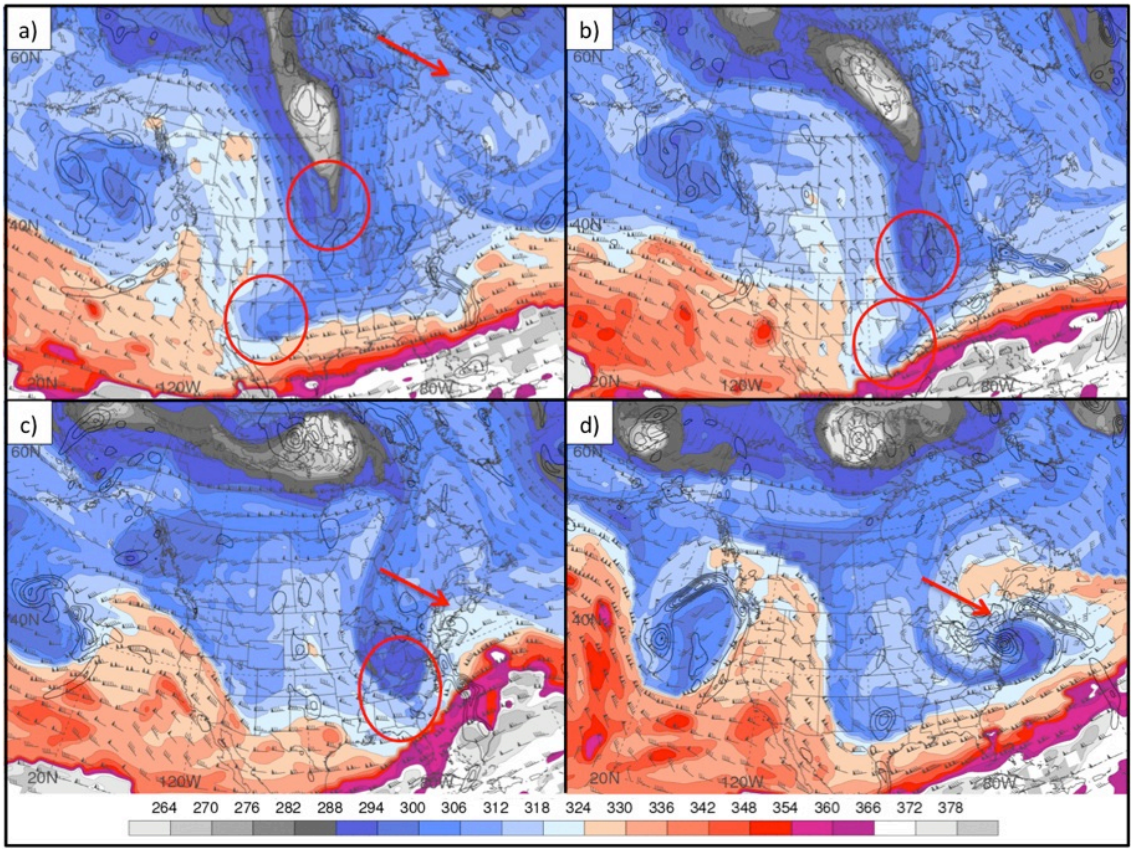

Fig. 4.18. As in Fig. 4.3, except at (a) 1200 UTC 23 February 2010, (b) 1200 UTC 24 February 2010, (c) 1200 UTC 25 February 2010, and (d) 1200 UTC 26 February 2010.

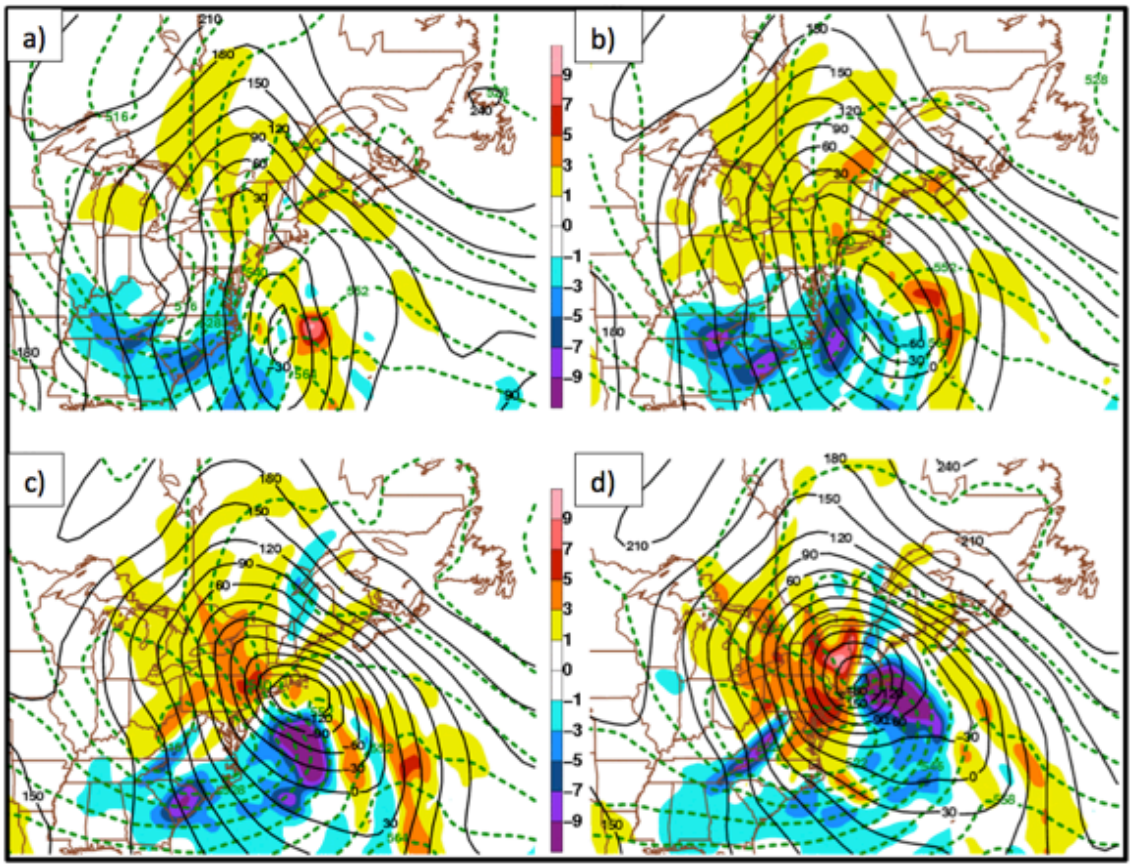

Fig. 4.19. As in Fig. 4.4, except at (a) 1200 UTC 25 February 2010, (b) 1800 UTC 25 February 2010, (c) 0000 UTC 26 February 2010, and (d) 0600 UTC 26 February 2010.

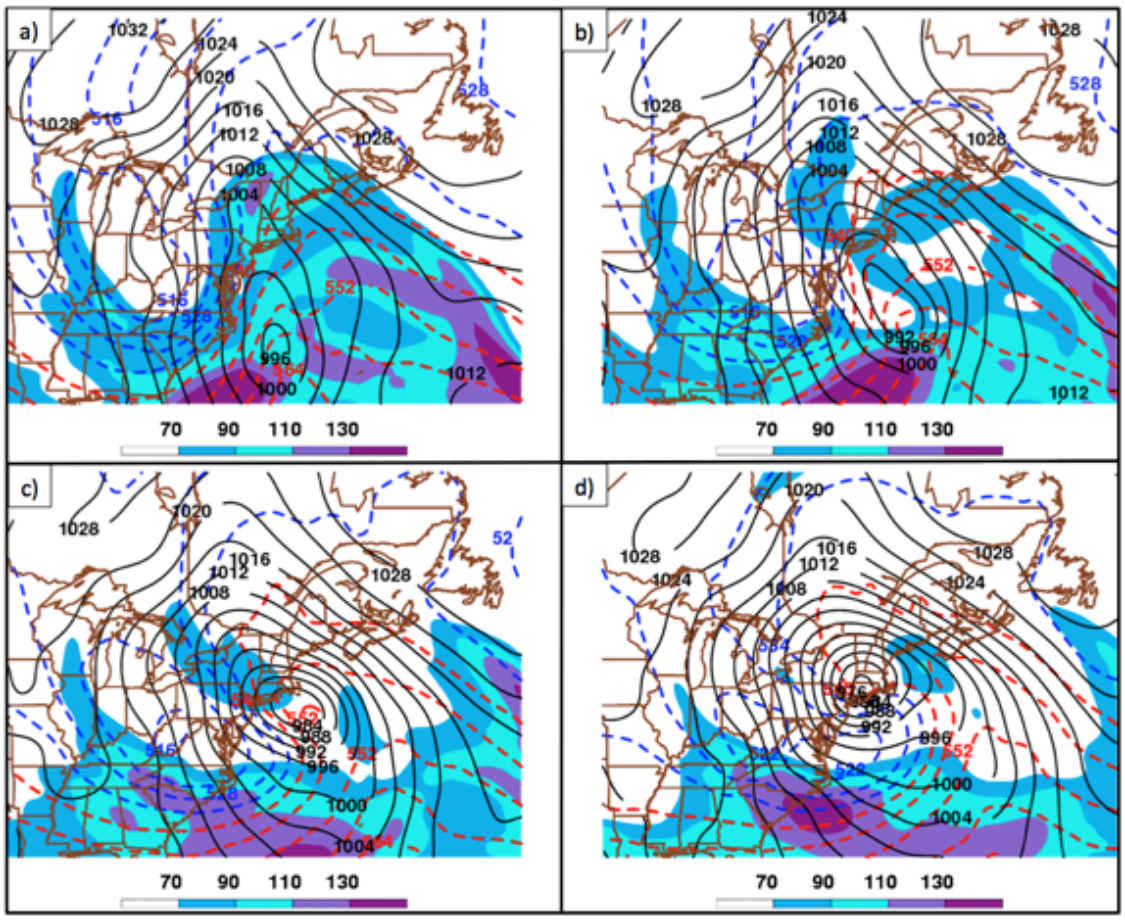

Fig. 4.20. As in Fig. 4.5, except at (a) 1200 UTC 25 February 2010, (b) 1800 UTC 25 February 2010, (c) 0000 UTC 26 February 2010, and (d) 0600 UTC 26 February 2010.

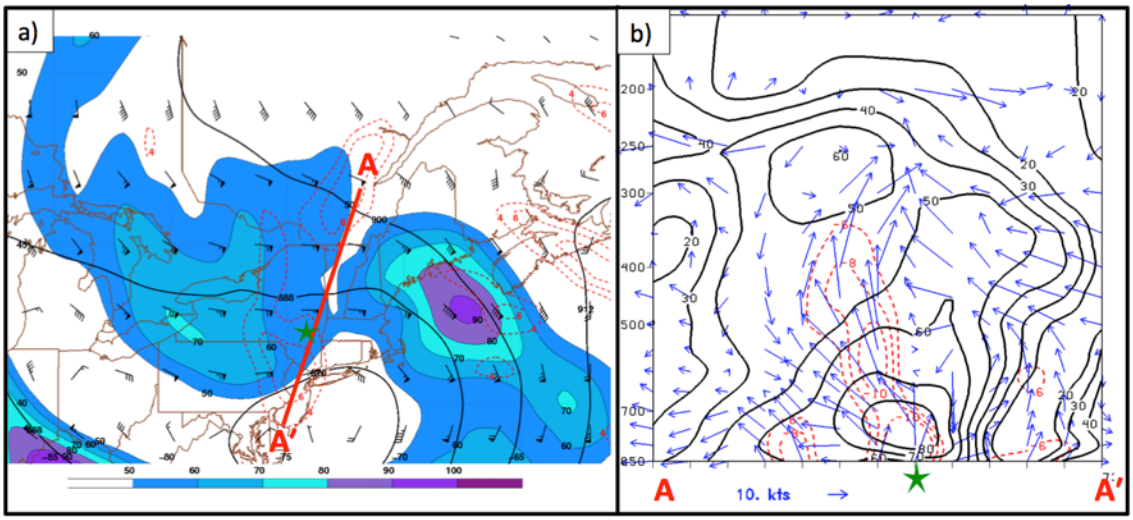

Fig. 4.21. As in Fig. 4.6, except at 0600 UTC 26 February 2010. Green star represents the approximate location of Hunter Mountain, NY.

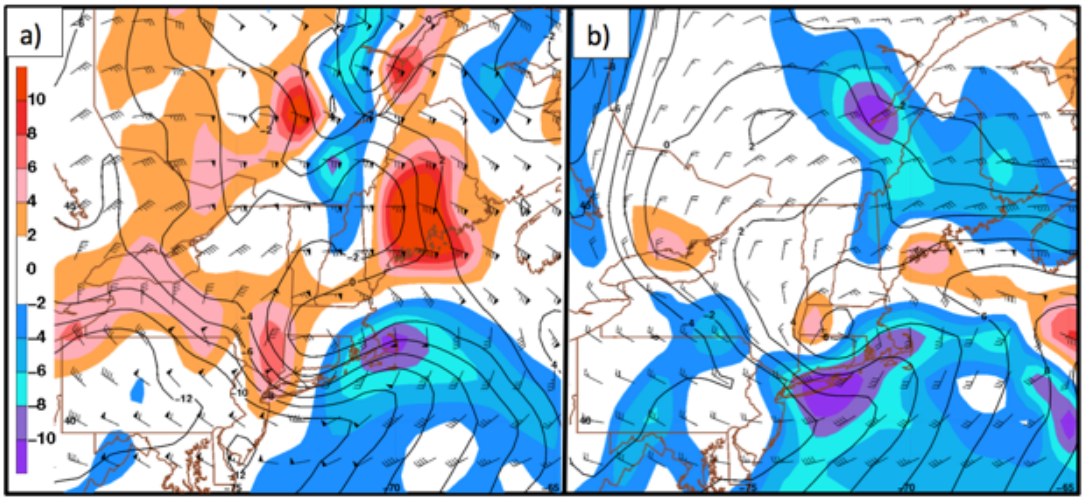

Fig. 4.22. As in Fig. 4.7, except at 0600 UTC 26 February 2010.

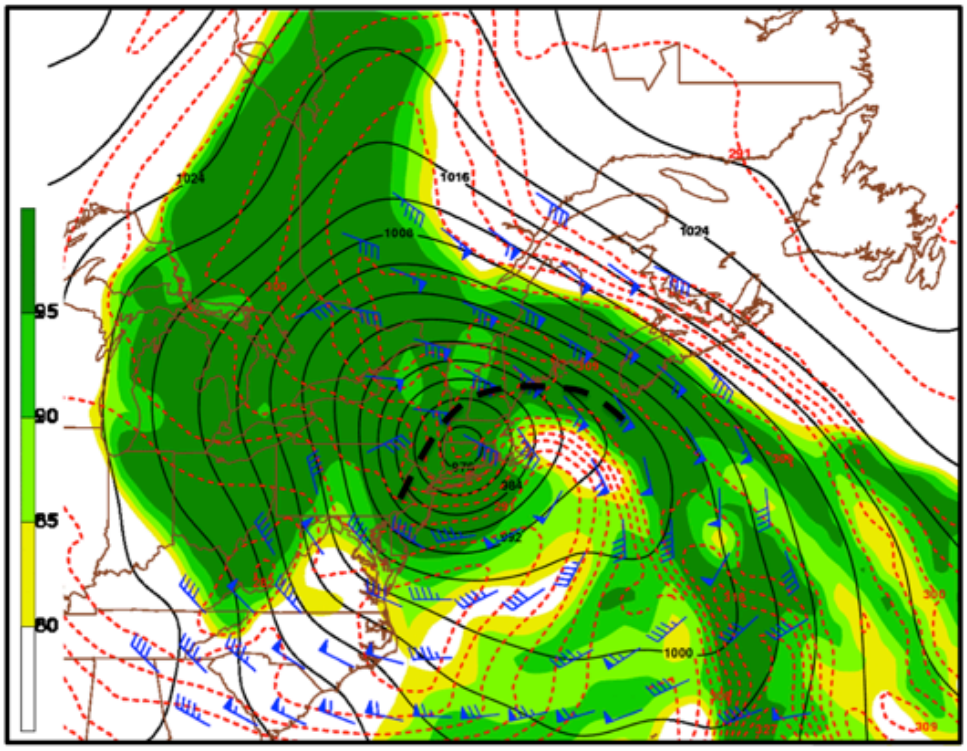

Fig. 4.23. As in Fig. 4.9, except at 0600 UTC 26 February 2010.

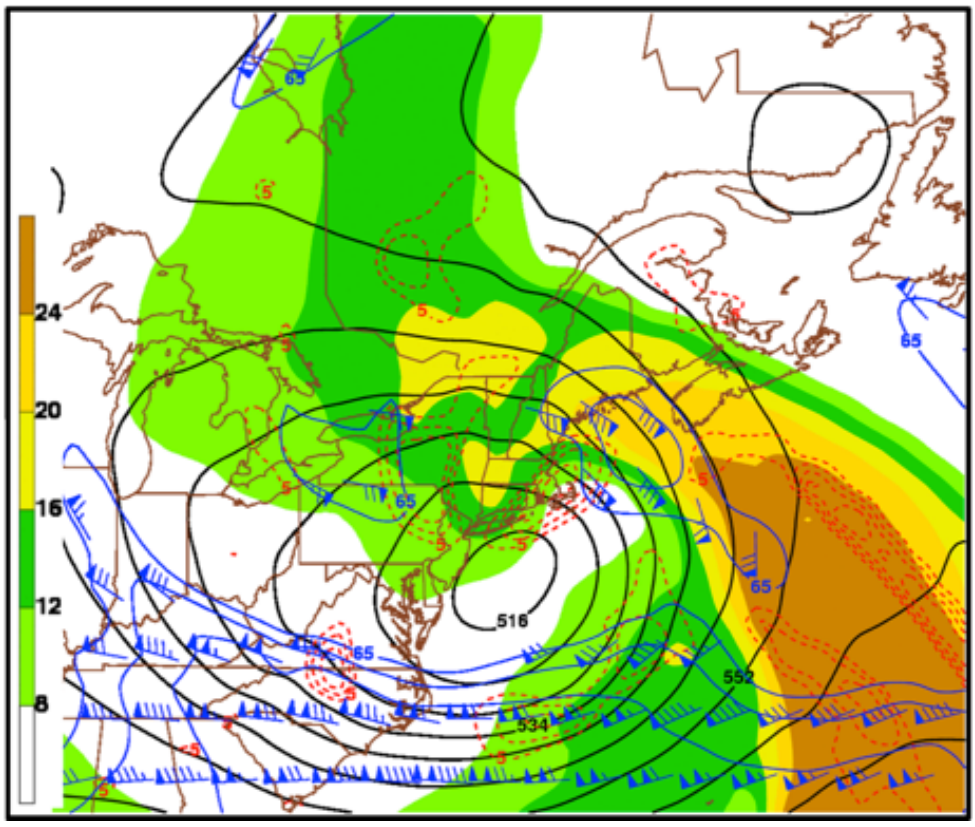

Fig. 4.24. As in Fig. 4.10, except at 0600 UTC 26 February 2010.

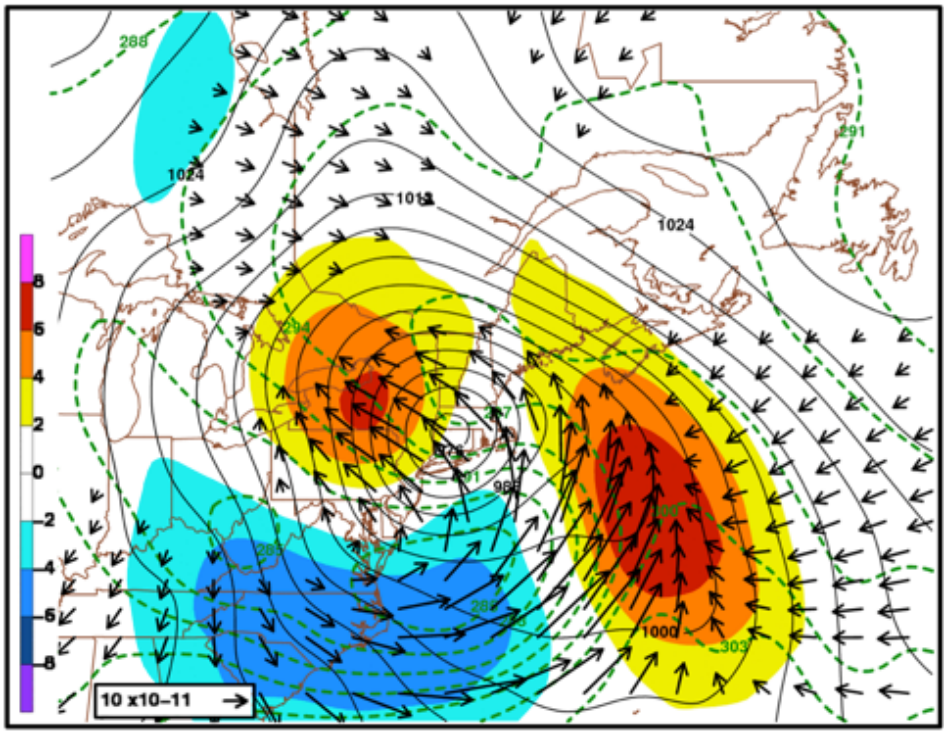

Fig. 4.25. As in Fig. 4.11, except at 0600 UTC 26 February 2010.

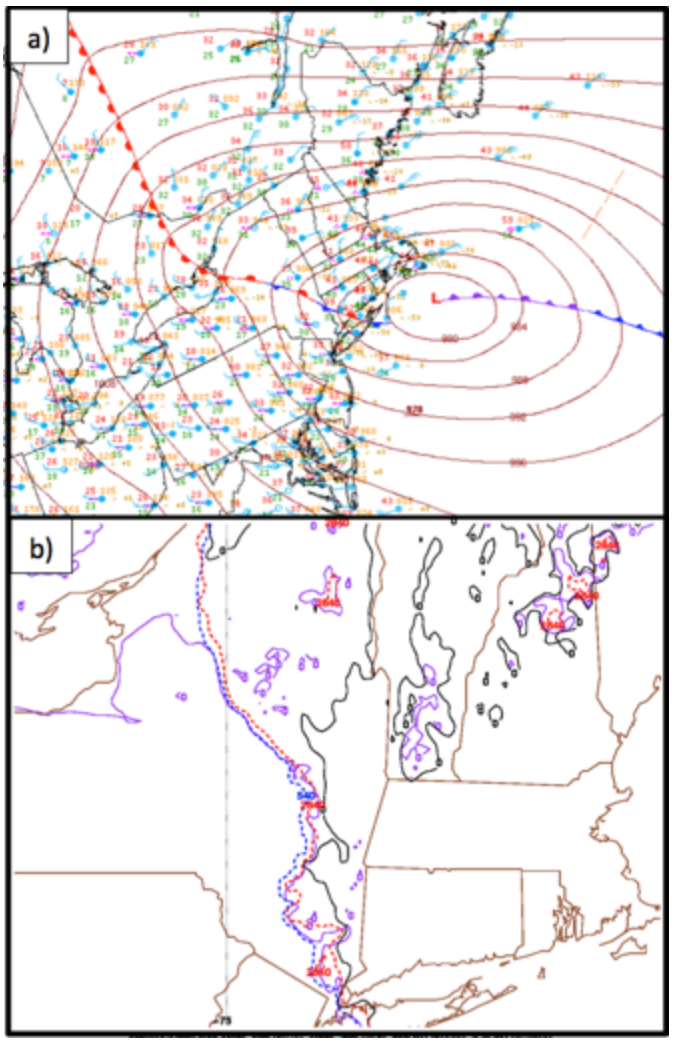

Fig. 4.26. (a) Weather Prediction Center (WPC) surface analysis and (b) 540 dam 1000–500-hPa thickness contour (blue), 2840 dam 1000–700-hPa thickness contour (red), 850-hPa 0°C isotherm (black), and 0°C 2-m temperature isotherm (purple) at 0000 UTC 26 February 2010.

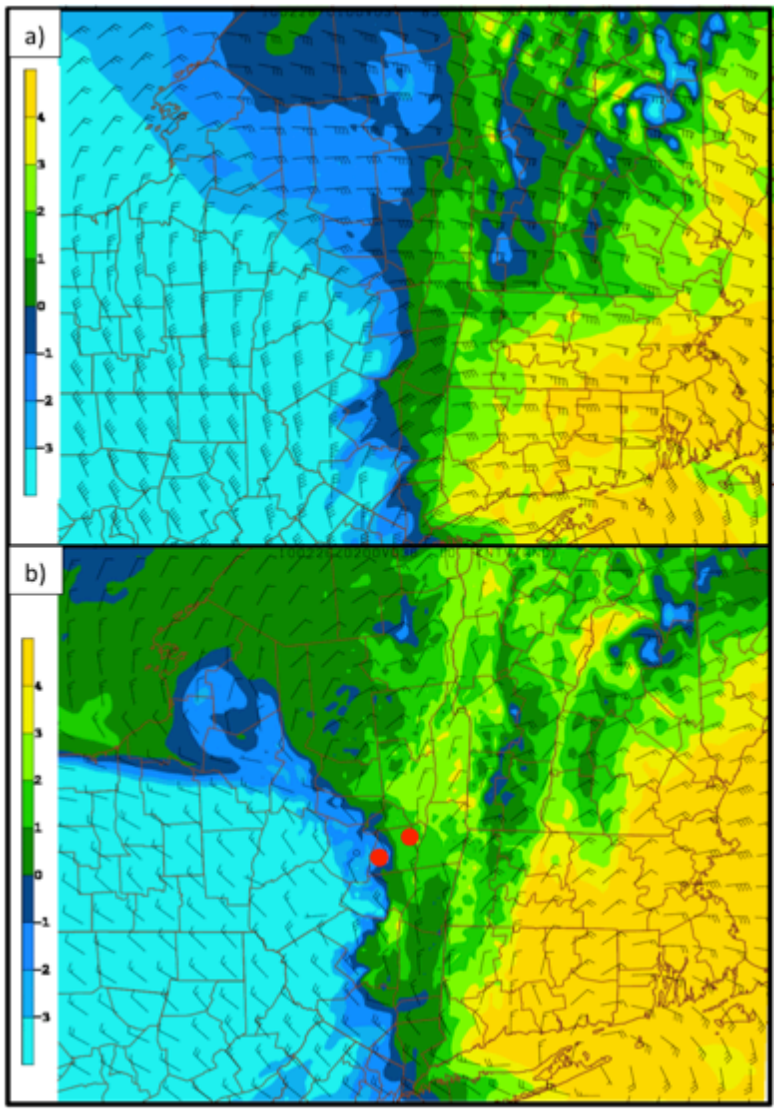

Fig. 4.27. (a) 850-hPa temperature (°C, shaded) and wind (kt, barbs) and (b) 2-m temperature (°C, shaded) and wind (kt, barbs) at 0600 UTC 26 February 2010. Red circles indicate the approximate locations of Albany and Potter Hollow, NY for the soundings shown in Figure 4.28.

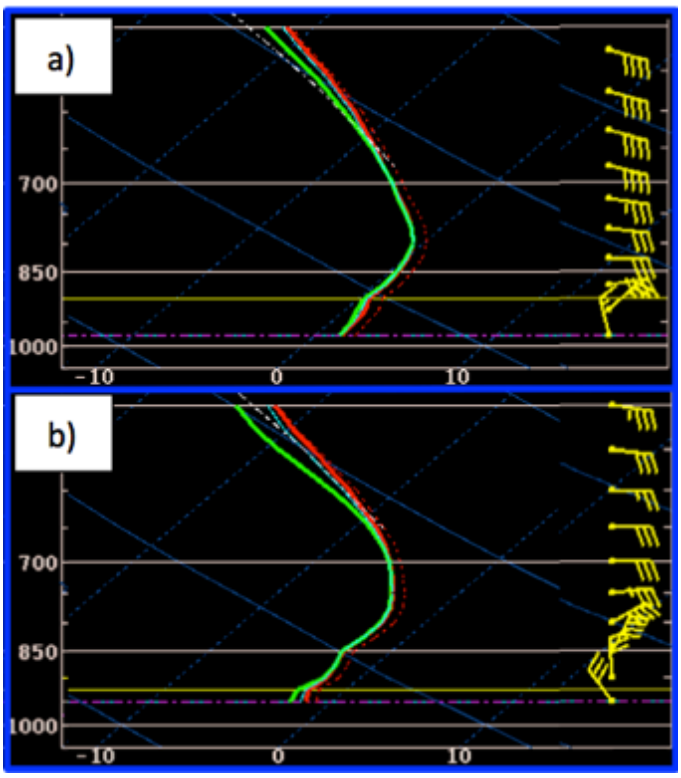

Fig. 4.28. WRF forecast skew-T log P soundings for (a) Albany, NY and (b) Potter Hollow, NY valid at 0600 UTC 26 February 2010.

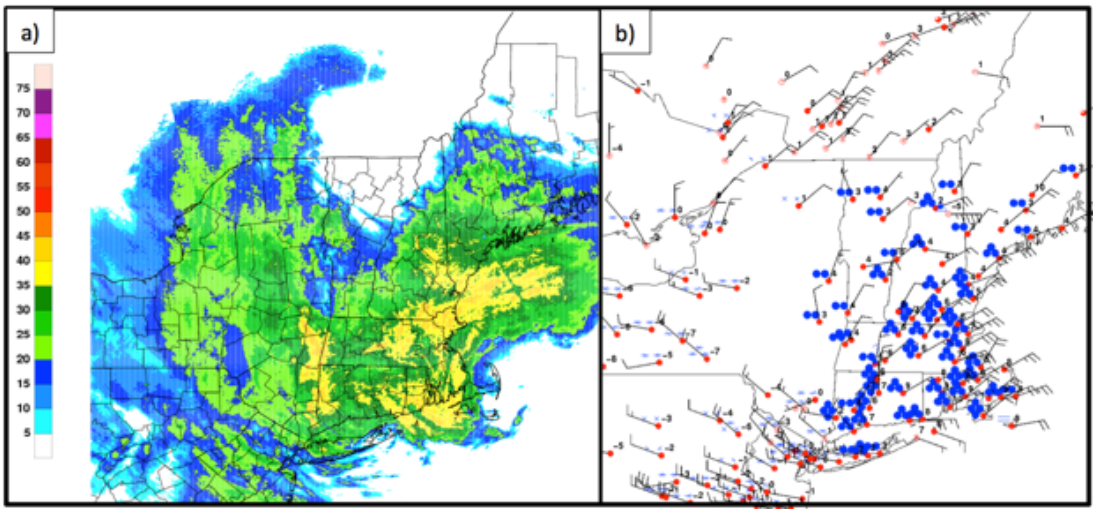

Fig. 4.29. As in Fig. 4.12, except at 0600 UTC 26 February 2010

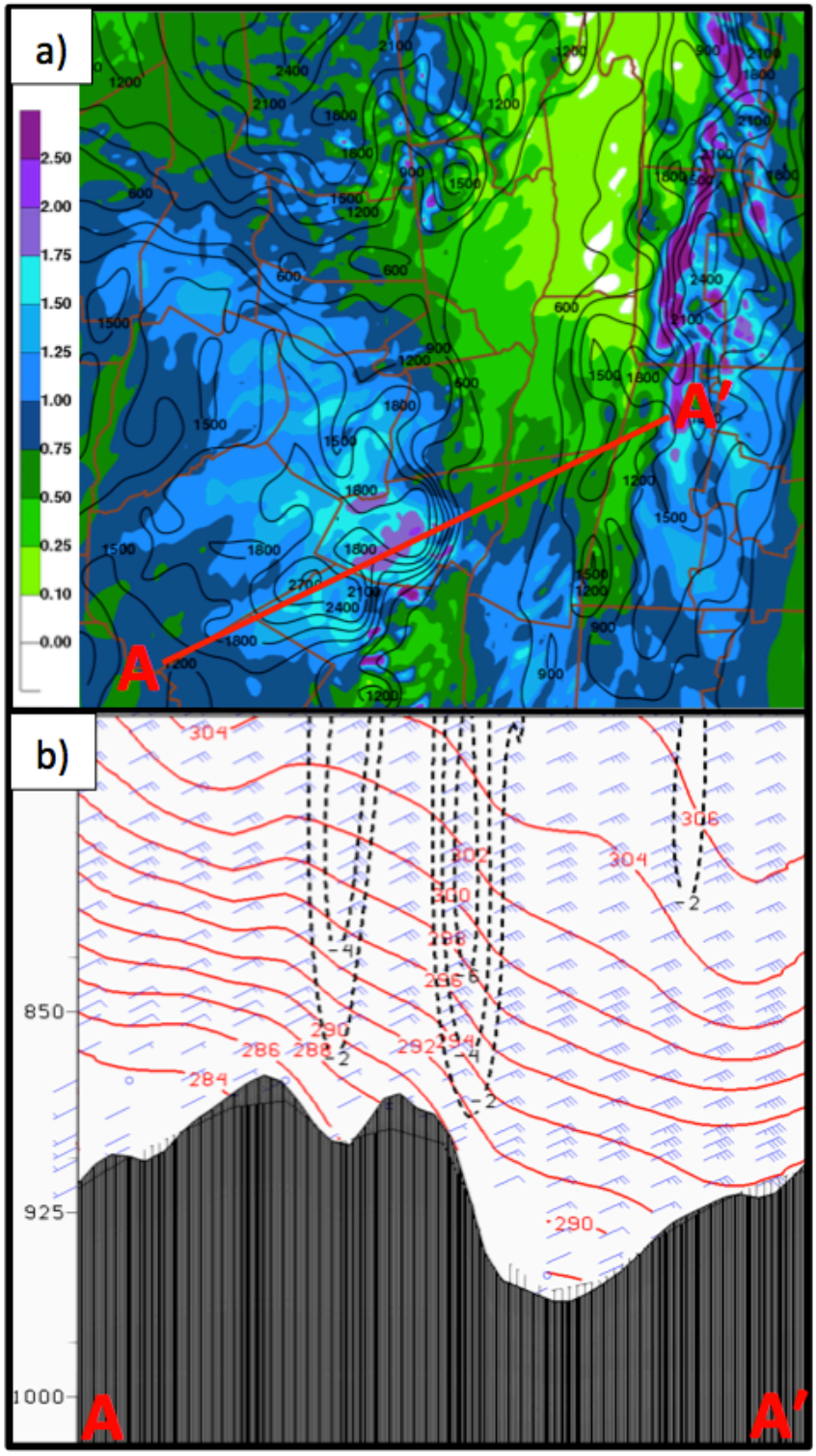

Fig. 4.30. (a) WRF forecast 48-h precipitation (in, shaded) valid at 0000 27 February 2010. (b) Cross-section of equivalent potential temperature (K, red contours), omega (μb s^{-1}, black contours), and cross-barrier wind speed (kt, barbs) valid at 0600 UTC 26 February 2010. Red line in (a) denotes the y-z cross-section in (b).

5. Discussion and Conclusions

5.1 Discussion

5.1.1 ACE Climatology and Statistics

Past studies have performed climatological analyses and developed numerous statistics regarding various aspects of Northeast U.S. cool season cyclones (e.g., Lackmann et al. 1996; Kocin and Uccellini 2004; Archambault et al. 2008, 2010). This current work represents the first attempt to explicitly define and analyze Northeast cool season cyclones associated with significant upper-level easterly wind anomalies, or ACEs, using similar methods. A climatological analysis of ACEs revealed that the majority of events occurred during the months of December through April, with a large increase in cutoff low events during the month of April (Fig. 3.3). This result is consistent with Payer (2010), who found that Northeast U.S. cool-season cutoff cyclone frequency was maximized during the month of April. The relative lack of ACEs during the beginning of the cool season is likely a result of weaker baroclinicity across the contiguous U.S., a poleward displaced mid-latitude jet stream, and a lack of maintained blocking regimes across the North Atlantic Ocean.

An inspection of ACE duration in the Northeast U.S. cyclone domain revealed that EJS events have the longest duration (46 h ± 3 h), while open wave events have the shortest duration (30 h ± 2 h; Fig. 3.4). This disparity is a result of significantly different upper-level flow regimes between the two types of ACEs. EJS events are associated with a deep, closed, upper tropospheric circulation and a domain average 300-hPa zonal wind

minimum of −67 kt, while open wave events are associated with a highly amplified, negatively tilted, upper tropospheric trough and a domain average zonal wind minimum of –25 kt. Strong easterly flow is prominent on the northern flank of the closed upper-level circulation during EJS events, while weaker easterly flow is present downstream of a negatively tilted upper-level trough axis during open wave events. The mean EJS event surface cyclone track displays a westward jog and a cyclonic loop as the upper-level low stalls and the entire system becomes vertically stacked, effectively increasing the duration of the event (Fig. 3.5). This process can be highly accentuated during individual EJS events, some of which initially progressed northeastward, only to track back westward across 4–6° of longitude. The mean open wave event surface cyclone tracks north-northeastward (Fig. 3.5), while remaining downstream of a slightly more progressive, yet highly amplified, upper tropospheric trough, leading to a shorter duration event. These results are consistent with Kocin and Uccellini (2004), who note that a small group of Northeast snowstorm cases display a preexisting closed circulation in the middle and upper troposphere, and are marked by a long duration snowfall and a slow moving surface cyclone.

Kocin and Uccellini (2004) describe a historical Northeast snowstorm referred to as the "Blizzard of '88" (11–14 March 1888), which is said to have, "initially raced northeastward from the Carolina coast to southern New England, then remained nearly stationary close to the southern New England coast for two days, performing a slow counterclockwise loop south of Rhode Island". This description, along with the observation of a north-south oriented stationary front along the Hudson Valley of New York (Kocin and Uccellini 2004), is consistent with EJS events observed in this study,

suggesting that the historical "Blizzard of '88" would fit into this category. Kocin and Uccellini (2004) attribute the unusual cyclone track to a process where the surface cyclone slows as the upper-level low cuts off directly over the surface cyclone. This idea can be built upon by considering the evolution of upper-level forcing in the presence of a closed upper-level circulation. In cases like the "Blizzard of '88", where there is a transition from an open to a closed upper-level circulation, the surface cyclone is pulled westward beneath the region of strongest upper-level divergence, collocated with the mid-level warm air advection maximum. This leads to a deceleration of the surface cyclone, allowing it to remain quasistationary or perform a small cyclonic loop before drifting eastward. Other cases display a preexisting northern stream cutoff circulation over the Northeast U.S., with a southern stream shortwave and cyclonic vorticity maximum approaching from the south. As the southern stream shortwave begins to interact with the northern stream, a surface low pressure develops and tracks northeastward, remaining downstream of the vorticity maximum in a region of cyclonic vorticity advection. As the vorticity maximum rotates around the periphery of the closed upper-level circulation, the attendant surface low pressure performs a large cyclonic loop while becoming vertically stacked. This leads to a more significant westward retrogression of the surface low pressure, and a more challenging forecast overall.

5.1.2 Teleconnection Responses

Prior work has shown that the negative phase of the AO/NAO is conducive for increased Northeast U.S. snowstorm frequency, with significant moisture transport inland

from the Atlantic Ocean during cyclone events (Kocin and Uccellini 2004; Archambault et al. 2008, 2010). The occurrence of high-latitude blocking, especially across the North Atlantic Ocean during negative AO/NAO periods (e.g., Woolings et al. 2008), favors a weak mid-latitude jet stream and frequent cold air outbreaks across the Northeast U.S. The mean daily AO and NAO values for all ACEs are −1.1 SD and −0.45 SD, respectively, with EJS events averaging more negative values than cutoff low and open wave events. This suggests that ACEs (especially EJS events) are more common during periods of maintained upper tropospheric ridging across the high latitudes. A lack of strong high-latitude ridging appears to preclude the development of EJS events in particular. The AO displayed a much stronger negative signal than the NAO for all events, indicating that the longitudinal axis of the upper-level block is paramount, and the NAO domain may be too spatially limited to display a useful signal in some cases. The AO domain, being much larger, provides a more robust signal during periods of extreme "west-based blocking" in which positive upper-level height anomalies are centered across northeastern North America or in the vicinity of the Hudson Strait.

The trend of the AO/NAO from one week prior to event occurrence to event occurrence was negative for all ACE categories, with EJS events averaging the most significant negative trend. The AO trend for EJS events was −0.93 SD while the NAO trend was −0.47 SD, indicating a substantial change in the high-latitude flow regime favoring upper-level ridging across North America and the North Atlantic Ocean and troughing across the Northeast U.S. The development of an ACE along the East Coast appeared to provide a positive feedback, transporting low PV air poleward and helping to reinforce the upper-level block and negative AO/NAO regime. This observation is

consistent with the results of Archambault et al. (2010) who found that during NAO^+ to NAO^- transitions, Northeast U.S. cyclones tend to enhance a North Atlantic ridge and develop a sustained blocking pattern. Kocin and Uccellini (2004) note that Northeast U.S. snowstorms are favored during negative NAO regimes in which there is a strong Greenland block or anticyclone. The current results supplement these conclusions and suggest that EJS events are favored during negative AO regimes in which there is a strong west-based block over the Hudson Strait.

Archambault et al. (2008) also found that during a positive PNA and negative NAO regime, a meridional flow pattern conducive for east coast cyclone development can present itself. An amplified ridge over the western U.S. helps deepen a downstream trough over the eastern U.S., increasing the likelihood of cyclogenesis along the East Coast. The preferred PNA phase for all ACEs was positive with a mean daily value of 0.49 SD. The mean PNA trend for all ACEs was +0.26 SD, indicating that a west coast ridge was amplifying significantly during the period leading up to cyclone development. The similarities between the results of the present study and Archambault et al. (2008, 2010) are encouraging and supportive. The current work suggests that a modestly rising PNA index coupled with a rapidly declining AO/NAO index is associated with the development of ACEs, assuming one or more potent upper level disturbances are present. ENSO displayed a much weaker signal during the majority of ACEs, indicating that it has less of an impact on ACE development.

5.1.3 Composite Analyses

Building upon the trend of various teleconnections, the earth- and cyclone-relative composites illustrate the physical mechanisms to which the teleconnection indices respond. The earth-relative composites seen in Figures 3.11–3.15 depict the evolution of the large-scale Rossby wave pattern accompanying the three types of ACEs. The lagged composites display general similarities to those of Lackmann et al. (1996), who explored the multiday period preceding explosive cyclogenesis in the western North Atlantic Ocean, yet some important distinctions exist. At t_{-48}, a region of positive standardized height anomalies exists across the western U.S. indicative of a developing ridge, while negative standardized height anomalies are in place across the south central U.S. (Figs. 3.13a–c). The same Rossby wave pattern is present at t_{-48} in the composite analyses from Lackmann et al. (1996); however, the greatest positive height anomalies are located further northwest over western British Columbia, and the greatest negative height anomalies are slightly weaker and further north (Fig. 1.6). The decreased distance between the negative and positive height anomaly centers (ridge and trough axis) in the ACE composites suggests a much more amplified, meridional flow pattern prior to ACE development.

The most notable feature in all ACE composites at t_{-24} is a large region of positive standardized height anomalies extending from northeast Canada toward southern Greenland (Figs. 3.14a–c). This is indicative of an upper-level block, of which the EJS composite displays the strongest, and open wave composite displays the weakest. The location of the block in all ACE composites is much further south and west than in the explosive cyclone composite (Fig. 1.6), suggesting that a block centered well west of Greenland is fundamental to ACE development. Prominent ridging across northeastern

Quebec acts twofold: first, to impede the progression of the upstream cyclogenetic trough, and second, to allow for a stronger height anomaly dipole and greater easterly flow aloft over southern Quebec (especially in the EJS composite).

A distinct region of negative height anomalies appears across the southern U.S. at t_{-48} (Figs. 3.13a–c) and amplifies significantly at t_{-24} (Figs. 3.14a–c), whereas this feature is lacking in the explosive cyclogenesis composites (Fig. 1.6). This indicates that a potent southern stream shortwave is also central to the development of ACEs, and that the rapid amplification of the cyclogenetic trough at t_{-24} is likely the result of a trough merger.

Consistent with Sanders and Gyakum (1980), intensification of each ACE composite surface low occurred downstream of the planetary-scale trough just off the East Coast of the U.S. The EJS event composite displayed the most rapidly intensifying surface low as a result of a more amplified, negatively tilted trough demonstrating the greatest decrease in the half wavelength between the trough axis and the downstream ridge (Fig. 3.14a). At t_0, the EJS and cutoff low composites exhibited cutoff low development similar to the LC2 scenario proposed by Thorncroft et al. (1993), in which a negatively tilted trough wraps up cyclonically allowing for a cutoff cyclone poleward of the mean jet stream. This suggests that cyclonic wave breaking is only associated with ACEs that occur in conjunction with a strong downstream block. As the upper-level low cuts off, a significant downstream response is evident, acting to further amplify the positive height anomaly across northeast Canada. This process is similar to that observed by Archambault et al. (2010), in which low PV air is brought poleward, downstream of a developing Northeast cyclone (Fig. 1.7). Archambault et al. (2010) notes that this process

is enhanced during cyclonic wave breaking events, such as during EJS and cutoff low events.

Common to all three types of ACEs is a negatively tilted large-scale trough, with a precipitable water axis downstream, directed from southeast to northwest toward the Northeast U.S. This bears great similarity to the composite analyses of cool-season Northeast precipitation events occurring during negative NAO regimes from Archambault et al. (2008); however, the tilt of the upper-level trough and precipitable water axes are more extreme. A coherent easterly jet streak is visible across northeast New England in the EJS composite, whereas in the cutoff low and open wave composites a more southerly jet streak exists further to the east. QG forcing for ascent is present in the equatorward exit region of an easterly jet streak in the EJS composite, contributing to forcing for ascent to the northwest of the surface low. Of greatest importance is the thermal advection pattern associated with each type of ACE. EJS events show the strongest thermal advection dipole, with warm air advection wrapping around the occluded sector of the cyclone. A well-defined trowal (i.e., θ_e) axis supports QG forcing for ascent at the nose of the warm sector and widespread wrap-around precipitation. Trowal development is slightly less pronounced in the cutoff low and open wave composites, as warm air advection does not extend as far northwest of the surface cyclone. The orientation of Q-vectors in the trowal region of EJS and cutoff low events implies that the convergence of Q_s is the predominant forcing mechanism for QG vertical motion, strongly supporting the work of Martin (1999). During open-wave events, increased low- to mid-level frontogenesis northwest of the surface cyclone likely supports distinct banded precipitation in the vicinity of the trowal. This inference is

consistent with Novak et al. (2010) and Kenyon (2013), who observed pivoting snowbands in the presence of trowals in conjunction with mid-level frontogenesis.

5.1.4 Case Studies of Two High Impact EJS Events

EJS events from 2–3 January and 25–27 February 2010 were chosen for case studies because of their high societal impact and marked resemblance to the EJS event composites. GEFS forecasts of 500-hPa height and mean sea level pressure displayed significant variability at lead times of only 48 h, leading to a low confidence forecast in both cases (Figs. 4.2, 4.17). The evolution of both events involved the interaction of northern and southern stream disturbances along the east coast of the U.S. (Figs. 4.3, 4.18), as a deepening surface low pressure retrograded westward from the North Atlantic Ocean toward the New England coast (Figs. 4.4, 4.19). Both cases displayed strikingly similar cyclonic wave breaking events, largely a result of a massive quasistationary upper-tropospheric block located directly downstream (Figs. 4.3, 4.18). Strong northerly warm air advection was present to the northwest of the surface low pressure in both cases (Figs. 4.7, 4.22), similar to the EJS event composite (Fig. 3.16b). QG forcing for ascent was most substantial in the occluded sector of both cyclones, along and northwest of the trowal axis. Cross sections taken through the exit regions of both easterly jet streaks revealed upward vertical motion beneath the equatorward jet exit region, in the ascending branch of a thermally indirect vertical circulation (Figs. 4.6, 4.21).

Mesoscale forcing embedded in synoptically driven circulations modified the total snowfall during both events, leading to strong and unusual gradients in the total snowfall

distributions (Figs. 4.1, 4.16). A WRF simulation of the 2–3 January 2010 event displayed moist low-level northwesterly flow, channeling down the Champlain Valley and converging in the vicinity of Burlington, VT. The presence of a stably stratified lower atmosphere prevented the low-level flow from directly ascending over the Green Mountain spine, and instead forced the flow to decelerate and turn down gradient. This mesoscale phenomenon, referred to as orographic blocking, led to a record snowfall of 33.1 in (84 cm) in Burlington, VT while only 6 to 12 in (15 to 30 cm) fell along and east of the mountain spine. This conclusion is consistent with Sisson et al. (2010) who found multiple signatures of orographic blocking during the event, and emphasizes the significance of lower tropospheric stratification during low-level northwesterly flow events in northern Vermont.

A WRF simulation of the 25–27 February 2010 event revealed that orography again played a central role. A north-south oriented thermal boundary became quasistationary along the Hudson River Valley on 25 February 2010 (Fig. 4.26), acting to focus heavy snowfall just to the west. Upward vertical motion was sustained in a region of upslope flow along the eastern Catskill and Helderberg Mountains, effectively reinforcing the stationary frontal boundary through adiabatic cooling (Fig. 4.30). Significant low-level wind shifts along New York's Mohawk and Hudson Valleys prevented the westward expansion of warm Atlantic air, leading to a rain-snow line approximately delineated by the valleys (Figs. 4.27, 4.29). Albany, NY received primarily rain during the event while New York City received upwards of 20 in of snow, largely as a result of northeasterly warm air advection in the upper Hudson Valley and westerly cold air advection across lower New York (Fig. 4.22). The anomalous

multiscale aspects of this case demonstrate just some of the fascinating complexities that can arise during EJS events.

5.1.5 Applications of Research to Operational Forecasting

Conceptual models for EJS, cutoff low and open wave events are shown in Figures 5.1a–c and provide an illustration of key synoptic-scale features present during ACE occurrence. To aid the operational forecaster in determining whether or not an ACE is dynamically possible at lead times greater than 48 h, a checklist was created. For an ACE to be possible, conditions 1–3 must be met, and for an ACE to likely, conditions 1–5 must be met:

1) A 300-hPa standardized zonal wind anomaly $\leq -3\sigma$ over the Northeast U.S. or southeast Canada.
2) A region of 500-hPa height anomalies $\geq 1\sigma$ over northeast Canada or the western North Atlantic Ocean.
3) A negatively tilted 500-hPa trough or cutoff low over the east-central U.S.
4) An active split flow regime favoring the interaction of multiple vorticity maxima across the east-central U.S.
5) A surface cyclone < 990 hPa along or off the East Coast.

5.2 Conclusions

This research sought to: 1) develop a case list of ACEs in the Northeast U.S. cyclone domain; 2) determine the climatological frequency of ACEs; 3) document the response of various teleconnection indices prior to and during ACE occurrence; 4) construct composite charts of ACEs, and 5) examine specific high-impact events that illustrate the synoptic and mesoscale forcing mechanisms unique to ACEs. To accomplish these objectives, a subjective classification scheme was developed, which identified 78 ACEs in the Northeast U.S. cyclone domain. ACEs were classified as EJS, cutoff low, or open wave based on synoptic scale structure, and then analyzed using climatological and composite methods. Two recent EJS events were chosen for case studies and were examined using 1° NCEP GFS analyses and high-resolution WRF simulations.

The greatest number of ACEs occurred throughout the 1950s, 1990s and during the months of December and April. ACEs were found to be most common during periods of substantial high-latitude blocking associated with a strongly negative AO/NAO and a modestly positive PNA index. The EJS category held the most events and was associated with the deepest and longest duration cyclones. A composite analysis revealed several synoptic-scale features responsible for the development of EJS events, including an amplified upper-tropospheric ridge over northeast Canada, a split flow regime across western North America, and an interaction of northern and southern stream shortwaves across the east-central U.S. The majority of precipitation in the EJS event composite was located in the occluded quadrant of the cyclone, highlighting the importance of the following forcing mechanisms: 1) the ascending branch of a thermally indirect vertical circulation beneath the equatorward exit region of an easterly jet streak; 2) northerly and

northeasterly low-level warm air advection beneath the equatorward jet exit region in the vicinity of the trowal axis, and 3) moist low-level northwesterly flow interacting with the complex terrain of the Northeast U.S. Both study cases further provided further evidence that mesoscale forcing was able to modify synoptically driven circulations, leading to strong snowfall gradients.

The three types of ACEs identified in this study can, in some respects, be regarded as three stages of Northeast U.S. cyclone development. The first stage (open wave event) is associated with the weakest downstream block, and lacks both an upper-level easterly jet streak poleward of the surface low and wrap-around low-level warm air advection precipitation. The second stage (cutoff low event) is associated with a more substantial west-based downstream block, and displays a developing easterly jet streak with more significant wrap-around low-level warm air advection precipitation. The third stage (EJS event) is associated with an immense west-based downstream block, and displays an easterly jet streak (> 60 kt) poleward of the surface cyclone, with significant wrap-around low-level warm air advection precipitation. Results from this study suggest that third stage cyclone events (EJS events) are the most anomalous and present the greatest forecast challenge.

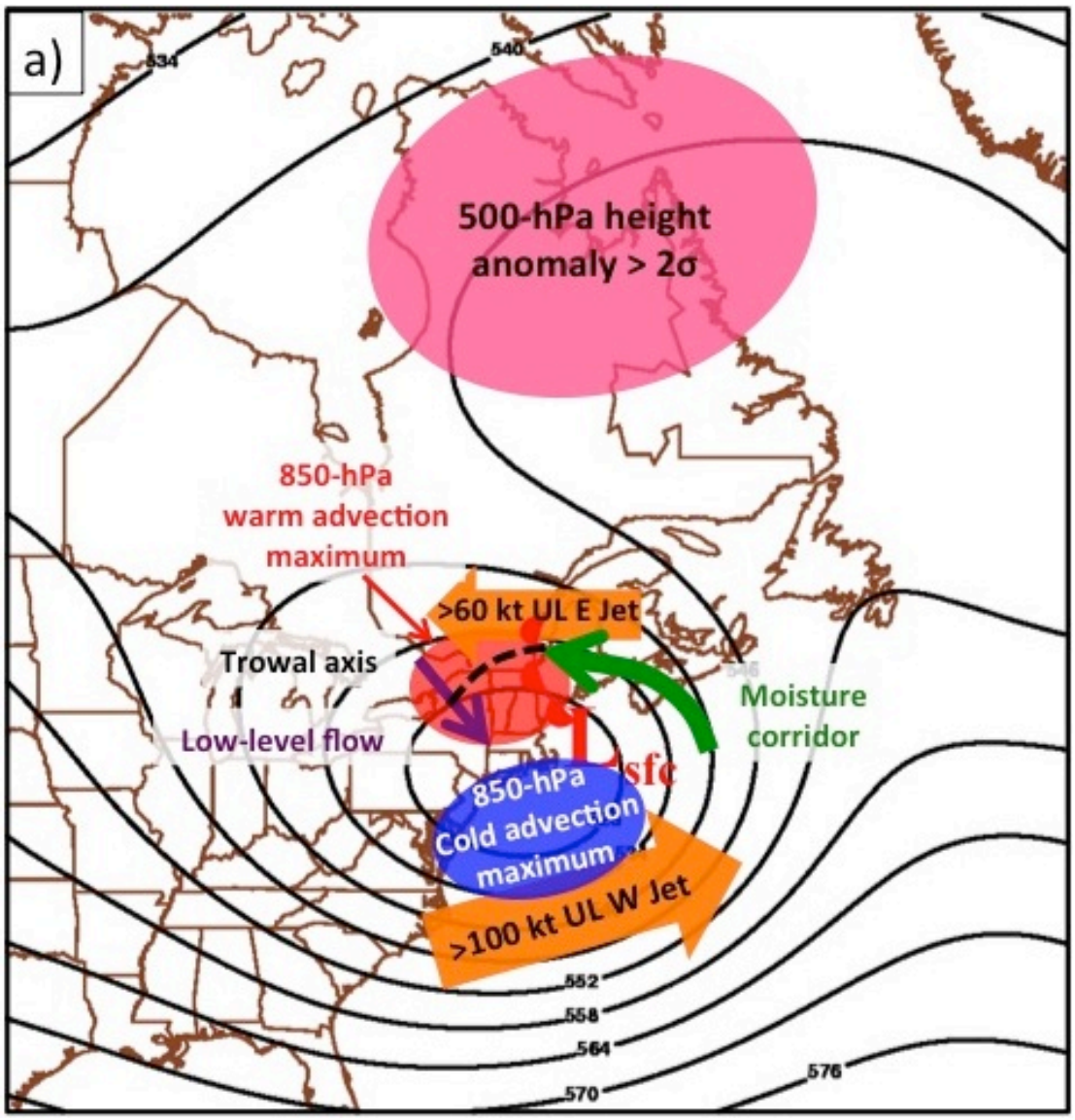
a)
534
540
500-hPa height
anomaly > 2σ
850-hPa
warm advection
maximum
>60 kt UL E Jet
Trowal axis
Low-level flow
Moisture
corridor
Sfc
850-hPa
Cold advection
maximum
>100 kt UL W Jet
552
558
564
570
576

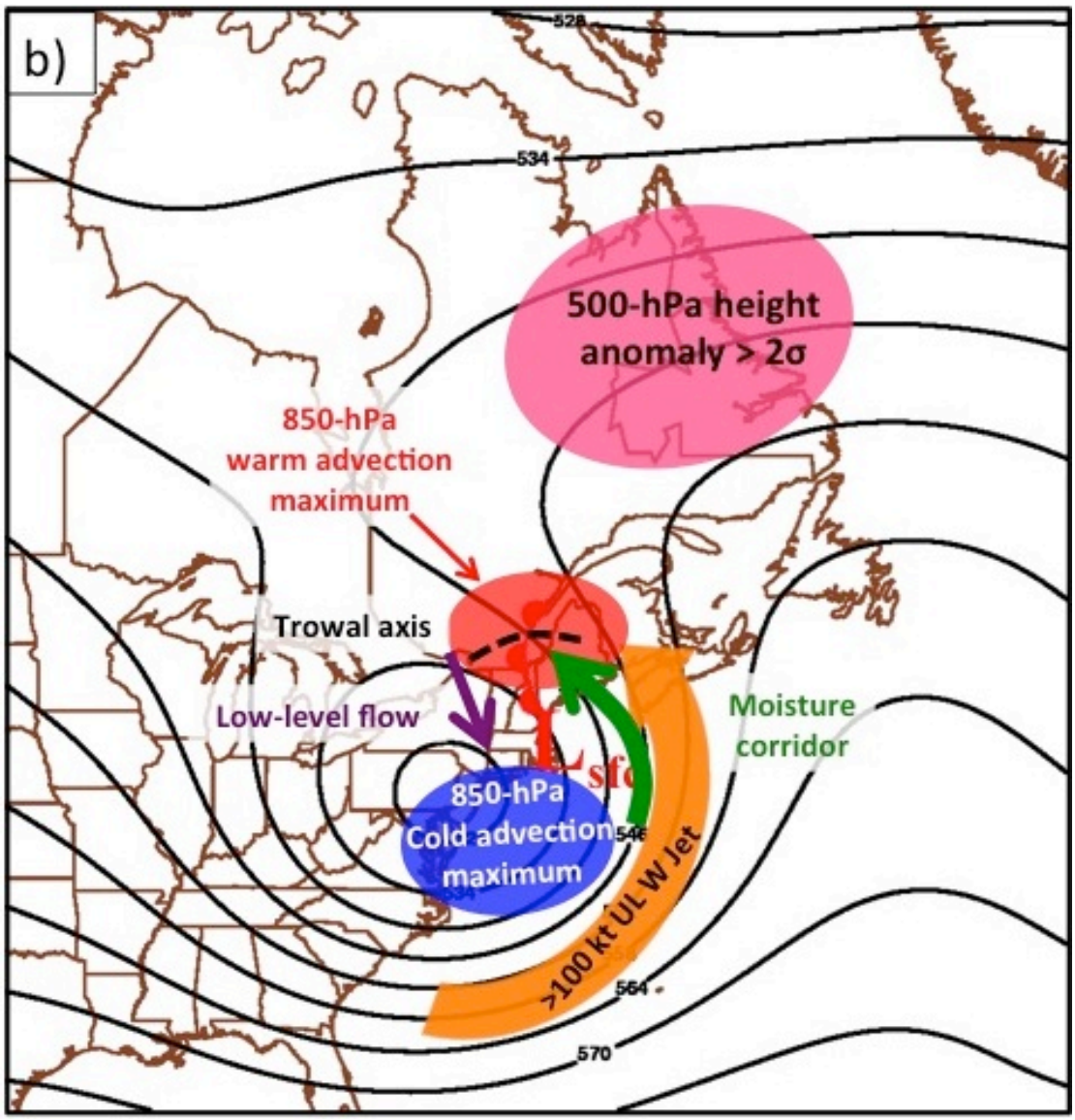
b)
528
534
500-hPa height
anomaly > 2σ
850-hPa
warm advection
maximum
Trowal axis
Low-level flow
Moisture
corridor
850-hPa
Cold advection
maximum
>100 kt UL W Jet
564
570

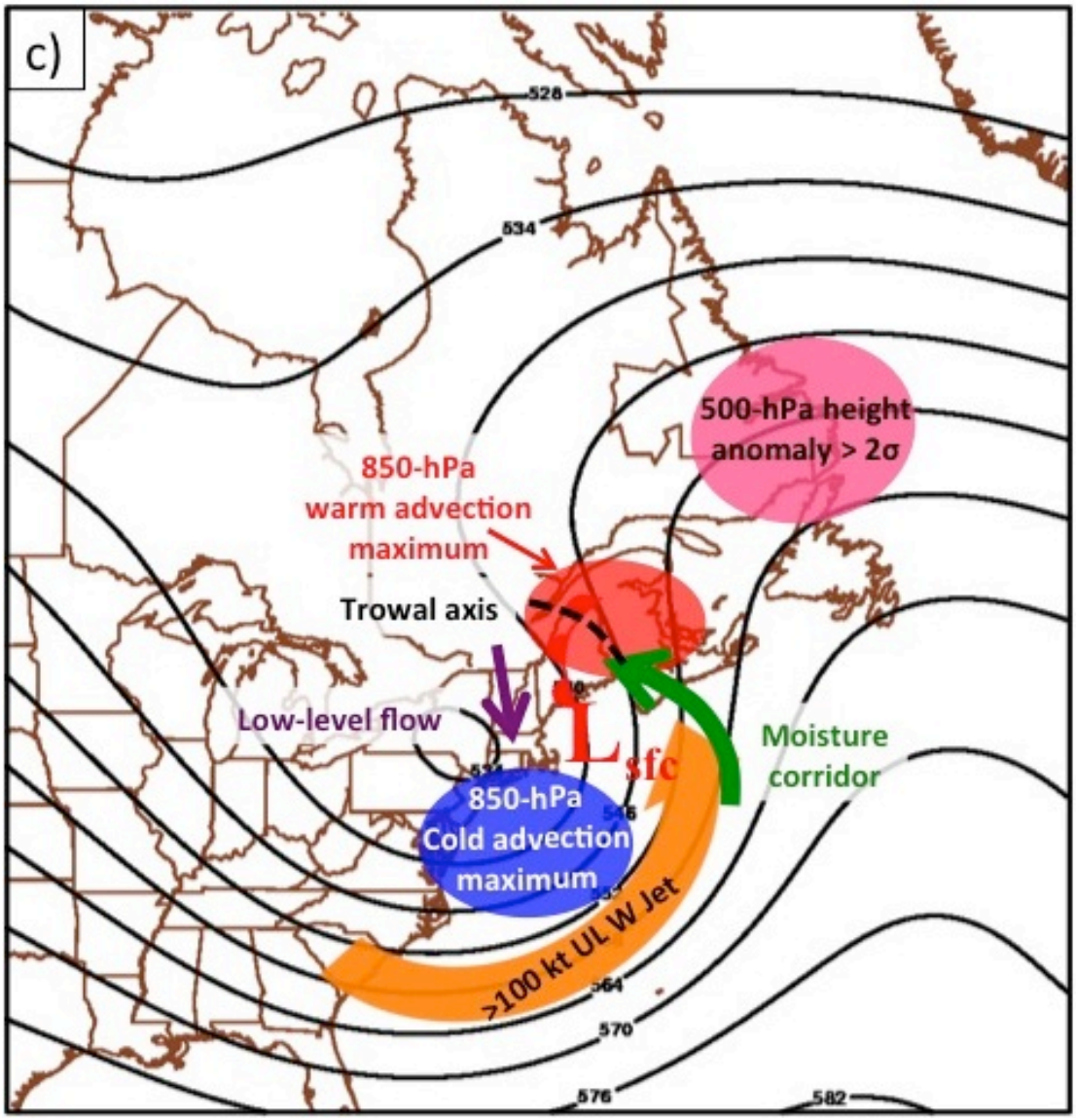

Fig. 5.1 Conceptual model depicting the 500-hPa geopotential height (dam, solid black contours) and key synoptic-scale features for (a) EJS events, (b) cutoff low events, and (c) open wave events.

REFERENCES

Archambault, H. M., D. Keyser, and L. F. Bosart, 2010: Relationships between large-scale regime transitions and major cool-season precipitation events in the northeastern United States. *Mon. Wea. Rev.,* **138**, 3454–3473.

_____, L. F. Bosart, D. Keyser, and A. Aiyyer, 2008: Influence of large-scale flow regimes on cool-season precipitation in the northeastern United States. *Mon. Wea. Rev.*, **136**, 2945–2963.

Austin, J. M., 1941: Favorable conditions for cyclogenesis near the Atlantic coast. *Bull. Amer. Meteor. Soc.*, **22**, 270–271.

Barnes, E. A., and D. L. Hartmann, 2010: Dynamical feedbacks and the persistence of the NAO. *J. Atmos. Sci.*, **67**, 851–865.

Barnston, A. G., and R. E. Livezey, 1987: Classification, seasonality and persistence of low-frequency atmospheric circulation patterns. *Mon. Wea. Rev.*, **115**, 1083–1126.

Bell, G. D., and L.F. Bosart, 1989: A 15-year climatology of Northern Hemisphere 500 mb closed cyclone and anticyclone centers. *Mon. Wea. Rev.*, **117**, 2142–2163.

_____, and L. F. Bosart, 1993: A case study diagnosis of the formation of an upper-level cutoff cyclonic circulation over the eastern United States. *Mon. Wea. Rev.*, **121**, 1635–1655.

_____, and D. Keyser, 1993: Shear and curvature vorticity and potential-vorticity interchanges: Interpretation and application to a cutoff cyclone event. *Mon. Wea. Rev.*, **122**, 76–102.

_____, and L. F. Bosart, 1994: Midtropospheric closed cyclone formation over the southwestern United States, the Eastern United States, and the Alps. *Mon. Wea. Rev.*, **122**, 791–813.

_____, and M. S. Halpert, 1998: Climate assessment for 1997. *Bull. Amer. Meteor. Soc.*, **79**, S1–S49.

Bjerknes, J., 1919: On the structure of moving cyclones. *Geogys. Publ., Norske Videnskaps-Akad. Oslo*, **1**, 1-8.

_____, 1969: Atmospheric teleconnections from the equatorial Pacific. *Mon. Wea. Rev.,*

97, 163–172.

Chang, Yehui, Siegfried Schubert, Max Suarez, 2012: Attribution of the Extreme U.S. East Coast Snowstorm Activity of 2010. *J. Climate*, **25**, 3771–3791.

Colucci, S. J., 1976: Winter cyclone frequencies over the eastern United States and adjacent western Atlantic, 1963-1973. *Bull. Amer. Meteor. Soc*., **57**, 548–553.

_____, 1985: Explosive cyclogenesis and large-scale circulation changes: Implications for atmospheric blocking. *J. Atmos. Sci.,* **42**, 2701–2717.

_____, 1987: Comparative diagnosis of blocking versus nonblocking planetary-scale circulation changes during synoptic-scale cyclogenesis. *J. Atmos. Sci*., **44**, 124–139.

Dean, D. B., and L. F. Bosart, 1996: Northern hemisphere 500-hPa trough merger and fracture: A climatology and case study. *Mon. Wea. Rev.,* **124**, 2644–2671.

desJardins, M. L., K. F. Brill, and S. S. Schotz, 1991: Use of GEMPAK on UNIX workstations. *Proc. Seventh Int. Conf. on Interactive Information and Processing Systems for Meteorology, Oceanography, and Hydrology,* New Orleans, LA, Amer. Meteor. Soc., 449–453.

Feldstein, S. B., 2002: Fundamental mechanisms of the growth and decay of the PNA teleconnection pattern. *Quart. J. Roy. Meteor. Soc.,* **128**, 775–796.

Gaza, R. S., and L. F. Bosart, 1990: Trough merger characteristics over North America. *Wea. Forecasting*, **5**, 314–331.

Grumm, R. H., and R. Hart, 2001: Standardized anomalies applied to significant cold season weather events: Preliminary findings. *Wea. Forecasting*, **16**, 736–754.

Hakim, G. J., L. F. Bosart, and D. Keyser, 1995: The Ohio Valley wave-merger cyclogenesis event of 25-26 January 1978. Part 1: Multiscale case study. *Mon. Wea. Rev.*, **123**, 2663–2692.

_____, D. Keyser, and L. F. Bosart, 1996: The Ohio Valley wave-merger cyclogenesis event of 25-26 January 1978: Part II: Diagnosis using quasigeostrophic potential vorticity inversion. *Mon. Wea. Rev.*, **124**, 2176–2205.

Halpert, M. S., and G. D. Bell, 1997: Climate assessment for 1996. *Bull. Amer. Meteor. Soc.*, **78**, S1-S49.

Hirsch, M. E., A. T. DeGaetano, and S. J. Colucci, 2001: An East Coast winter storm climatology. *J. Climate*, **14**, 882–899.

Hoerling, M., 2010: Understanding the mid-Atlantic snowstorms during the winter of 2009-2010. Expert assessment report of the National Oceanic and Atmospheric Administration, 16 pp.

Hong S.Y., J. Dudhia, S. H. Chen, 2004: A revised approach to ice- microphysical processes for the bulk parameterization of clouds and precipitation. *Mon. Weather Rev.* **132**, 103–120.

Kalnay, E., M. Kanamitsu, R. Kistler, W. Collins, D. Deaven, L. Gandin, M. Iredell, S. Saha, G. White, J. Woollen, Y. Zhu, A. Leetmaa, B. Reynolds, M. Chelliah, W. Ebisuzaki, W. Higgins, J. Janowiak, K. C. Mo, C. Ropelewski, J. Wang, R. Jenne, and D. Joseph, 1996: The NCEP/NCAR 40-year reanalysis project. *Bull. Amer. Meteor. Soc*., **77**, 437–471.

Kenyon, J. S., 2013: The Motion of Mesoscale Snowbands in Northeast U.S. Winter Storms. Masters of Science Thesis, Department of Earth and Atmospheric Sciences, University at Albany/SUNY, Albany, NY, 108 pp.

Keyser, D., and M. A. Shapiro, 1986: A review of the structure and dynamics of upper-level frontal zones. *Mon. Wea. Rev.,* **114**, 452–499.

_____, Reeder, M. J., and Reed, R. J., 1988: A Generalization of Petterssen's Frontogenesis Function and Its Relation to the Forcing of Vertical Motion. *Mon. Wea. Rev.*, **116**, 762–781.

Kim, B. M., G. H. Lim, and K. Y. Kim, 2006: A new look at the midlatitude-MJO teleconnection in the northern hemisphere winter. *Quart. J. Roy. Meteor. Soc*., **132**, 485–503.

Kistler, R., E. Kalnay, W. Collins, S. Saha, G. White, J. Woolen, M. Chelliah, W. Ebisuzaki, M. Kanamitsu, V. Kousky, H. Van den Dool, R. Jenne, and M. Fiorino, 2001: The NCEP-NCAR 50-year reanalysis: Monthly means CD-ROM and documentation. *Bull. Amer. Meteor. Soc*., **82**, 247–267.

Kocin, P. J., and L. W. Uccellini, 2004: *Northeast Snowstorms (Volume I: Overview, Volume II: The Cases). Meteor. Monogr.*, No. 54, Amer. Meteor. Soc., 818 pp.

Konrad, C. E., and S. J. Colucci, 1988: Synoptic climatology of 500 mb circulation changes during explosive cyclogenesis. *Mon. Wea. Rev.*, **116**, 1431–1443.

Kocin, P. J., and L. W. Uccellini, 1990: *Snowstorms along the Northeastern Coast of the United States: 1955-985. Meteor. Monogr.*, No. 44, Amer. Meteor. Soc., 280 pp.

Lackmann, G. M., L. F. Bosart, and D. Keyser, 1996: Planetary- and synoptic-scale characteristics of explosive wintertime cyclogenesis over the western North Atlantic Ocean. *Mon. Wea. Rev.*, **124**, 2672–2702.

Lefevre, R. J., and J. W. Nielsen-Gammon, 1995: An objective climatology of mobile troughs in the northern hemisphere. *Tellus*, **47**, 638–655.

Madden, R. A., and P. R. Julian, 1972: Description of global scale circulation cells in the tropics with a 40–50 day period. *J. Atmos. Sci.*, **29**, 1109–1123.

_____, and P. R. Julian, 1994: Observations of the 40–50-day tropical oscillation—A review. *Mon. Wea. Rev.*, **122**, 814–837.

Maglaras, G. J., J. S. Waldstreicher, P.J. Kocin, A. F. Gigi, and R. A. Marine, 1995: Winter weather forecasting throughout the eastern United States. Part I: An overview. *Wea. Forecasting*, **10**, 5–20.

Martin, J. E., 1999: Quasigeostrophic Forcing of Ascent in the Occluded Sector of Cyclones and the Trowal Airstream. *Mon. Wea. Rev.*, **127**, 70–88.

Matthews, A. J., B. J. Hoskins, and M. Masutani, 2004: The global response to tropical heating in the Madden-Julian oscillation during northern winter. *Quart. J. Roy. Meteor. Soc.*, **130**, 1991–2011.

Miller, J. E., 1946: Cyclogenesis in the Atlantic coastal region of the United States. *J. Meteor.*, **3**, 31–44.

Noel, J., and D. Changnon, 1998: A pilot study examining U.S. winter cyclone frequency patterns associated with three ENSO parameters. *J. Climate,* **11**, 2152–2159.

Novak, D. R., and A. R. Aiyyer, 2010: Evolution of mesoscale precipitation band environments within the comma head of northeast U.S. Cyclones. *Mon. Wea. Rev.*, **138**, 2354–2374.

Palmén, E., 1949: Origin and structure of high-level cyclones south of the maximum westerlies. *Tellus*, **1**, 22–31.

_____, and K.M. Nagler, 1949: The formation and structure of a large-scale disturbance in the westerlies. *J. Meteorol.*, **6**, 227–242.

_____, and C. W. Newton, 1969: *Atmospheric Circulation Systems.* Academic Press,

603 pp.

Payer, M. D., 2010: Forecasting precipitation distributions associated with cool-season 500-hPa cutoff cyclones in the northeastern United States. Masters of Science Thesis, Department of Earth and Atmospheric Sciences, University at Albany/SUNY, Albany, NY, 130 pp.

Pelly, J. L., and B. J. Hoskins, 2003: A new perspective on blocking. *J. Atmos. Sci*., **60**, 743–755.

Petterssen, S., 1956: *Weather Analysis and Forecasting.* Vol. 1. McGraw-Hill, 428 pp.

Rex, D. F., 1950: Blocking action in the middle tropospheric westerlies and its effect on regional climate: 1. An aerological study of blocking action. *Tellus*, **2**, 196–211.

Rochette, S. M., and P. S. Market, 2011: A case study of an anomalous cold-season easterly jet streak in the mid-latitudes. *Electronic Journal of Operational Meteorology*, 2011-EJ6.

Roebber, P. J., 1984: Statistical analysis and updated climatology of explosive cyclones. *Mon. Wea. Rev.*, **112**, 1577–1589.

Rogers, J. C., 1990: Patterns of low-frequency monthly sea level pressure variability (1899–1986) and associated wave cyclone frequencies. *J. Climate*, **3**, 1364–1379.

Salmon, E., and P. J. Smith, 1980: A synoptic analysis of the 25-56 January 1978 blizzard cyclone in the central United States. *Bull. Amer. Soc.*, **61**, 453-460.

Sanders, F., 1988: Life history of mobile troughs in the upper westerlies. *Mon. Wea. Rev.*, **116**, 2629–2648.

_____, and J. R Gyakum, 1980: Synoptic-dynamic climatology of the "bomb." *Mon. Wea. Rev.,* **108**, 1590–1606.

Seager, R., Y. Kushnir, J. Nakamura, M. Ting, and N. Naik, 2010: Northern Hemisphere winter snow anomalies: ENSO, NAO and the winter of 2009/10. *Geophys. Res. Lett.,* **37**, L14703, doi:10.1029/2010GL043830.

Shapiro, M. A., and D. Keyser, 1990: Fronts, jet streams and the tropopause. *Extratropical Cyclones: The Erik Palmén Memorial Volume*, C. W. Newton and E. O. Holopainen, Eds., Amer. Meteor. Soc., 167–193.

Sisson, P.A., D. St. Jean, E. Evenson, W.E. Murray, S.F. Hogan, L.F. Bosart, D. Keyser,

and B. Smith, 2004: Applying local research to National Weather Service operations: Forecasting heavy mountain snowfalls in Vermont and northern New York. Preprints, 11th Conference on Mountain Meteorology, Seattle, WA, Amer. Meteor. Soc., CD-ROM, 17.5.

_____, P. Banacos, and B. Taber, 2010: Champlain powder: The historic Burlington Vermont snowfall of 2–3 January 2010. 35th Annual Northeastern Storm Conference, Saratoga Springs, NY, Lyndon State College.

Skamarock, W. C., J. B. Klemp, J. Dudhia, D. O. Gill, D. M. Barker, M. G. Duda, X.-Y. Huang, W. Wang, and J. G. Powers, 2008: A description of the Advanced Research WRF version 3. NCAR Technical Note 475, http://www.mmm.ucar.edu/wrf/users/docs/arw_v3.pdf.

Smith, S. R., and J. J. O'Brien, 2001: Regional snowfall distributions associated with ENSO: Implications for seasonal forecasting. *Bull. Amer. Meteor. Soc.,* **82**, 1179–1191.

St. Jean, D., P. A. Sisson, L.F. Bosart, D. Keyser, and B. Smith, 2004: Characteristics Of Upslope Snowfall Events In Northern New York State and Northern Vermont: Diagnostics And Model Simulations Of Several Northwest-Flow Cases. Preprints, 20th Conference on Weather Analysis and Forecasting, Seattle, WA, Amer. Meteor. Soc., CD-ROM, 18.4

Straus, D. M., and J. Shukla, 2002: Does ENSO force the PNA? *J. Climate*, **15**, 2340–2358.

Stuart, N. A., and R.H. Grumm, 2006: Using wind anomalies to forecast East Coast winter storms. *Wea. Forecasting*, **21**, 952–968.

_____, cited 2010a: Post New Year's Day 2010 Storm. [Available online at http://cstar.cestm.albany.edu/PostMortems/CSTARPostMortems/2010/jan1-4/jan2010storm.htm.]

_____, cited 2010b: Historic End of February 2010 Storm: Stage 2. [Available online at http://cstar.cestm.albany.edu/PostMortems/CSTARPostMortems/2010/feb2010storm5/snowicanestage2.htm]

Sutcliffe, R. C., 1947: A contribution to the problem of development. *Quart. J. Roy. Meteor. Soc.,* **73**, 370–383.

_____, and A. G. Forsdyke, 1950: The theory and use of upper air thickness patterns in forecasting. *Quart. J. Roy. Meteor. Soc.,* **76**, 189–217.

Thompson, D. W., and J. M. Wallace, 1998: The Arctic Oscillation signature in the wintertime geopotential height and temperature fields. *Geophys. Res. Lett.,* **25**, 1297–1300.

Thompson, G., R. M. Rasmussen, and K. Manning, 2004: Explicit forecasts of winter precipitation using an improved bulk microphysics scheme. Part I: Description and sensitivity analysis. *Mon. Wea. Rev*., **132**, 519–542.

Thorncroft, C.D., B.J. Hoskins, and M.E. McIntyre, 1993: Two paradigms of baroclinic-wave life-cycle behaviour. *Quart. J. Roy. Meteor. Soc.,* **119**, 17–55.

Uccellini, L. W., and P. J. Kocin, 1987: An examination of vertical circulations associated with heavy snow events along the East Coast of the United States. *Wea. Forecasting*, **2***,* 289–308.

_____, and D. R. Johnson, 1979: The coupling of upper and lower tropospheric jet streaks and implications for the development of sever convective storms. *Mon. Wea. Rev*., **107**, 682-703.

Walker, G. T., and E. W. Bliss, 1932: World Weather V. *Mem. Roy. Meteor. Soc.,* **44**, 53–84.

Wallace, J. M., and D. S. Gutzler, 1981: Teleconnections in the geopotential height field during the Northern Hemisphere winter. *Mon. Wea. Rev.,* **109**, 784–812.

_____, and _____, 2000: Annular modes in the extratropical circulation. Part I: Month-to-month variability. *J. Climate,* **13**, 1000–1016.

Wang, C., H. Liu, and S. Lee (2010), The record‐breaking cold tempera- tures during the winter of 2009/2010 in the Northern Hemisphere, Atmos. Sci. Lett., doi:10.1002/asl.278.

Zhou, S., M. L'Heureux, S. Weaver, and A. Kumar, 2012: A composite study of the MJO influence on the surface air temperature and precipitation over the Continental United States. *Climate Dyn*., **38**, 1459-1471